Supplementary Information (SI) for Chemical Science.
This journal is © The Royal Society of Chemistry 2026

This version of the Supplementary Information was published on 30/01/26

Supporting Information for

Formation of Tungsten Ethylidene Complexes from Diethyl Complexes Through a Proton-Catalyzed Rearrangement of Ethylene

Milan Maji, Landley Zeng, Richard R. Schrock,[a]* Matthew P. Conley,[a] and Veronica Carta[a]

Department of Chemistry, University of California at Riverside, Riverside, California 92521

Contents

1. General Considerations

Unless otherwise stated, all manipulations were carried out using standard Schlenk or glovebox techniques under an N_2 atmosphere. Pentane, diethyl ether, dichloromethane, benzene and toluene were dried and deoxygenated by argon purge followed by passage through activated alumina in a solvent purification system followed by storage over 4 Å molecular sieves. Non-halogenated and non-nitrile containing solvents were tested with a standard purple solution of sodium benzophenone ketyl in THF to confirm effective oxygen and moisture removal prior to use. W(NAr)$_2$Cl$_2$(DME) was prepared according to reported procedure.[1] Perfluoro-*t*-butanol and hexafluoro-*t*-butanol were purchased from Oakwood chemical and Alfa chemical respectively and stored over activated 4 Å molecular sieves. 1,4-TMS benzene, Isopropyl magnesium chloride and n-propyl magnesium chloride were purchased from Sigma-Aldrich; $B(C_6F_5)_3$ was purchased from Alfa chemical and sublimed before use. Elemental analyses were performed by Atlantic Microlab, Inc., Norcross, GA. Deuterated solvents were purchased from Cambridge Isotope Laboratories Inc., degassed, and dried over activated 4 Å molecular sieves for at least 24 h prior to use. NMR spectra were recorded on Bruker Avance 600 MHz and Bruker Avance 500 MHz spectrometers. ^{1}H and ^{13}C chemical shifts are reported in ppm relative to tetramethylsilane using residual solvent as an internal standard.^{19}F chemical shifts are reported in ppm relative to trichlorofluoromethane as an external standard.

2. NMR spectra

W(NAr)$_2$Et$_2$. ^{1}H NMR (600 MHz, C_6D_6, 298K): δ 7.07 (d, *J* = 7.6 Hz, 4H), 6.97 (t, *J* = 7.6 Hz, 2H), 3.66 (sept, *J* = 6.9 Hz, 4H), 2.11 (q, *J* = 8.0 Hz, 4H), 1.58 (t, *J* = 8.0 Hz, 6H), 1.18 (d, *J* = 6.9 Hz, 24H). **^{13}C{^{1}H} NMR** (151 MHz, C_6D_6, 298K): δ 152.62, 142.28, 125.19, 122.52, 57.71, 28.72, 23.50, 10.70.

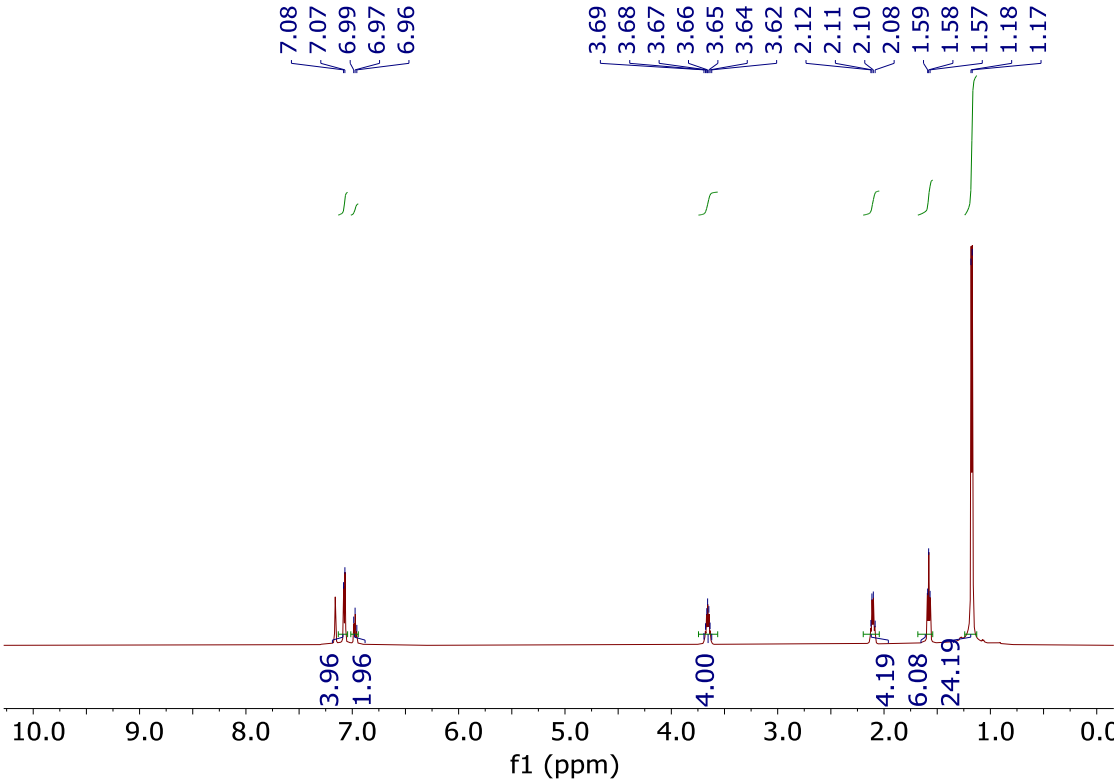

Figure S1. ^{1}H NMR spectrum of $W(NAr)_2Et_2$ (600 MHz, 298K) in C_6D_6.

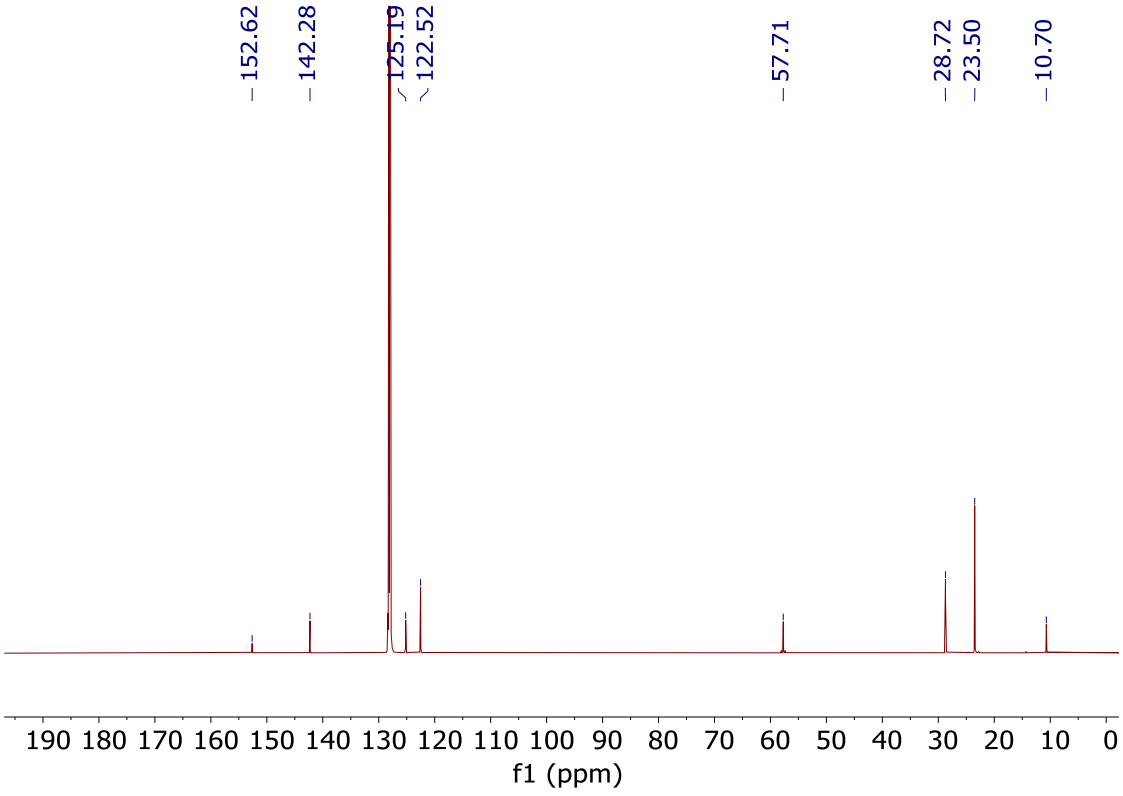

Figure S2. ^{13}C NMR spectrum of $W(NAr)_2Et_2$ (151 MHz, 298K) in C_6D_6.

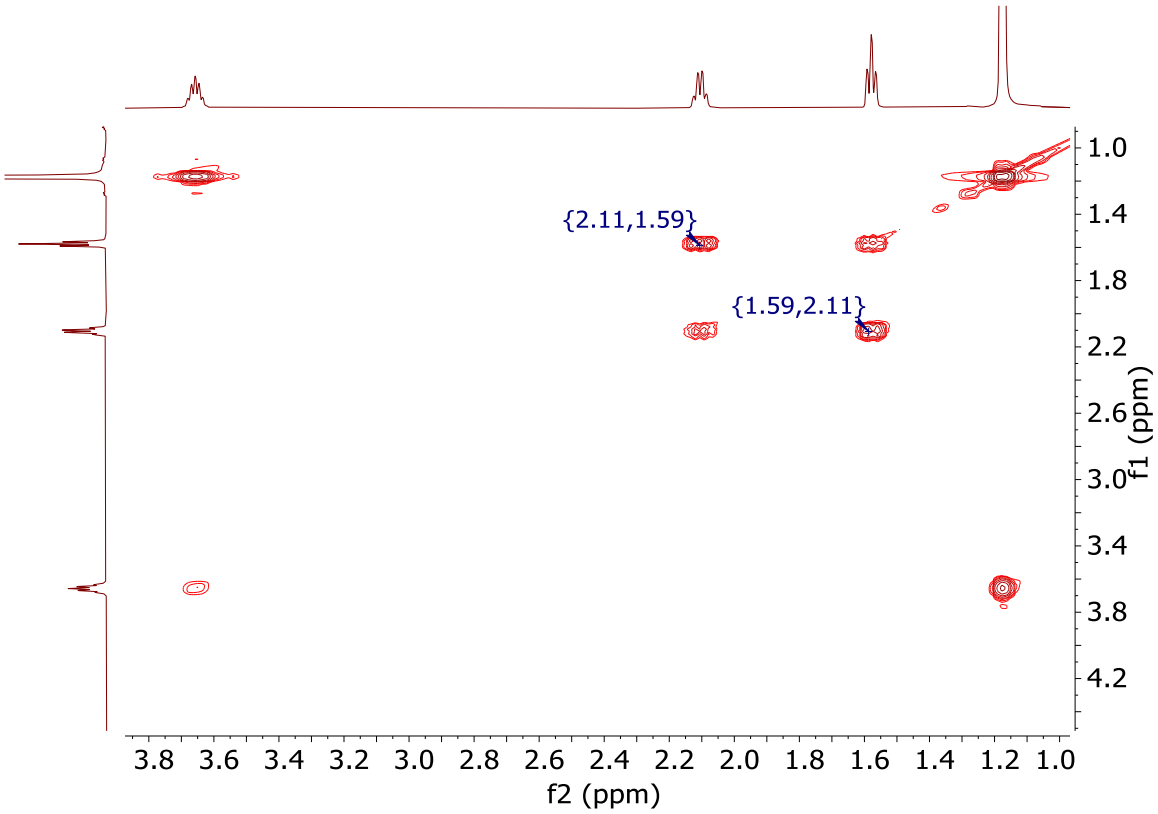

Figure S3. ^{1}H-COSY spectrum W(NAr)$_2$Et$_2$ (600 MHz, 298K) in C_6D_6.

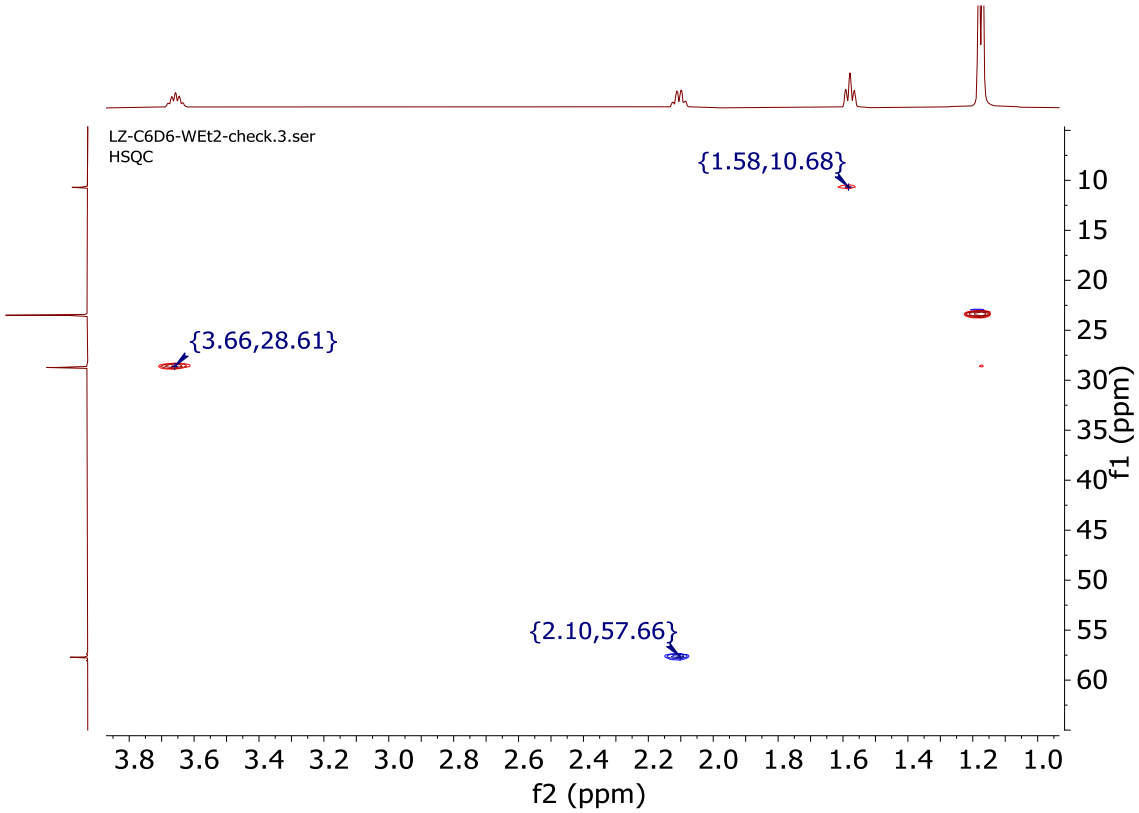

Figure S4. The aliphatic area of an HSQC{^{1}H;^{13}C} spectrum of W(NAr)$_2$Et$_2$ (600 MHz, 298K) in C_6D_6.

W(NAr)(OR$_{F9}$)$_2$(C$_2$H$_4$)(ArNH$_2$). ^{1}H NMR (600 MHz, C$_6$D$_6$, 298K): δ 7.06 (d, 2H), 6.94 (d, 3H), 6.91 (t, 1H), 3.53 (sept, 4H), 3.27 (s, 1H), 2.81 (s, 2H), 2.65 (sept, 2H), 1.13 (d, *J* = 6.5 Hz, 24H)**. ^{13}C NMR** (151 MHz, C$_6$D$_6$, 298K): δ 152.05, 146.76, 128.97, 123.23, 123.05, 121.94, 59.37, 28.94, 28.13, 23.50, 22.64. **^{19}F NMR** (564 MHz, C$_6$D$_6$, 298K): δ −73.65.

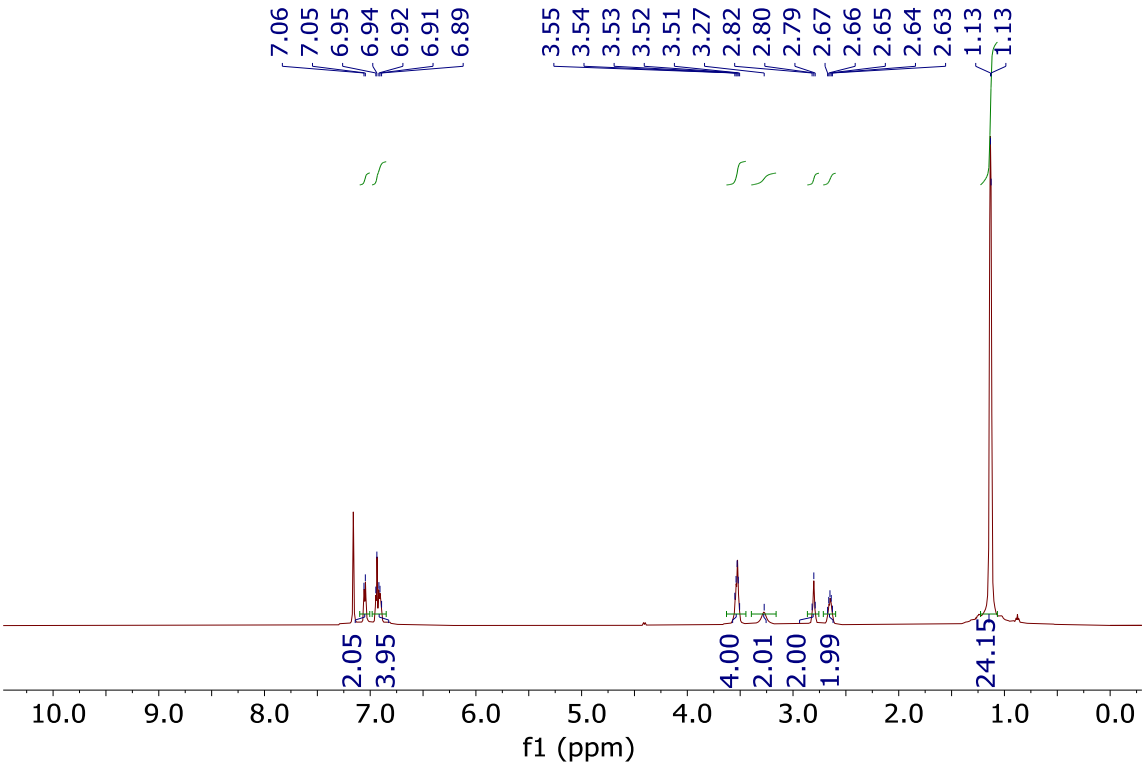

Figure S5. ^{1}H NMR spectrum of W(NAr)(NH$_2$Ar)(OR$_{F9}$)$_2$(C$_2$H$_4$) (600 MHz, 298K) in C$_6$D$_6$.

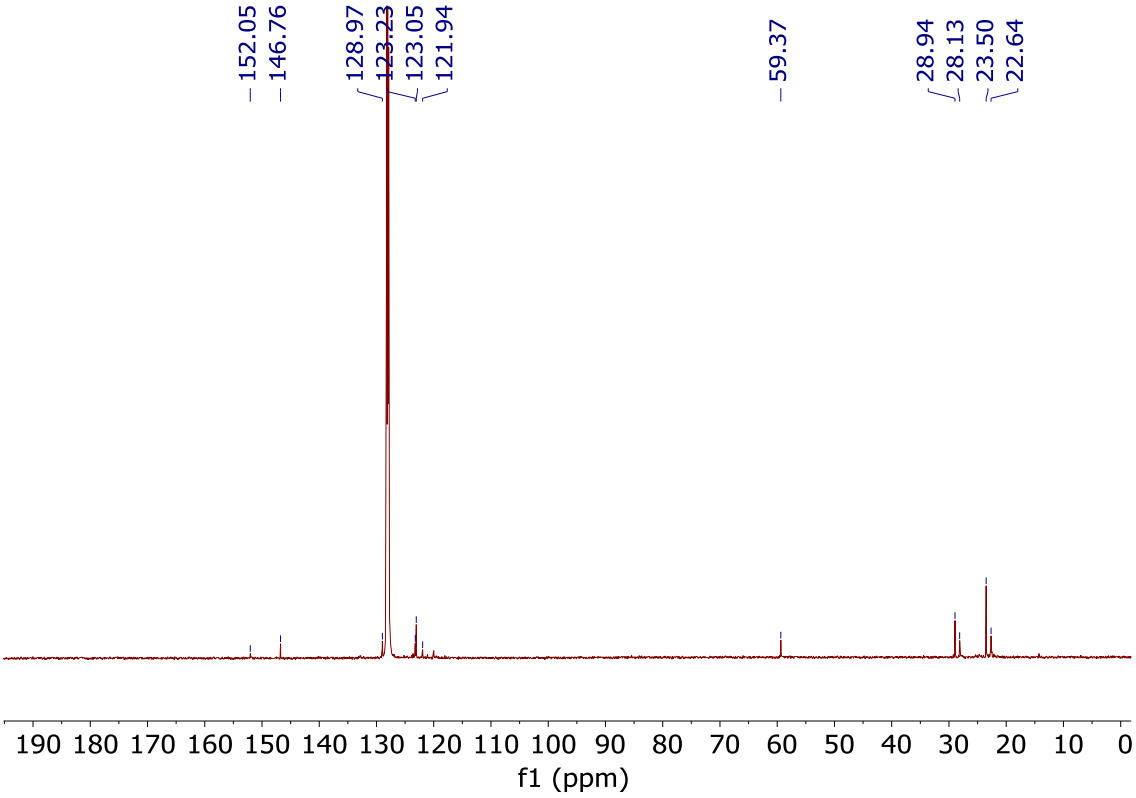

Figure S6. ^{13}C NMR spectrum of W(NAr)(NH_2Ar)(OR_{F9})$_2$(C_2H_4) (151 MHz, 298K) in C_6D_6.

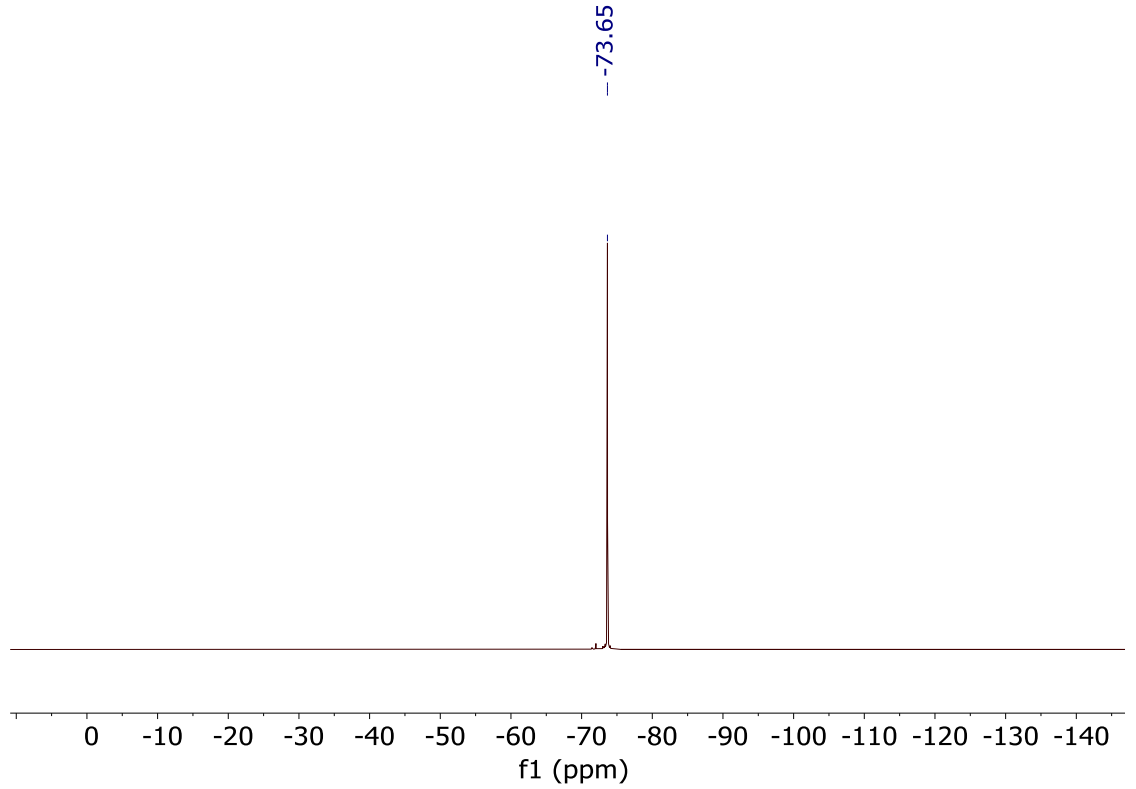

Figure S7. ^{19}F NMR spectrum of W(NAr)(NH_2Ar)(OR_{F9})$_2$(C_2H_4) (564 MHz, 298K) in C_6D_6.

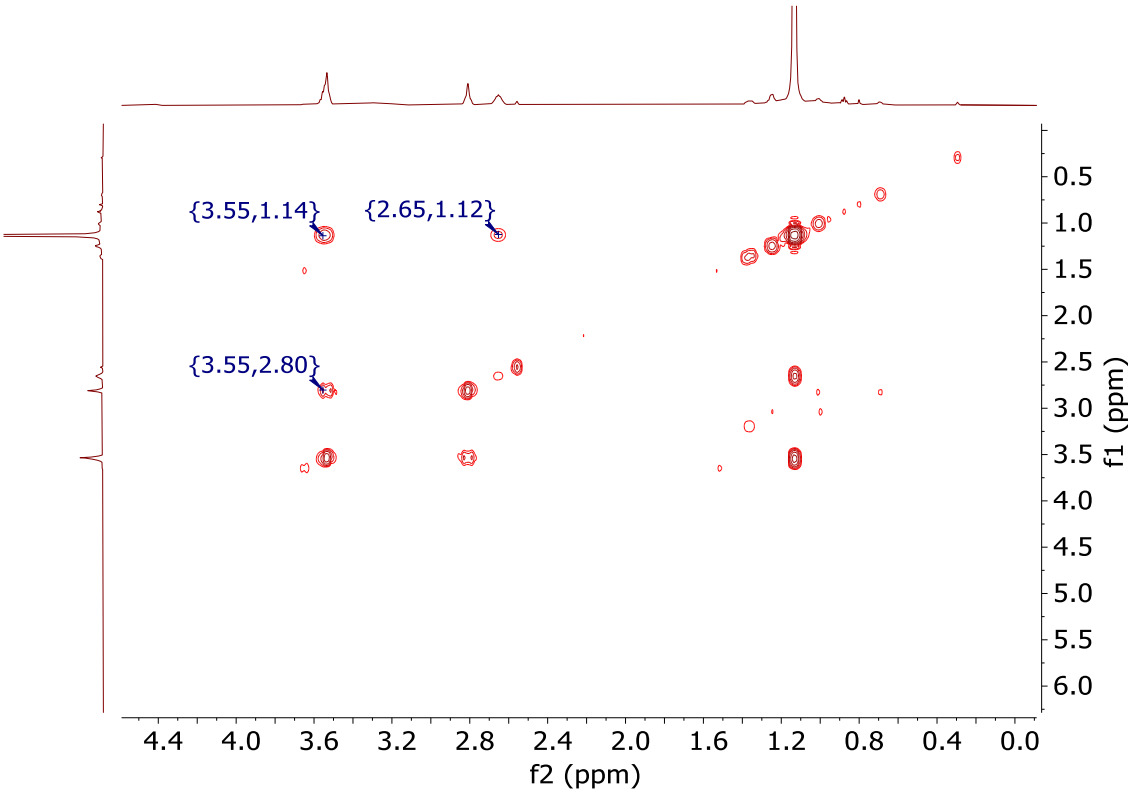

Figure S8. ^{1}H-COSY spectrum W(NAr)(NH_2Ar)(OR_{F9})$_2$(C_2H_4) (600 MHz, 298K) in C_6D_6.

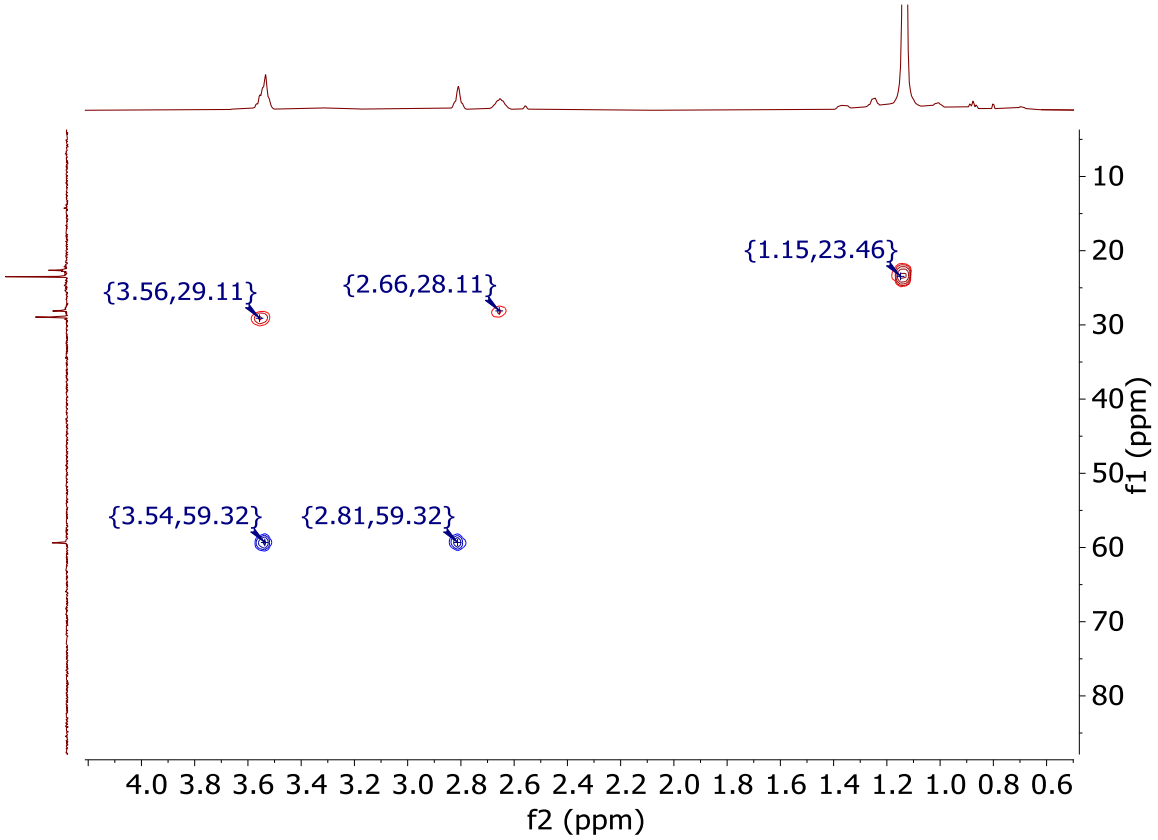

Figure S9. Aliphatic area of an HSQC{ ^{1}H;^{13}C} spectrum of W(NAr)(NH_2Ar)(OR_{F9})$_2$(C_2H_4) (600 MHz, 298K) in C_6D_6.

W(NAr')(ArNH)(ArNH$_2$)(OR$_{F9}$). **^{1}H NMR** (600 MHz, C_6D_6, 298K): δ 8.81 (s, 1H), 7.12 (d, *J* = 7.4 Hz, 1H), 7.04 – 6.98 (m, 4H), 6.91 – 6.89 (m, 3H), 6.74 (s, 1H), 5.94 (d, *J* = 12.1 Hz, 1H), 5.57 (d, *J* = 12.1 Hz, 1H), 3.82 (s, 1H), 3.74 (s, 1H), 3.66 (d, *J* = 8.1 Hz, 1H), 3.21 – 3.18 (m, 1H), 3.05 – 3.03 (m, 1H), 2.84 – 2.80 (m, 1H), 2.56 (s, 3H), 1.53 (d, *J* = 9.8 Hz, 1H), 1.38 – 1.36 (m, 9H), 1.25 – 1.24 (m, 9H), 1.01 – 0.96 (m, 12H), 0.69 (d, *J* = 6.9 Hz, 3H). **^{13}C{^{1}H} NMR** (151 MHz, C_6D_6, 298K): δ 158.40, 151.82, 147.51, 143.89, 140.18, 138.54, 132.92, 132.21, 127.11, 126.92, 125.22, 123.63, 123.21, 122.10, 121.09, 92.19, 85.45, 29.22, 28.92, 28.31, 28.03, 25.33, 24.71, 23.00, 22.49, 22.17, 22.09, 14.29. **^{19}F{^{1}H} NMR** (282 Hz, C_6D_6, 298K): δ –73.46 (s, 9F)

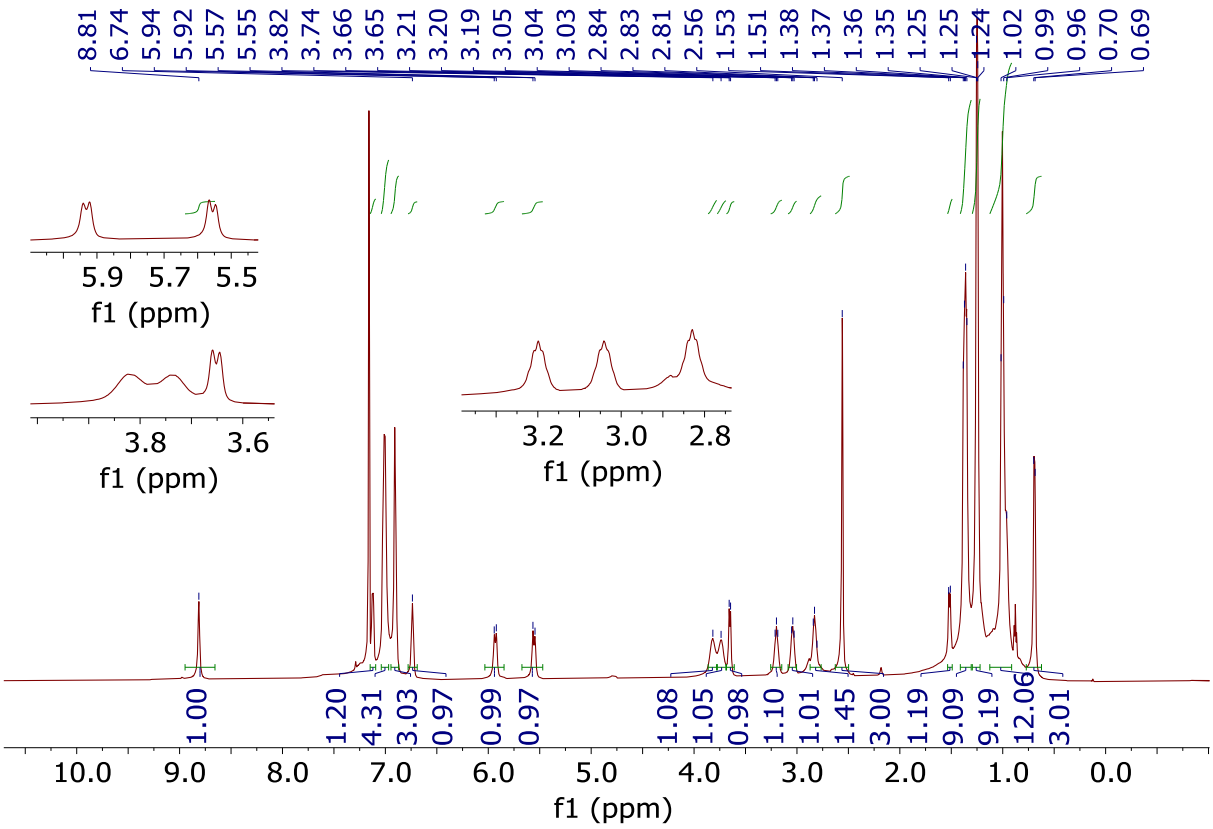

Figure S10. ^{1}H NMR spectrum of W(NAr)(Ar'NH)(ArNH$_2$)(OR$_{F9}$) (600 MHz, 298K) in C_6D_6.

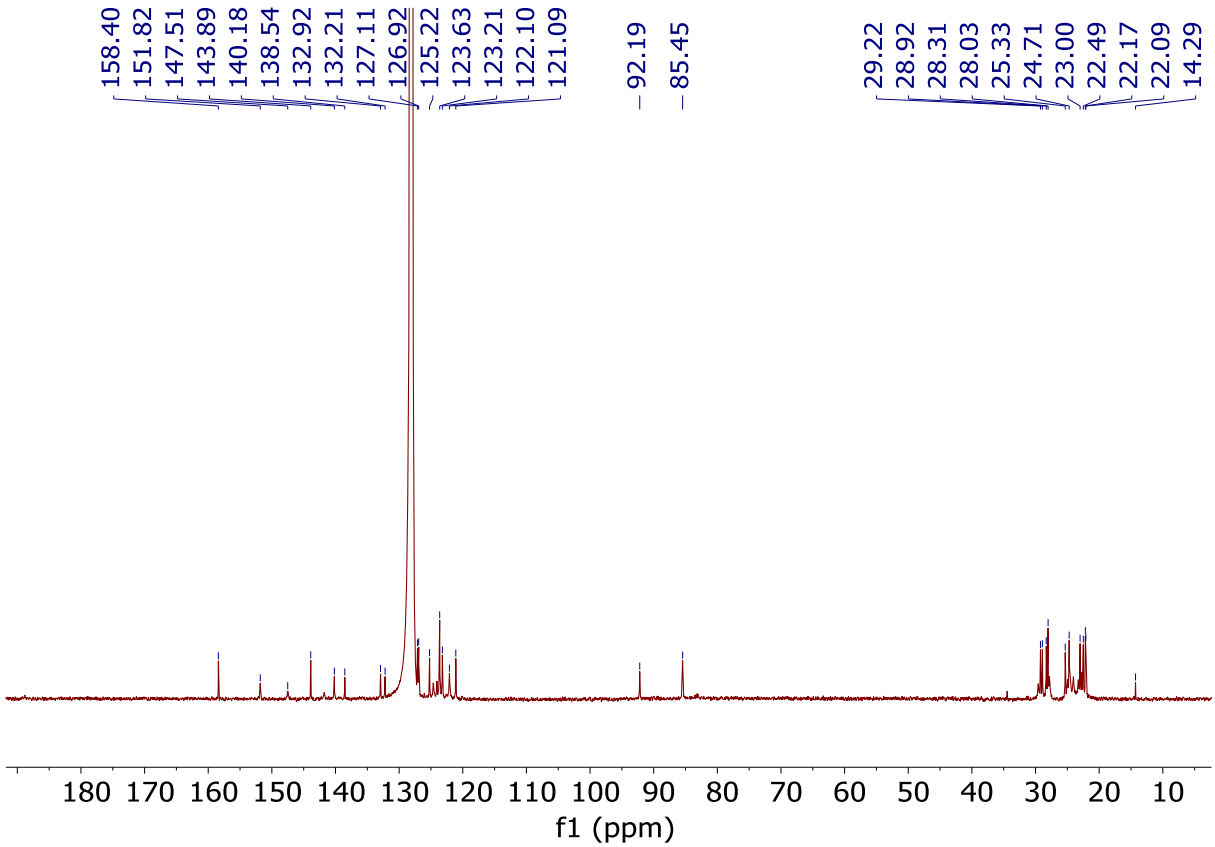

Figure S11. ^{13}C NMR spectrum of W(NAr)(Ar'NH)($ArNH_2$)(OR_{F9}) (151 MHz, 298K) in C_6D_6.

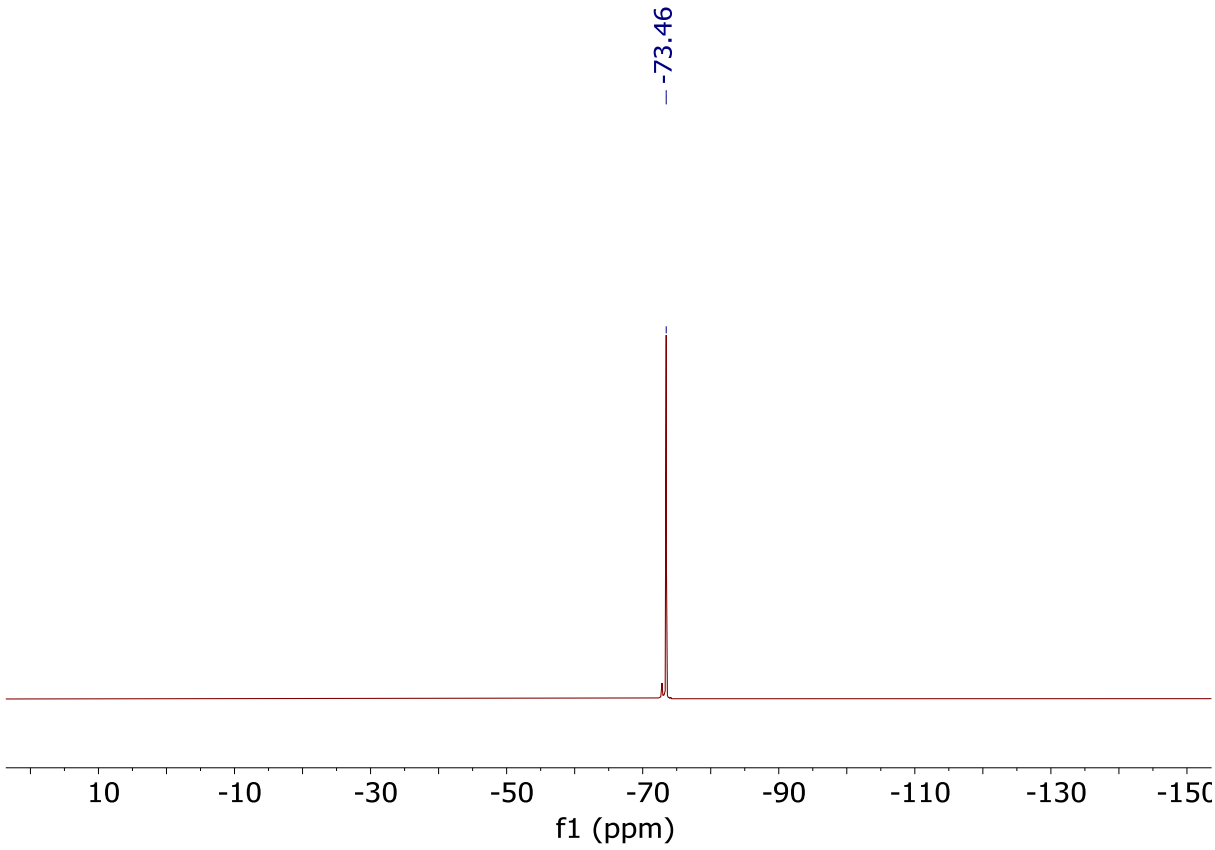

Figure S12. ^{19}F NMR spectrum of W(NAr)(Ar'NH)($ArNH_2$)(OR_{F9}) (564 MHz, 298K) in C_6D_6.

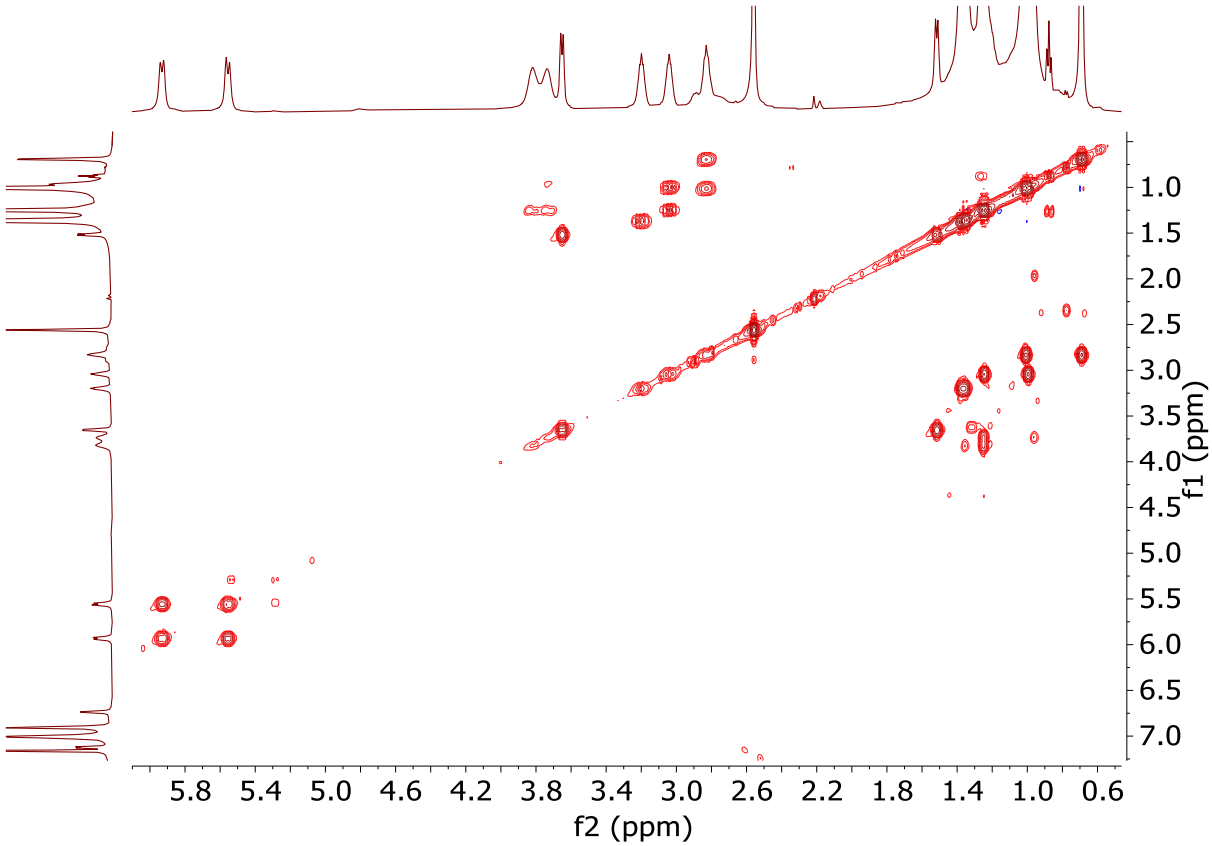

Figure S13. ^{1}H-COSY spectrum W(NAr)(Ar'NH)($ArNH_2$)(OR_{F9}) (600 MHz, 298K) in C_6D_6.

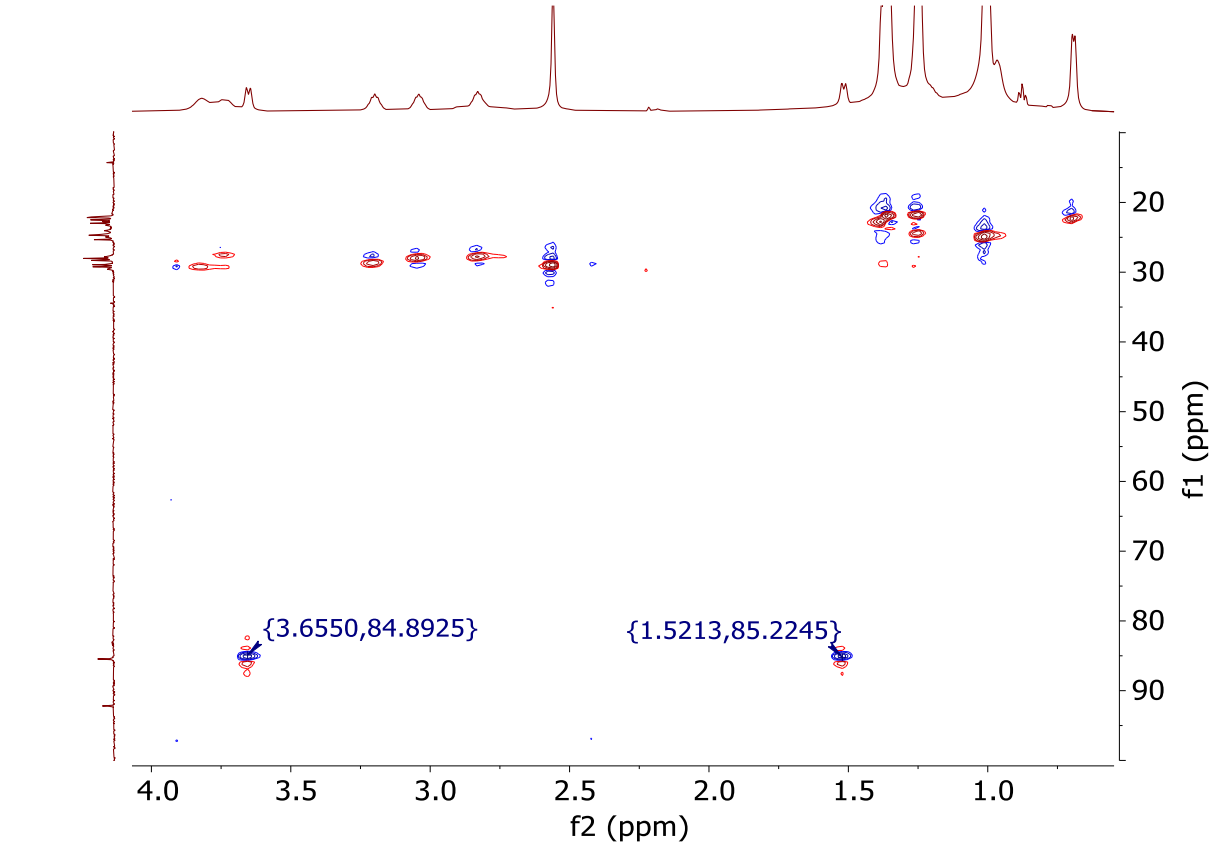

Figure S14. The Aliphatic area of HSQC{ ^{1}H;^{13}C} spectrum of W(NAr)(Ar'NH)($ArNH_2$)(OR_{F9}) (600 MHz, 298K) in C_6D_6.

W(NAr)(OR$_{F6}$)$_2$(C$_2$H$_4$)(ArNH$_2$). **^{1}H NMR** (600 MHz, C$_6$D$_6$, 298K): δ 7.06 (d, *J* = 7.6 Hz, 2H), 6.98 – 6.95 (m, 3H), 6.91 (t, *J* = 7.6 Hz, 1H), 3.61 (sept, *J* = 6.9 Hz, 2H), 3.22 (br s, 2H, ArNH$_2$), 3.20 – 3.14 (m, 2H), 2.64 (sept, *J* = 6.8 Hz, 2H), 2.35 – 2.26 (m, 2H), 1.33 (s, 6H), 1.17 (d, *J* = 6.9 Hz, 12H), 1.14 (d, *J* = 6.8 Hz, 12H). **^{13}C NMR** (151 MHz, C$_6$D$_6$, 298K): δ 152.10, 145.82, 140.64, 132.39, 123.14, 122.96, 119.05, 83.62, 83.42, 83.23, 52.92, 28.75, 28.16, 23.54, 22.60, 18.25. **^{19}F NMR** (282 MHz, C$_6$D$_6$, 298K): δ –77.14, –77.32.

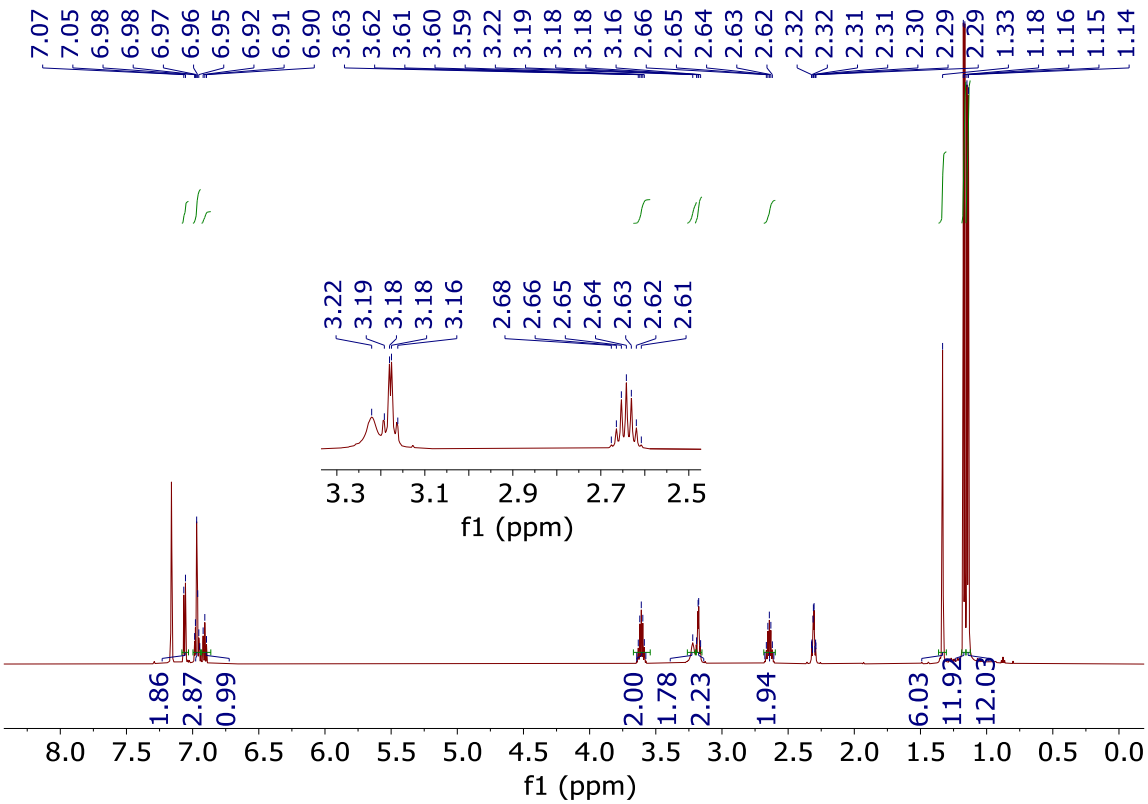

Figure S15. ^{1}H NMR spectrum of W(NAr)(OR$_{F6}$)$_2$(C$_2$H$_4$)(ArNH$_2$) (600 MHz, 298K) in C$_6$D$_6$.

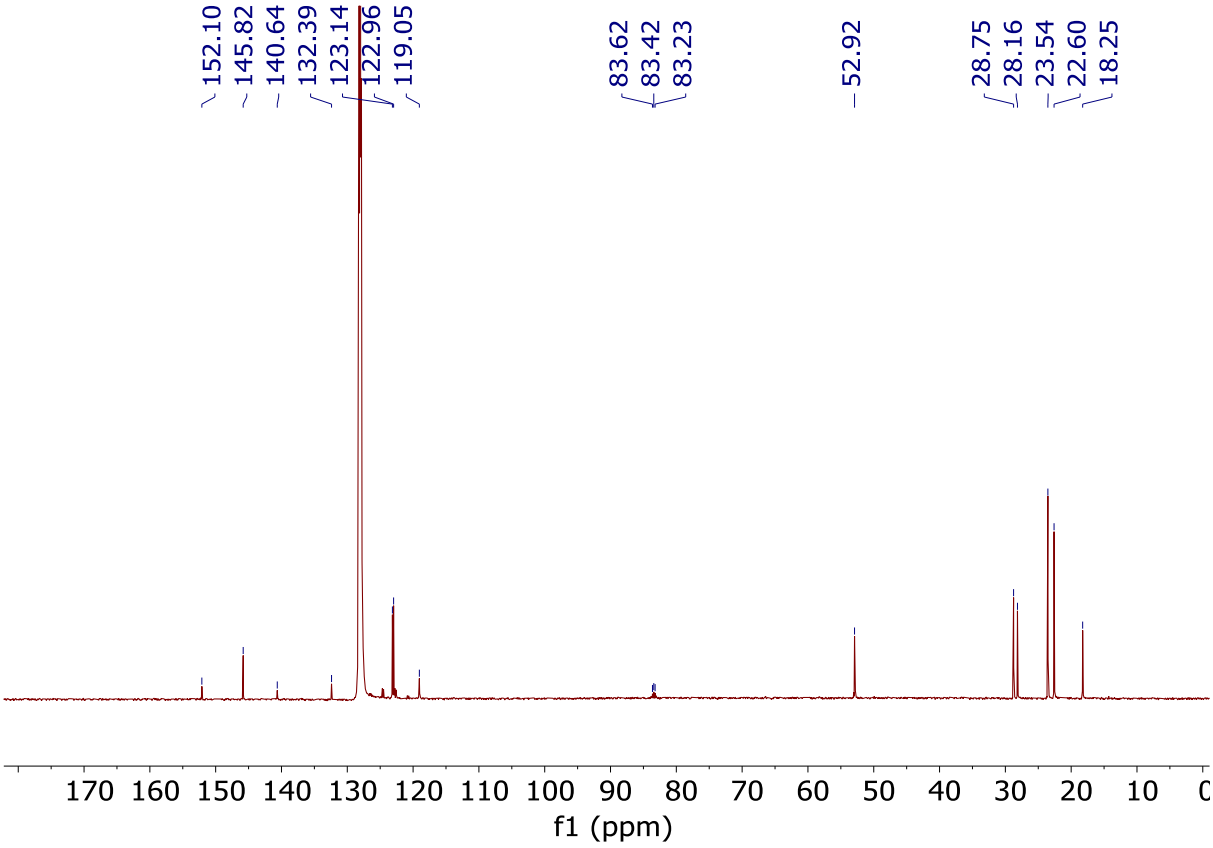

Figure S16. ^{13}C NMR spectrum of $W(NAr)(OR_{F6})_2(C_2H_4)(ArNH_2)$ (151 MHz, 298K) in C_6D_6.

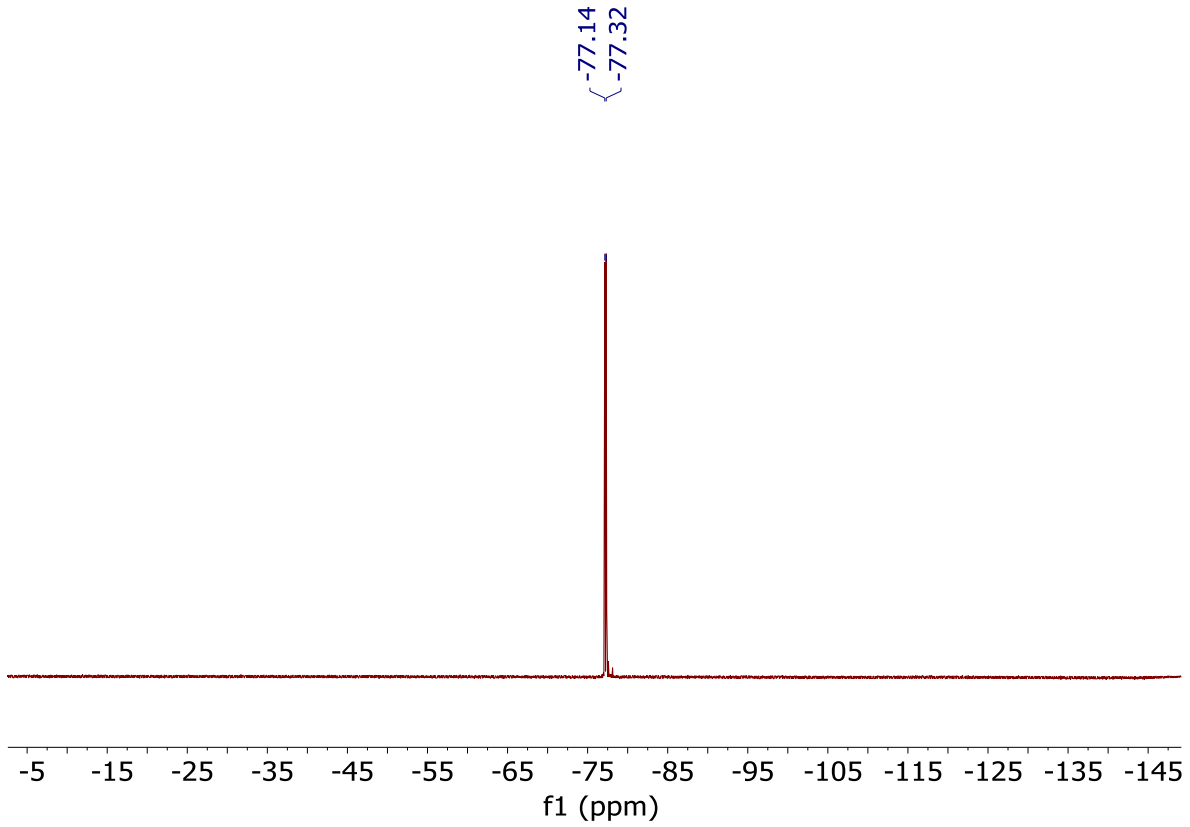

Figure S17. ^{19}F NMR spectrum of $W(NAr)(OR_{F6})_2(C_2H_4)(ArNH_2)$ (282 MHz, 298K) in C_6D_6.

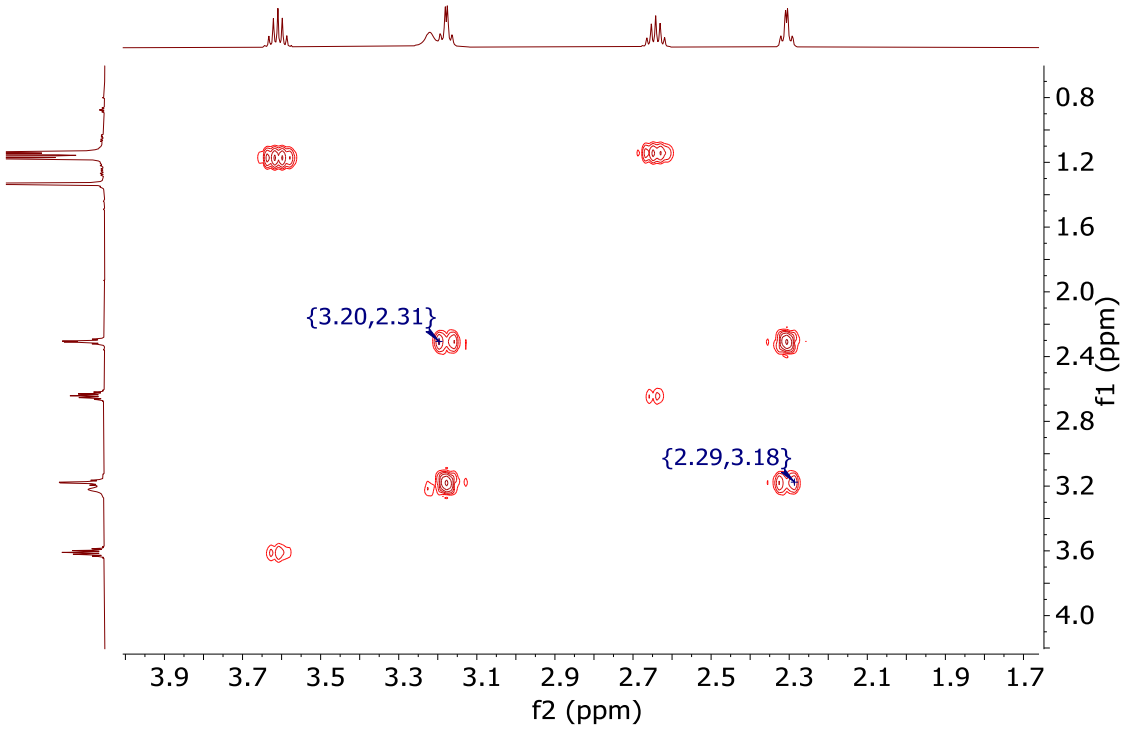

Figure S18. ^{1}H-COSY spectrum W(NAr)(OR_{F6})$_2$(C_2H_4)($ArNH_2$) (600 MHz, 298K) in C_6D_6.

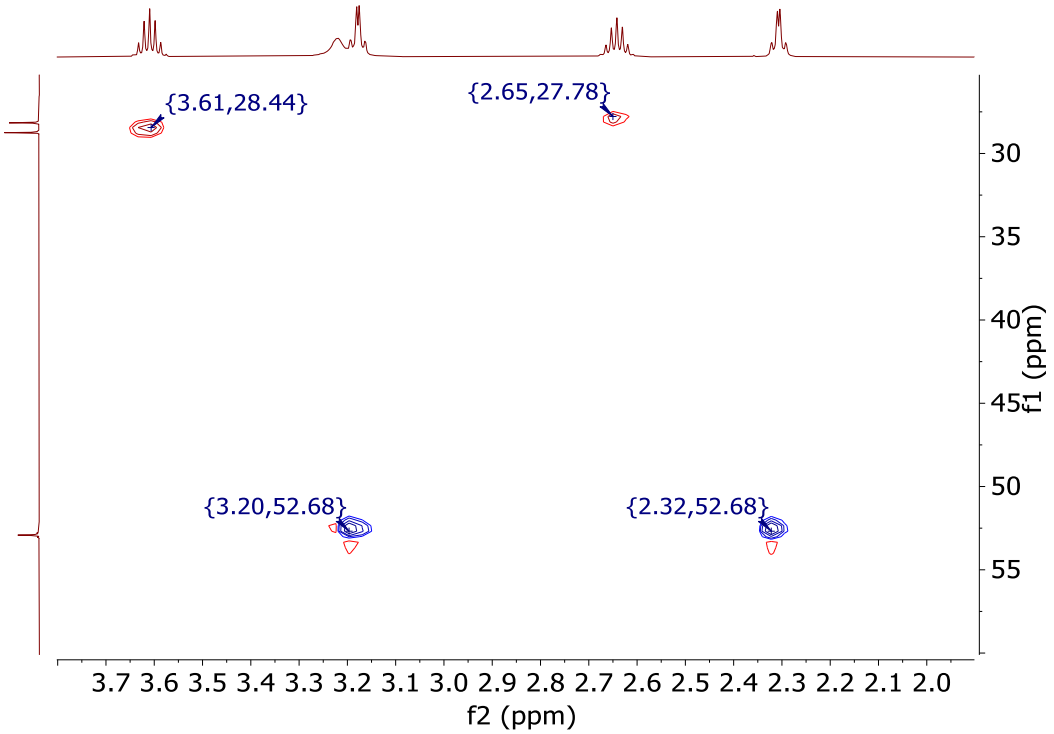

Figure S19. The aliphatic area of an HSQC{ ^{1}H;^{13}C} spectrum of W(NAr)(OR_{F6})$_2$(C_2H_4)($ArNH_2$) (600 MHz, 298K) in C_6D_6.

W(NAr)(OR$_{F3}$)$_2$(C$_2$H$_4$)(ArNH$_2$). **^{1}H NMR** (300 MHz, C$_6$D$_6$, 298K): δ 7.17 – 7.11 (m, 5H), 7.0 (t, *J* = 7.6 Hz, 1H), 3.85 (sept, *J* = 6.9 Hz, 2H), 3.30 (brs, 2H), 3.13 – 3.07 (m, 2H), 2.76 (sept, *J* = 6.7 Hz, 2H), 2.21 – 2.14 (m, 2H), 1.39 (s, 12H), 1.32 (d, *J* = 6.9 Hz, 12H), 1.25 (d, *J* = 6.8 Hz, 12H). **^{13}C NMR** (75 MHz, C$_6$D$_6$, 298K): δ 152.38, 146.62, 144.93, 142.71, 140.69, 132.39, 126.56, 123.14, 122.87, 122.50, 119.01, 82.22, 81.83, 81.44, 69.08, 48.71, 35.36, 28.62, 28.19, 24.51, 24.45, 23.62, 22.61. **^{19}F NMR** (282 MHz, C$_6$D$_6$, 298K): δ –81.9.

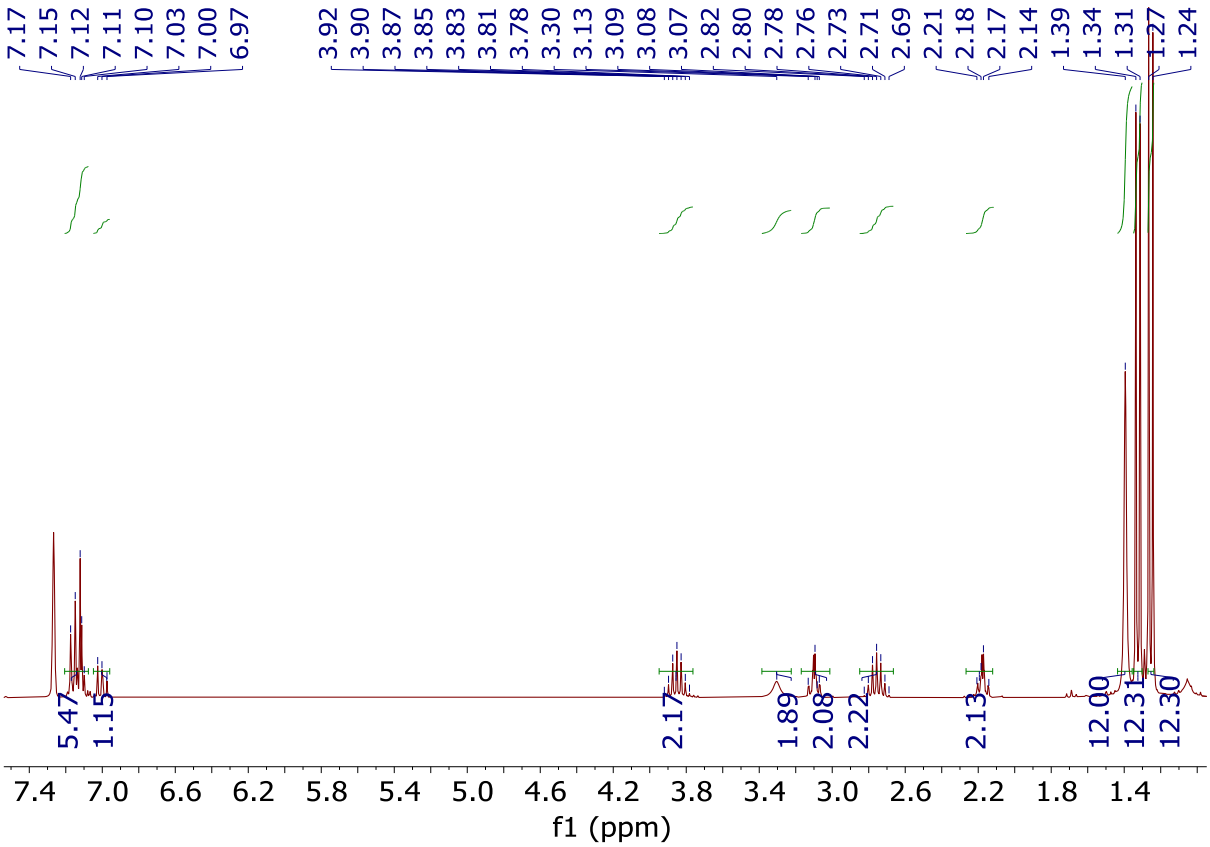

Figure S20. ^{1}H NMR spectrum of W(NAr)(OR$_{F3}$)$_2$(C$_2$H$_4$)(ArNH$_2$) (300 MHz, 298K) in C$_6$D$_6$.

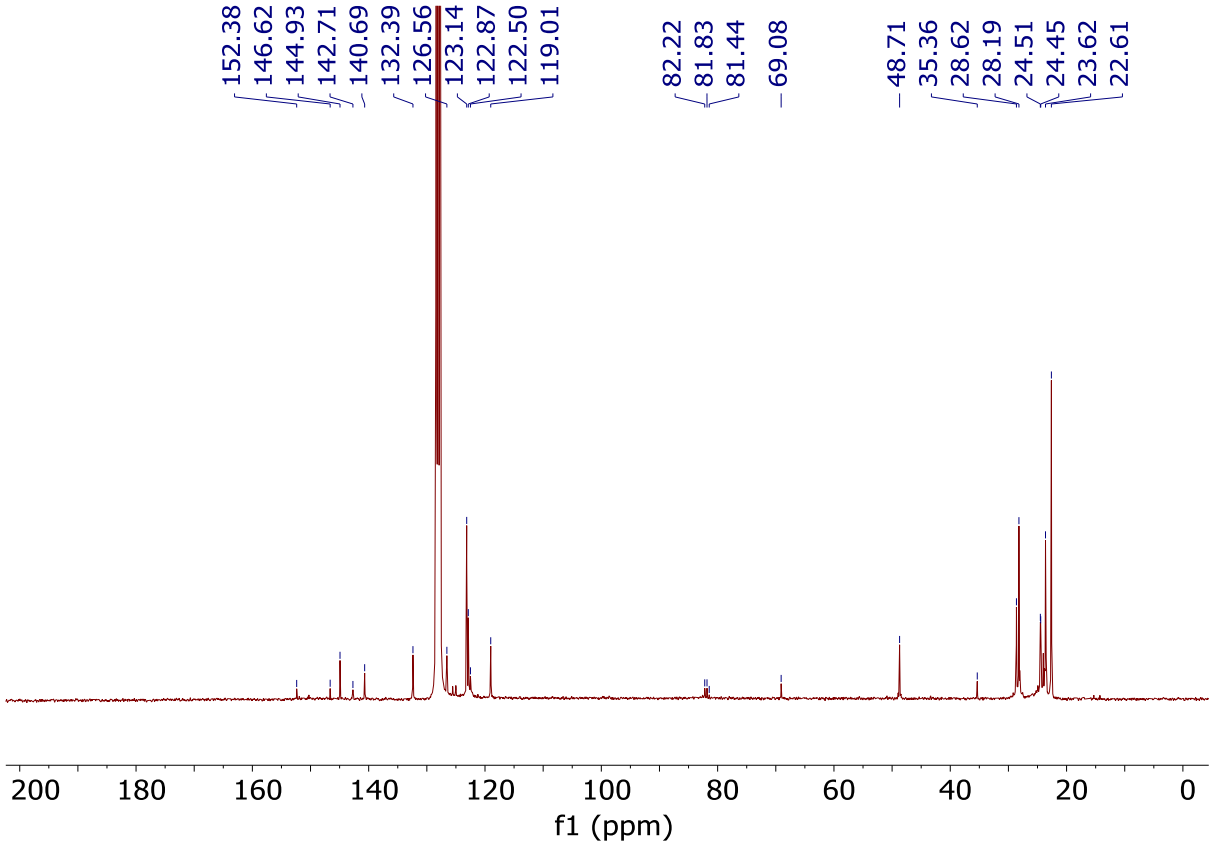

Figure S21. ^{13}C NMR spectrum of $W(NAr)(OR_{F3})_2(C_2H_4)(ArNH_2)$ (75 MHz, 298K) in C_6D_6.

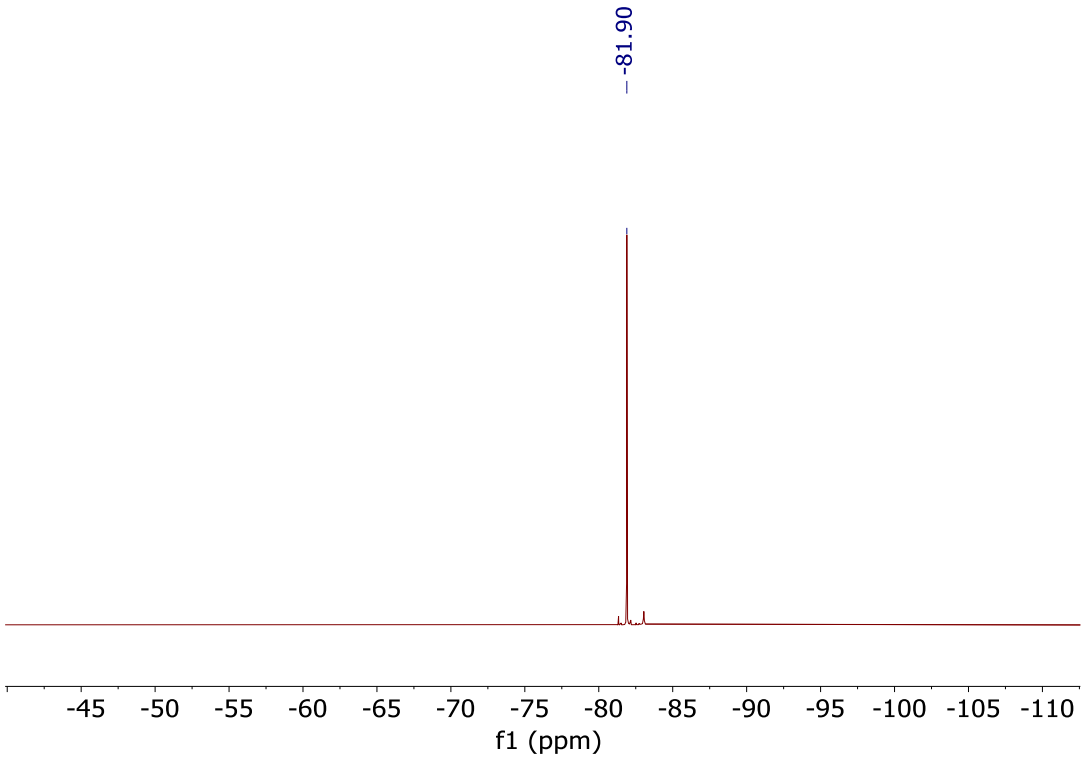

Figure S22. ^{19}F NMR spectrum of $W(NAr)(OR_{F3})_2(C_2H_4)(ArNH_2)$ (282 MHz, 298K) in C_6D_6.

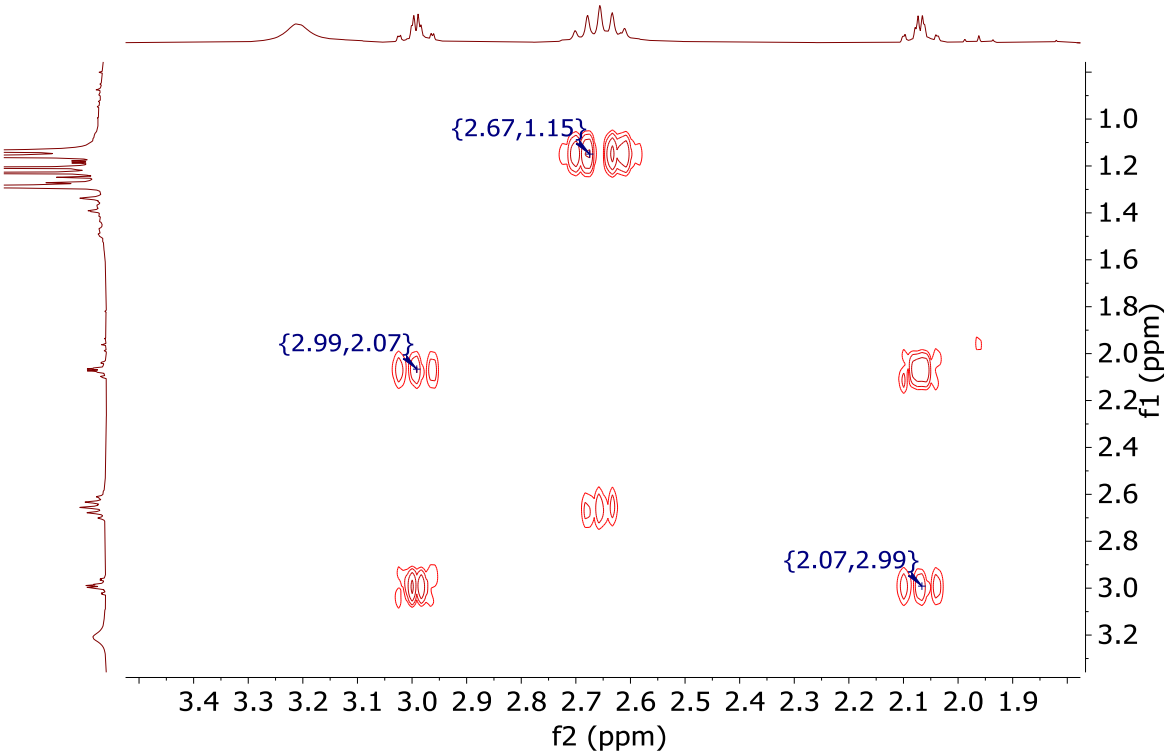

Figure S23. ^{1}H-COSY spectrum W(NAr)(OR_{F3})$_2$(C_2H_4)($ArNH_2$) (300 MHz, 298K) in C_6D_6.

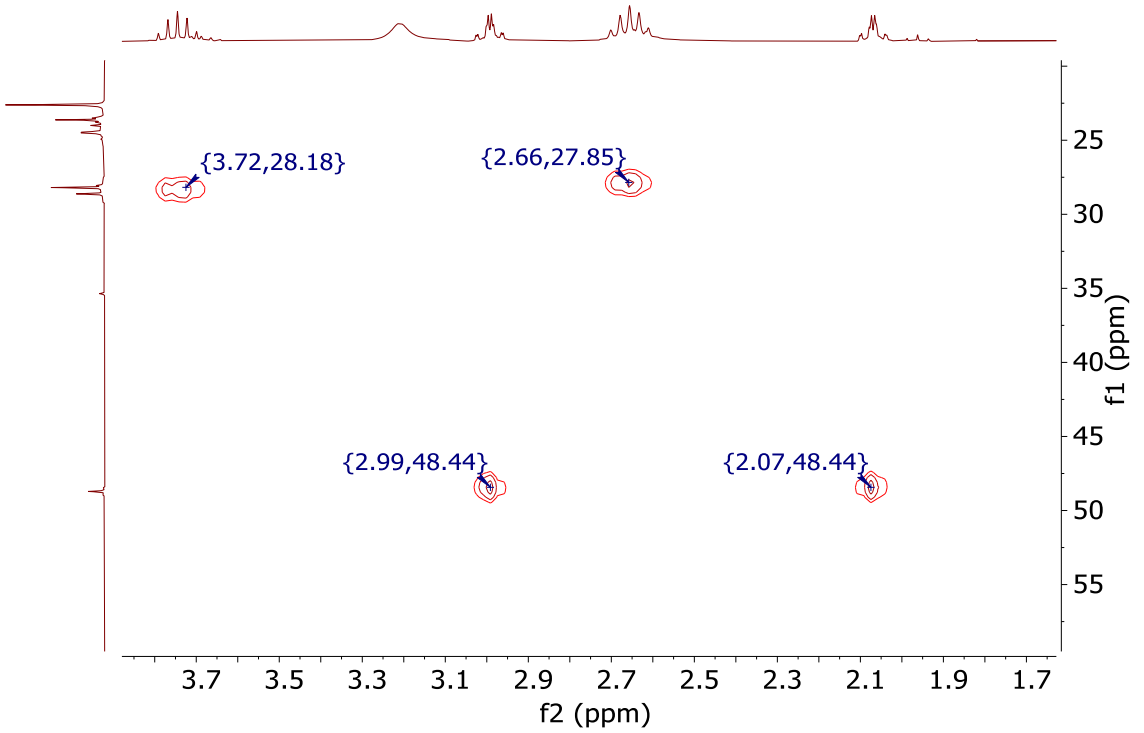

Figure S24. The Aliphatic area of HSQC{ ^{1}H;^{13}C} spectrum of W(NAr)(OR_{F3})$_2$(C_2H_4)($ArNH_2$) (300 MHz, 298K) in C_6D_6.

W(NAr)(py)[(μ-NAr')(μ-HNAr'')]W(NAr)(OR$_{F9}$)

^{1}H NMR (600 MHz, C_6D_6) δ 9.03 (d, *J* = 5.6 Hz, 2H), 7.32 (d, *J* = 7.7 Hz, 2H), 7.23 (d, *J* = 7.6 Hz, 1H), 7.12 (t, *J* = 7.7 Hz, 2H), 7.09 – 7.06 (m, 3H), 7.02 (t, *J* = 7.7 Hz, 1H), 6.81 (t, *J* = 7.6 Hz, 1H), 6.78 (t, *J* = 7.4 Hz, 1H), 6.58 (d, *J* = 8.0 Hz, 1H), 6.50 (d, *J* = 7.3 Hz, 1H), 6.46 (t, *J* = 6.8 Hz, 2H), 4.37 (sept, *J* = 6.8 Hz, 1H), 4.09 (s, 1H), 3.69 (sept, *J* = 6.7 Hz, 2H), 3.63 (s, 3H), 3.45 (sept, *J* = 6.8 Hz, 2H), 3.17 (d, *J* = 5.3 Hz, 1H), 3.08 (sept, *J* = 6.8 Hz, 1H), 2.62 (s, 3H), 2.31 (d, *J* = 5.3 Hz, 1H), 1.55 (d, *J* = 6.8 Hz, 3H), 1.51 (d, *J* = 6.8 Hz, 3H), 1.46 (d, *J* = 6.6 Hz, 3H), 1.41 (d, *J* = 6.6 Hz, 3H), 1.32 (d, *J* = 6.8 Hz, 3H), 1.27 (d, *J* = 6.9 Hz, 3H), 1.14 – 1.09 (m, 18H). **^{13}C NMR** (151 MHz, C_6D_6, 298K): δ 301.05, 158.04, 156.57, 152.90, 151.77, 150.45, 149.59, 149.06, 148.45, 148.19, 147.44, 144.73, 140.46, 138.51, 125.11, 124.21, 122.75, 121.90, 120.43, 120.38, 115.38, 77.37, 65.52, 63.73, 31.27, 30.88, 30.44, 28.78, 26.93, 26.48, 26.34, 26.24, 22.42, 21.48, 15.19. **^{19}F NMR** (282 MHz, C_6D_6, 298K): δ –73.42.

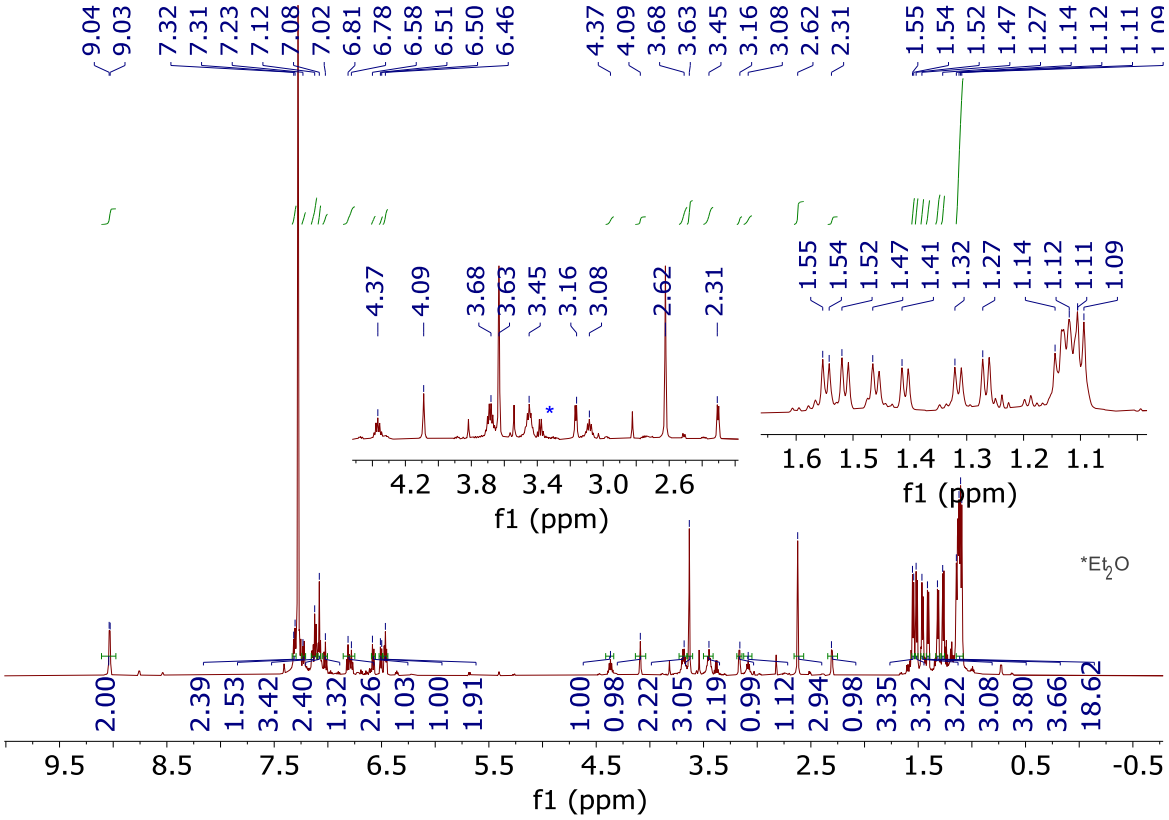

Figure S25. ^{1}H NMR spectrum of W(NAr)(py)[(μ-NAr')(μ-NHAr'')]W(NAr)(OR$_{F9}$) (600 MHz, 298K) in C_6D_6.

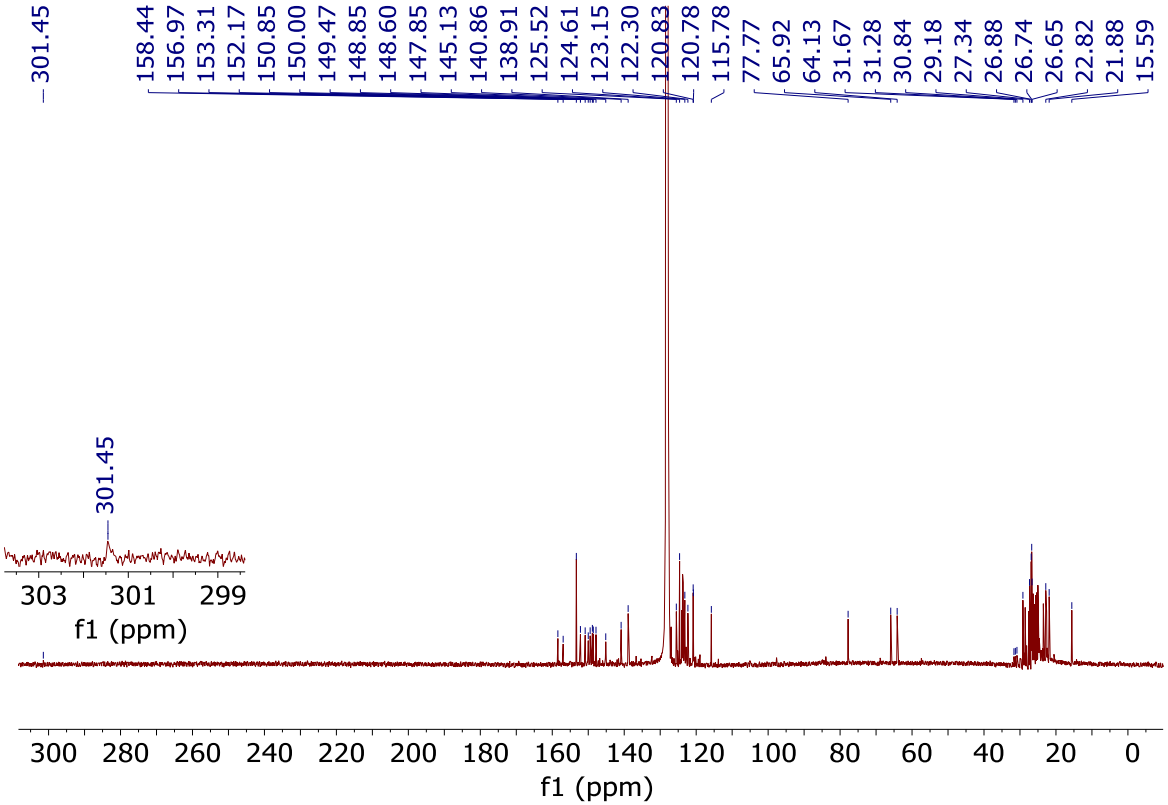

Figure S26. ^{13}C NMR spectrum of W(NAr)(py)[(μ-NAr')(μ-NHAr'')]W(NAr)(OR_{F9}) (151 MHz, 298K) in C_6D_6.

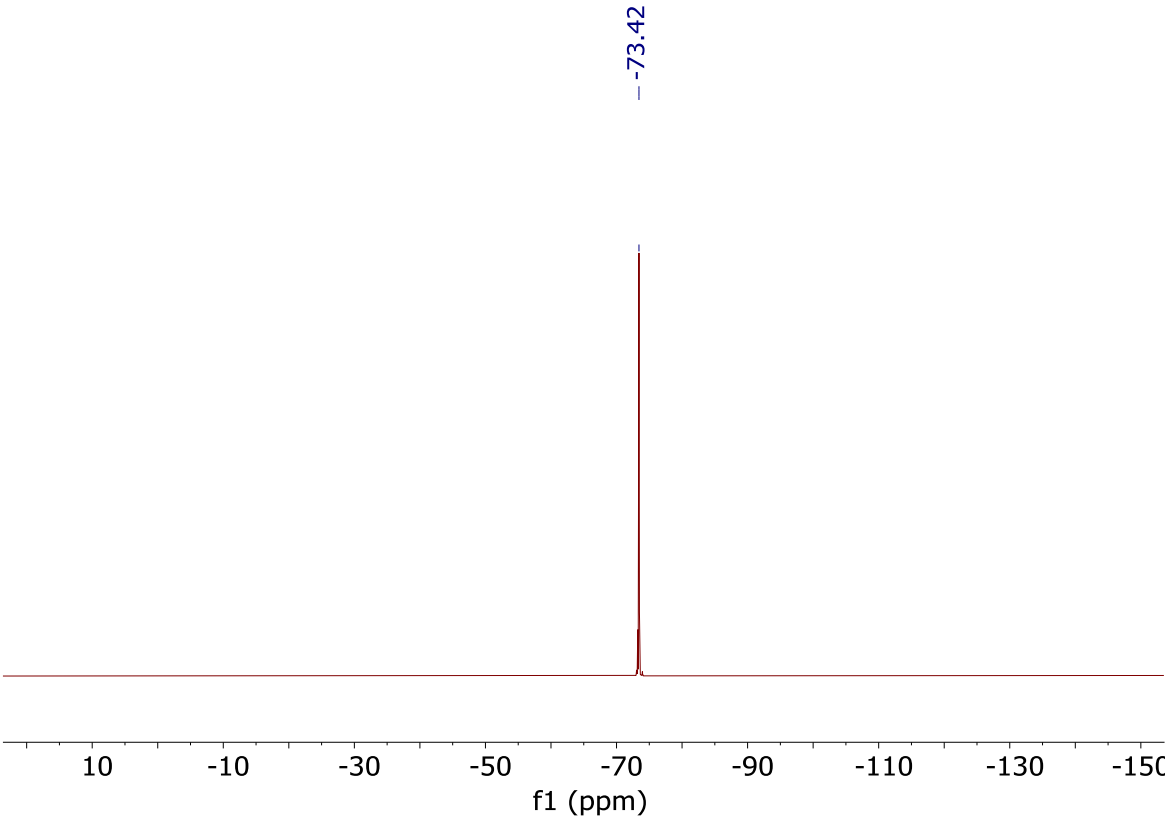

Figure S27. ^{19}F NMR spectrum of W(NAr)(py)[(μ-NAr')(μ-NHAr'')]W(NAr)(OR_{F9}) (564 MHz, 298K) in C_6D_6.

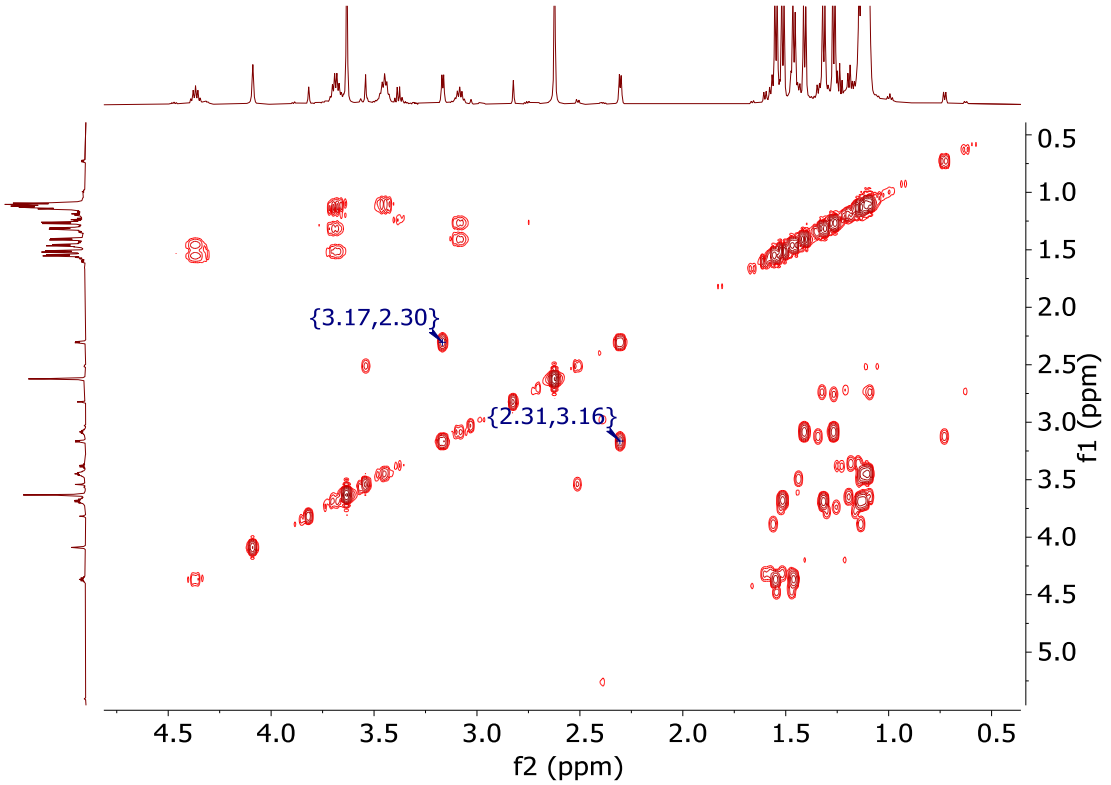

Figure S28. ^{1}H-COSY spectrum W(NAr)(py)[(μ-NAr')(μ-NHAr")]W(NAr)(OR_{F9}) (600 MHz, 298K) in C_6D_6.

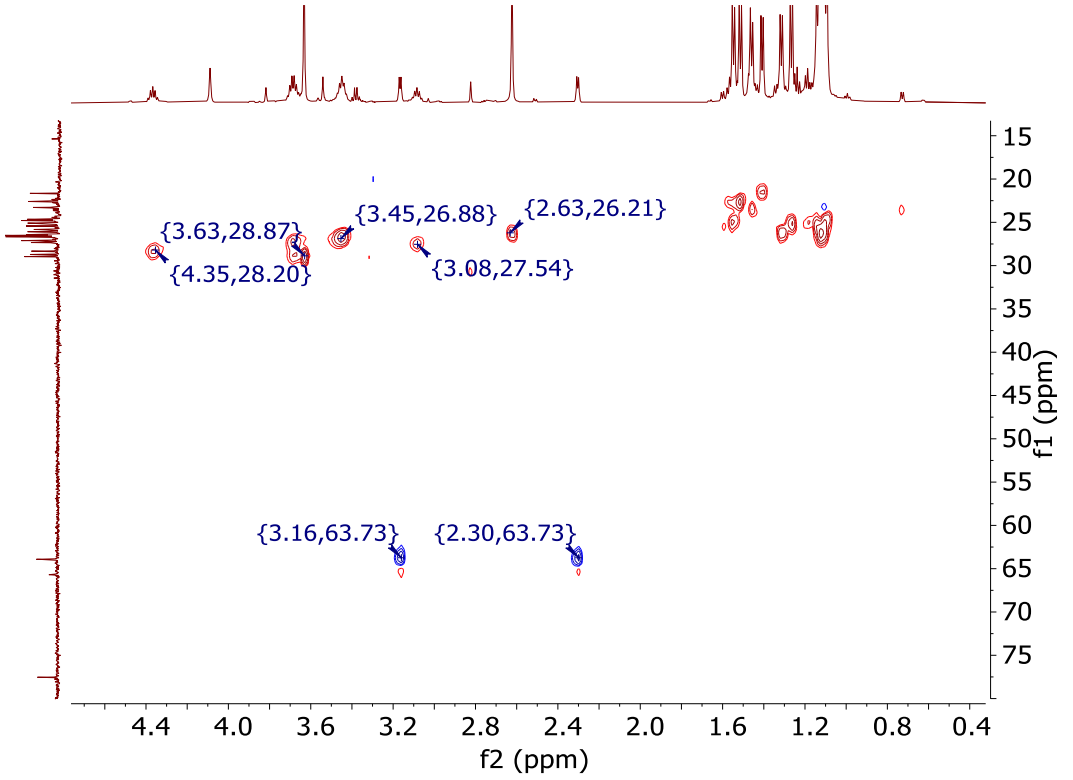

Figure S29. The Aliphatic area of HSQC{^{1}H;^{13}C} spectrum of W(NAr)(py)[(μ-NAr')(μ-NHAr")]W(NAr)(OR_{F9}) (600 MHz, 298K) in C_6D_6.

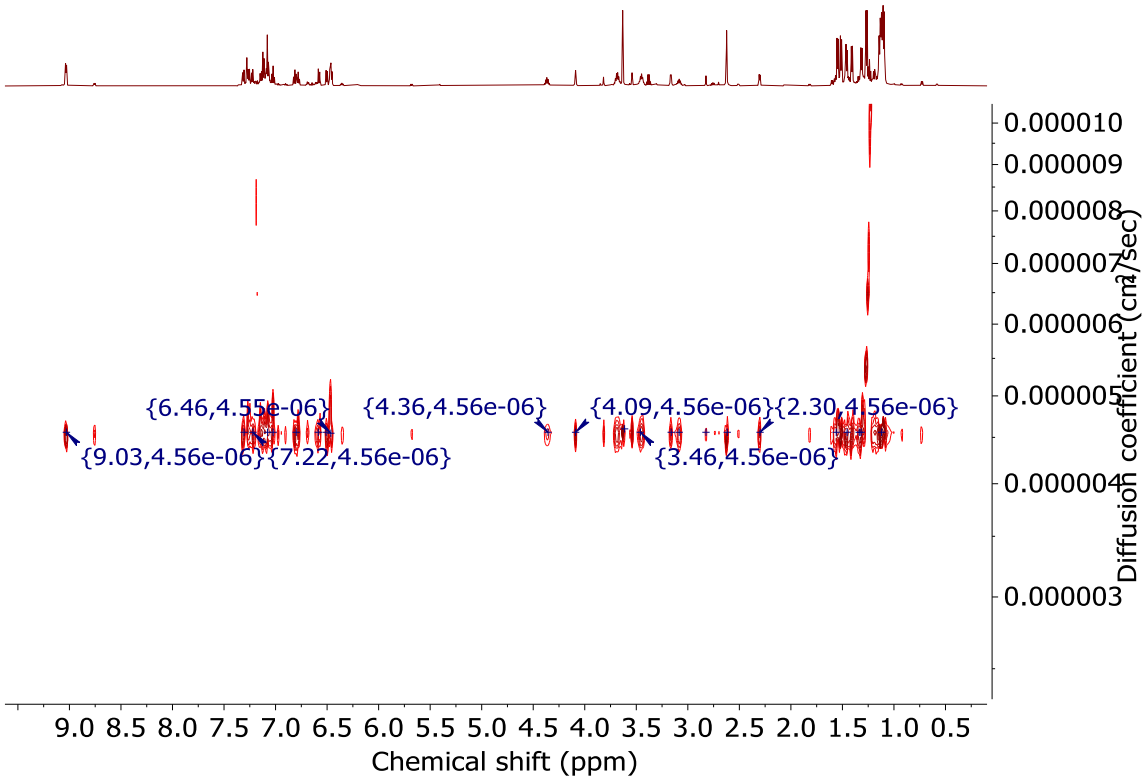

Figure S30. The DOSY spectrum of W(NAr)(py)[(μ-NAr')(μ-NHAr")]W(NAr)(OR_{F9}) (600 MHz, 298K) in C_6D_6.

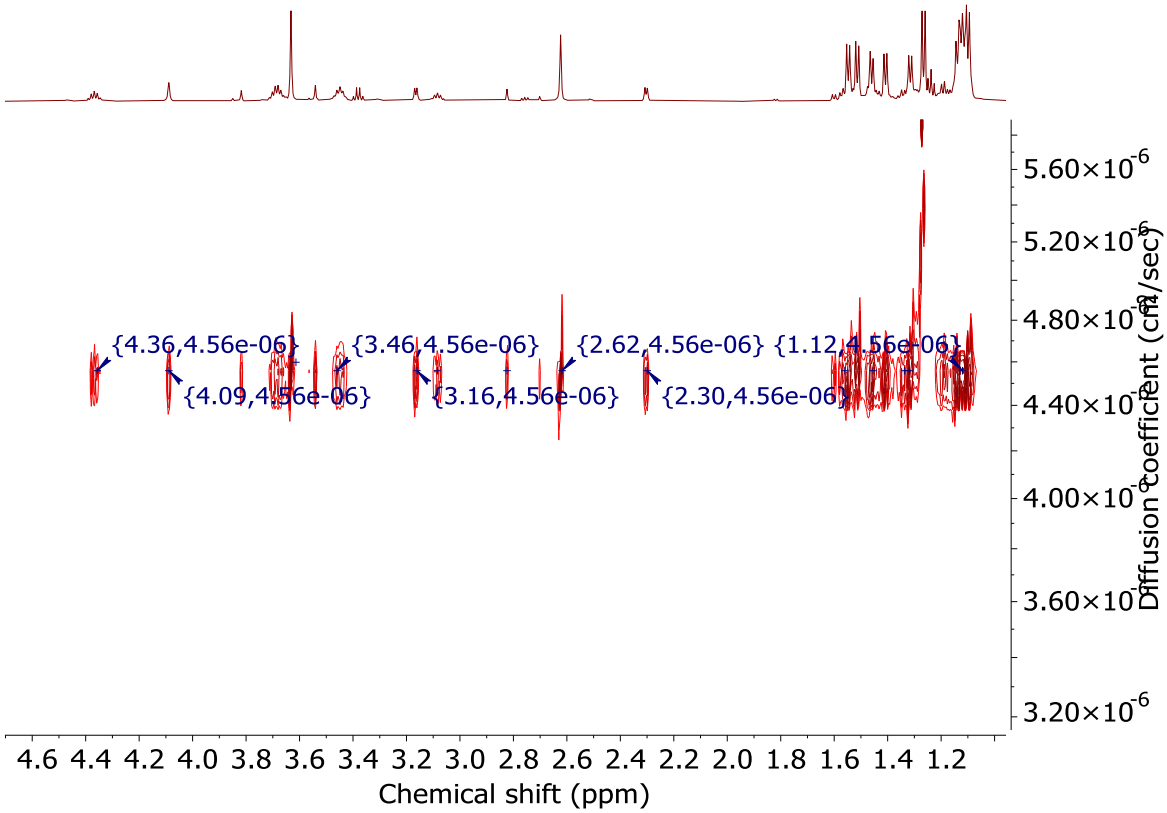

Figure S31. The aliphatic area of a DOSY spectrum of W(NAr)(py)[(μ-NAr')(μ-NHAr")]W(NAr)(OR_{F9}) (600 MHz, 298K) in C_6D_6.

3. Mechanistic Experiments

Solution stability of $W(NAr)(ArNH_2)(OR_{F9})_2(C_2H_4)$

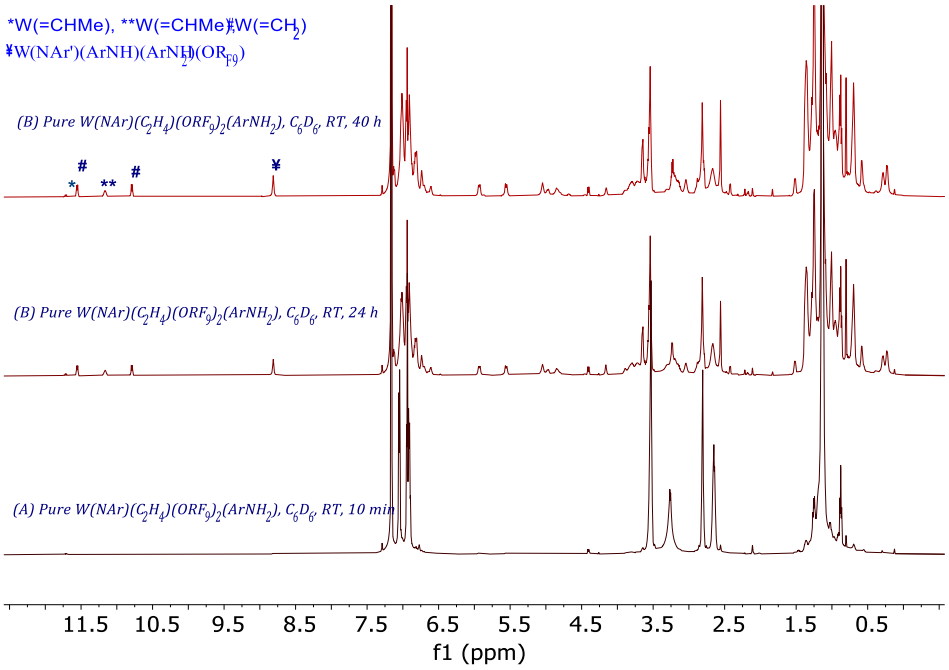

Figure S32. ^{1}H NMR spectra of $W(NAr)(ArNH_2)(OR_{F9})_2(C_2H_4)$ in C_6D_6 after A) 10 min and B) 24 h, and C) 40 h (600 MHz, 298K).

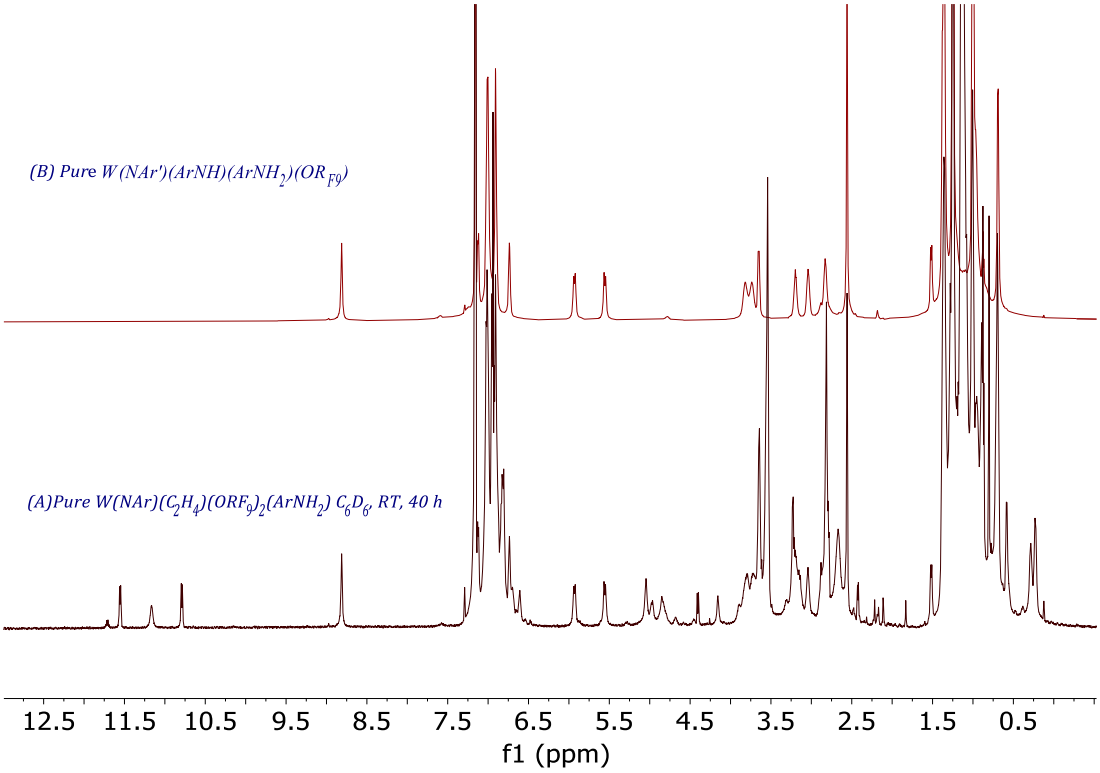

Figure S33. ^{1}H NMR spectra of A) $W(NAr)(ArNH_2)(OR_{F9})_2(C_2H_4)$ in C_6D_6 40 h and B) pure sample of $W(NAr')(ArNH)(ArNH_2)(OR_{F9})$ (600 MHz, 298K).

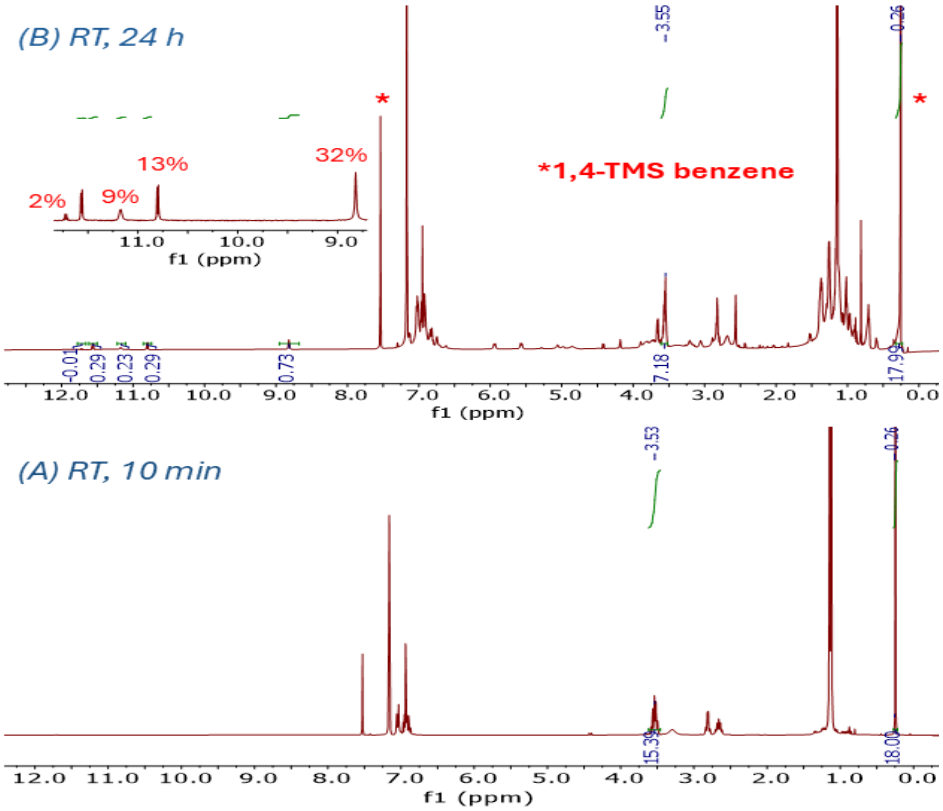

Figure S34. Quantification of the decomposition products in the above reaction mixture using 1,4-TMS benzene as internal standard (600 MHz, 298K).

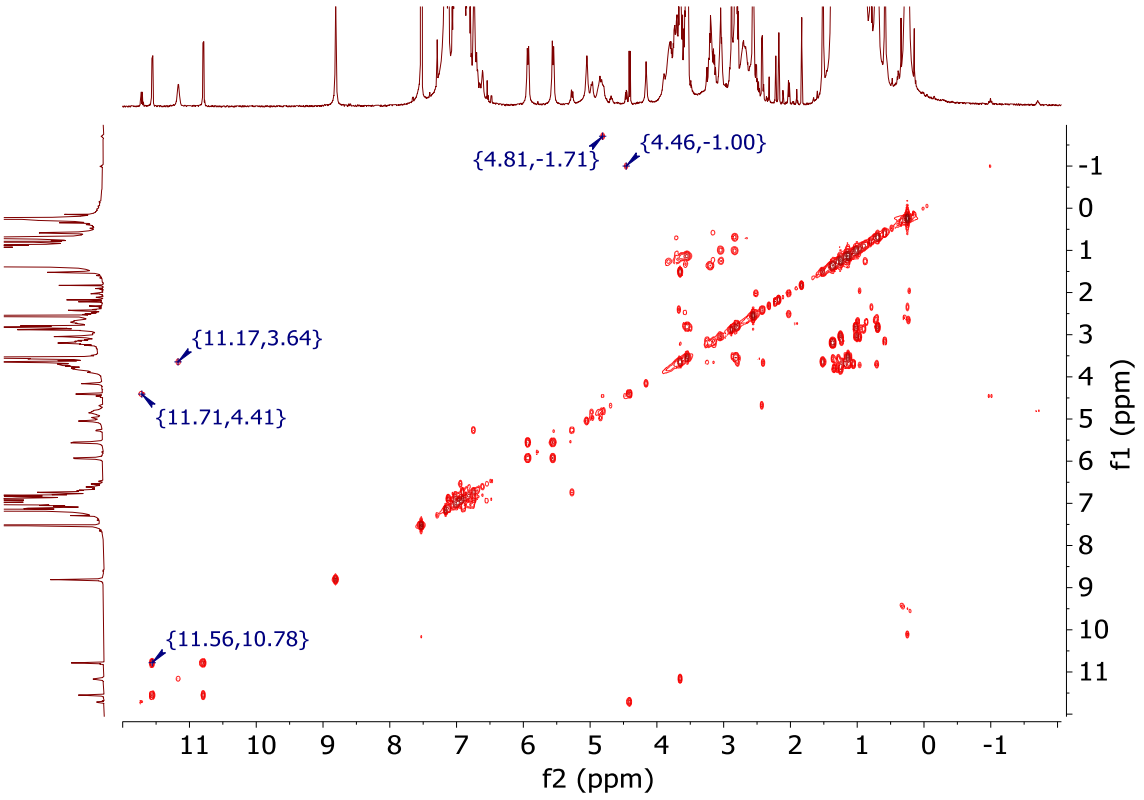

Figure S35. The ^{1}H-COSY spectrum of the above reaction mixture (600 MHz, 298K) in C_6D_6.

Reaction of $W(NAr)(ArNH_2)(OR_{F9})_2(C_2H_4)$ with $B(C_6F_5)_3$

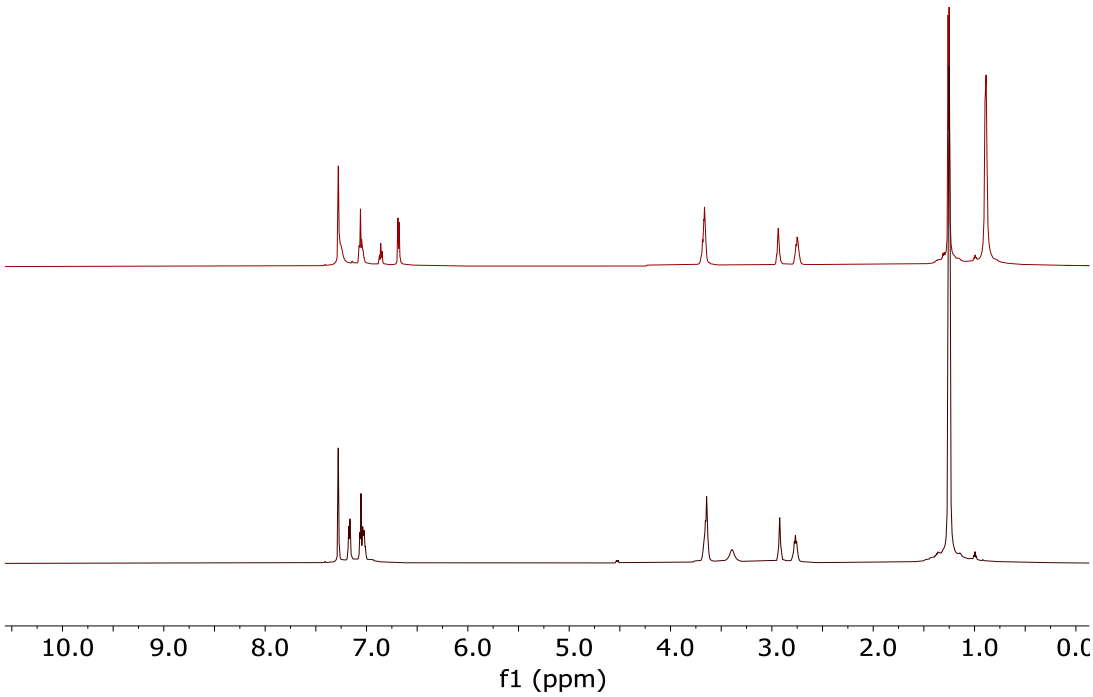

Figure S36. ^{1}H NMR spectra of A) $W(NAr)(ArNH_2)(OR_{F9})_2(C_2H_4)$ and B) 10 min after addition of $B(C_6F_5)_3$ in C_6D_6 (600 MHz, 298K).

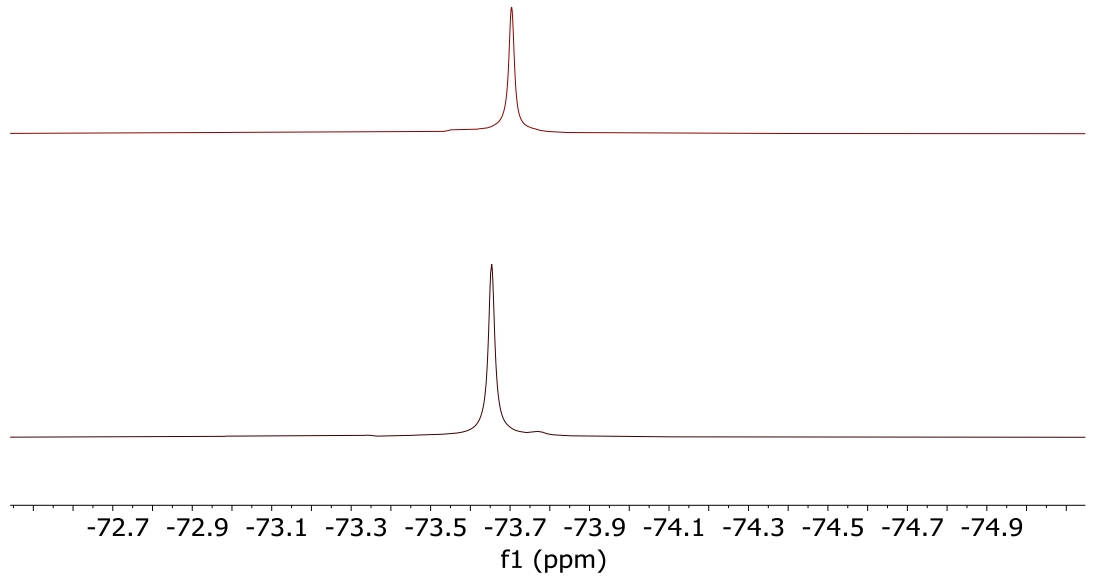

Figure S37. ^{19}F NMR spectra of A) $W(NAr)(ArNH_2)(OR_{F9})_2(C_2H_4)$ and B) 10 min after addition of $B(C_6F_5)_3$ in C_6D_6 (564 MHz, 298K).

Solution stability of $W(NAr)(OR_{F9})_2(C_2H_4)$

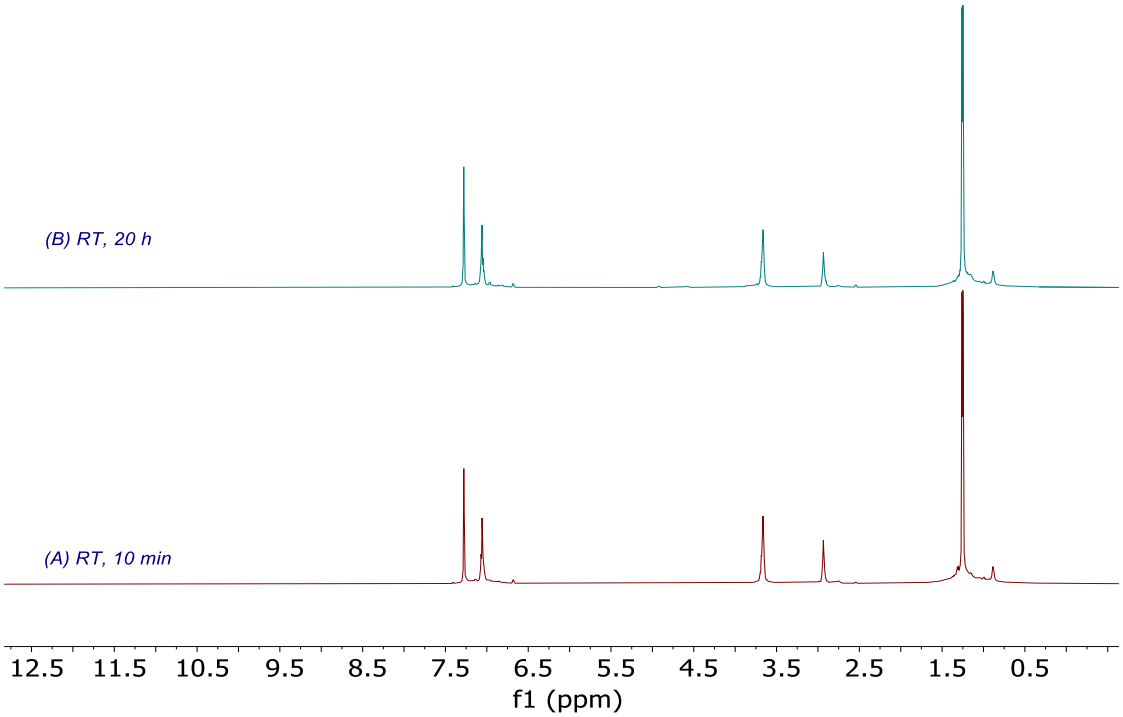

Figure S38. ^{1}H NMR spectra of $W(NAr)(OR_{F9})_2(C_2H_4)$ in C_6D_6 after A) 10 min and B) 20 h (600 MHz, 298K) in C_6D_6.

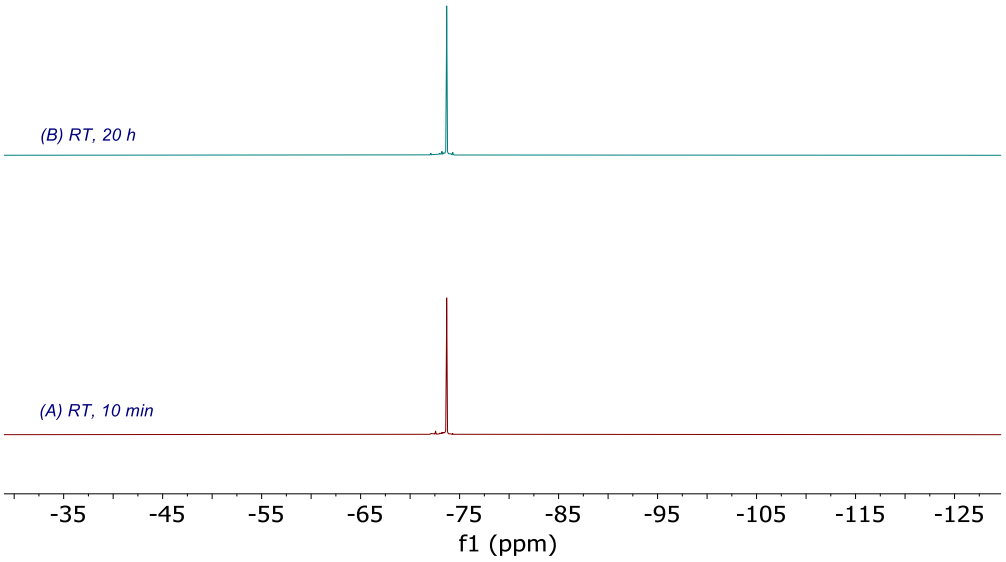

Figure S39. ^{19}F NMR spectra of $W(NAr)(OR_{F9})_2(C_2H_4)$ in C_6D_6 after A) 10 min and B) 20 h (564 MHz, 298K) in C_6D_6.

Reaction of W(NAr)(ArNH$_2$)(OR$_{F9}$)$_2$(C$_2$H$_4$) with ethylene

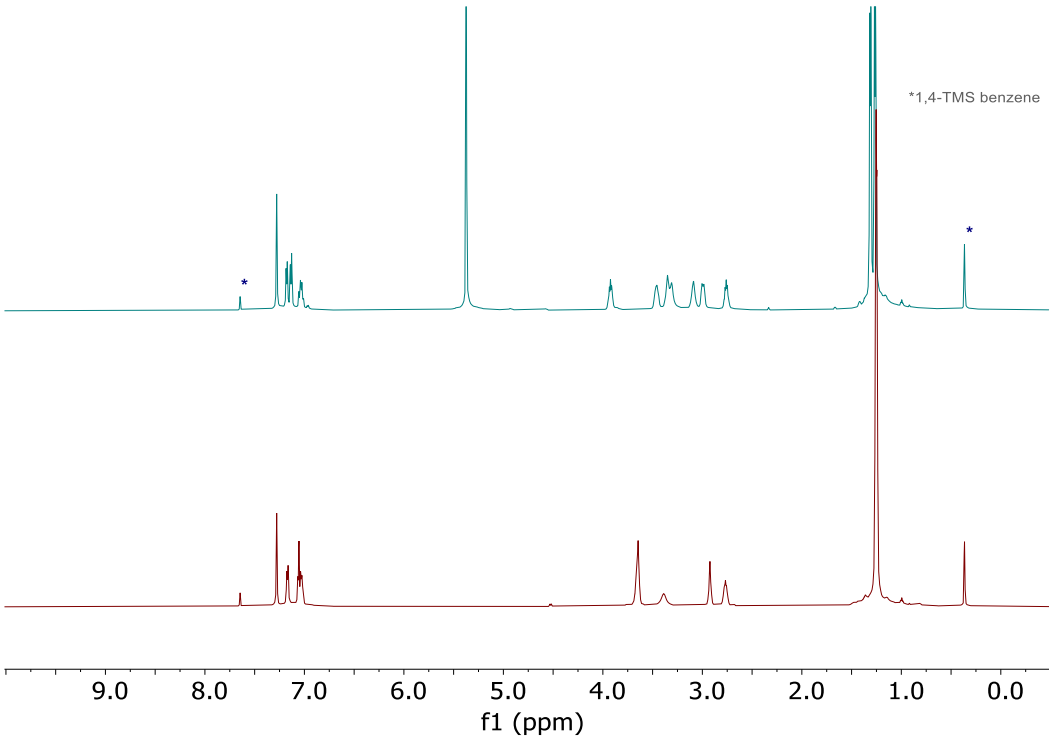

Figure S40. ^{1}H NMR spectra of A) W(NAr)(ArNH$_2$)(OR$_{F9}$)$_2$(C$_2$H$_4$), and B) after 10 min of addition of ethylene (600 MHz, 298K) in C$_6$D$_6$.

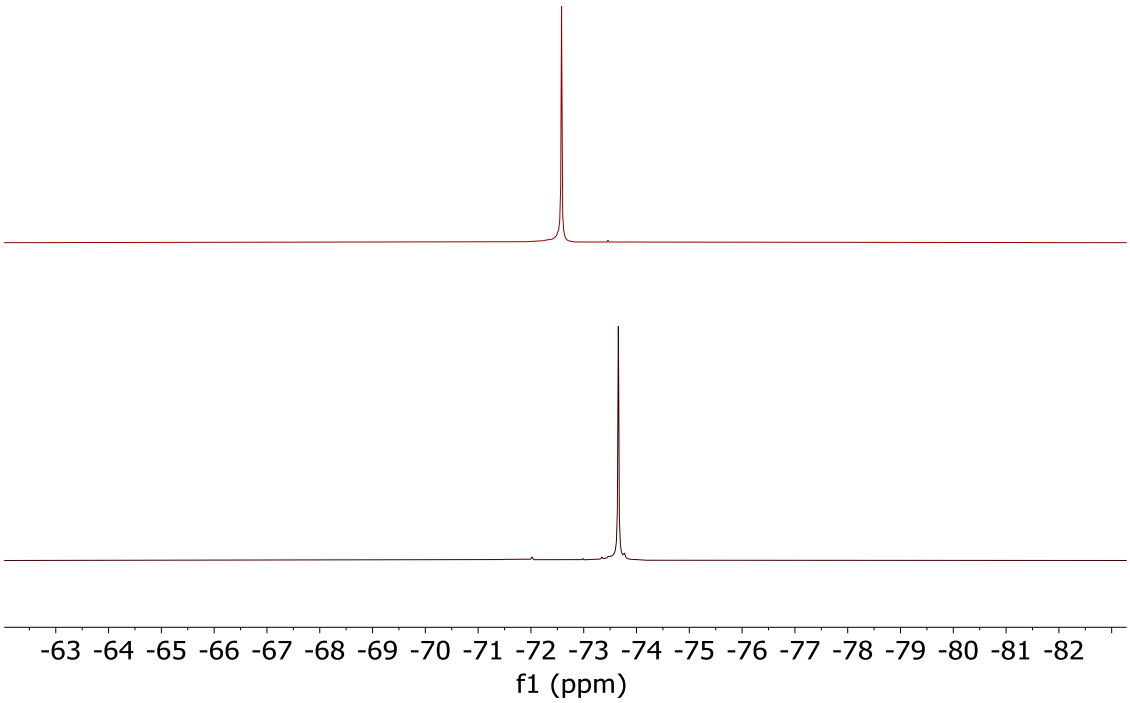

Figure S41. ^{19}F NMR spectra of A) W(NAr)(ArNH$_2$)(OR$_{F9}$)$_2$(C$_2$H$_4$), and B) after 10 min of addition of ethylene (564 MHz, 298K) in C$_6$D$_6$.

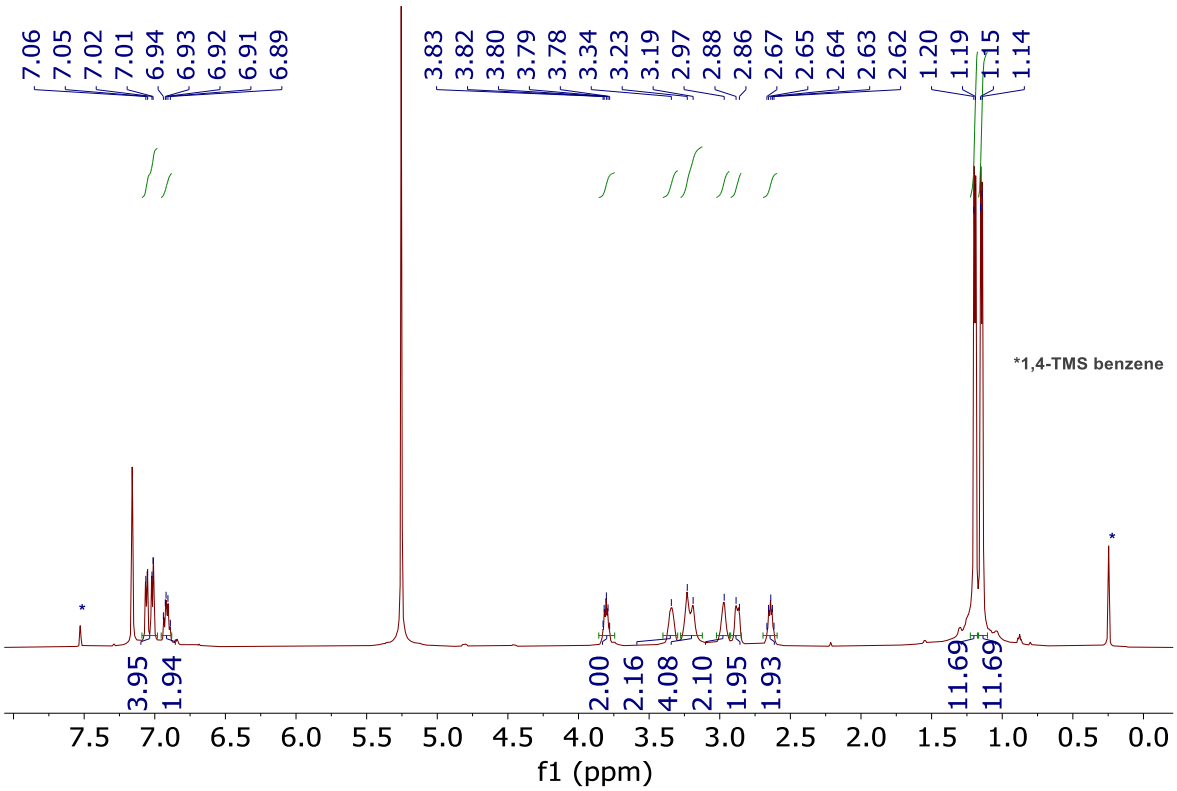

Figure S42. ^{1}H NMR spectra of W(NAr)(ArNH$_2$)(OR$_{F9}$)$_2$(C$_2$H$_4$) after 10 min of addition of ethylene (600 MHz, 298K) in C_6D_6.

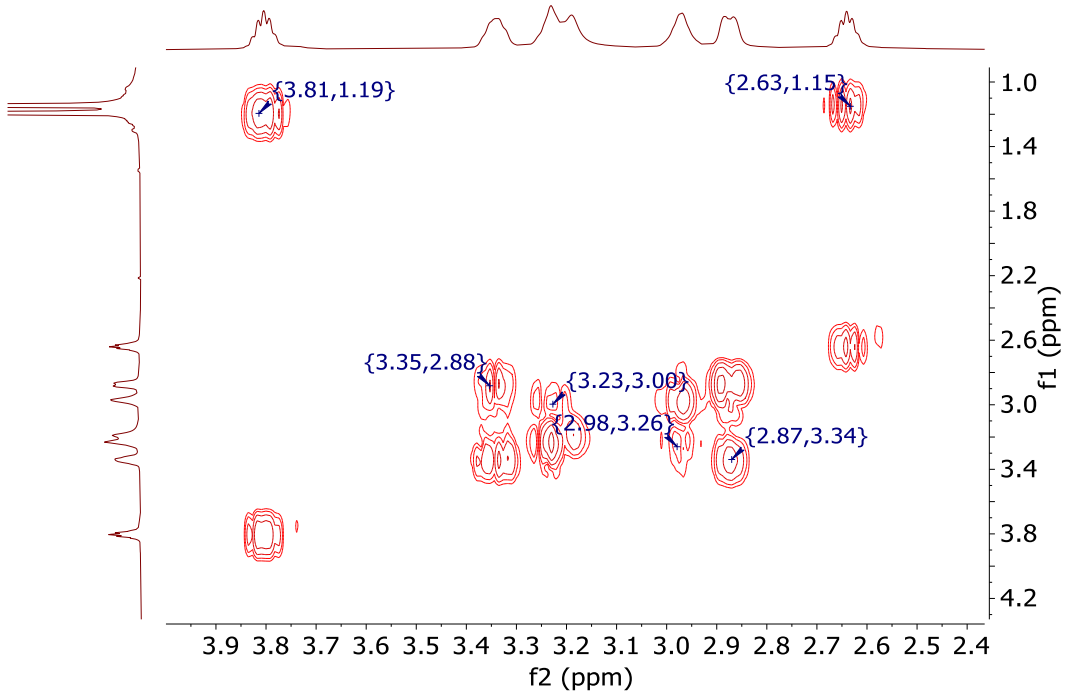

Figure S43. The aliphatic area of COSY spectrum of the above reaction mixture (600 MHz, 298K) in C_6D_6.

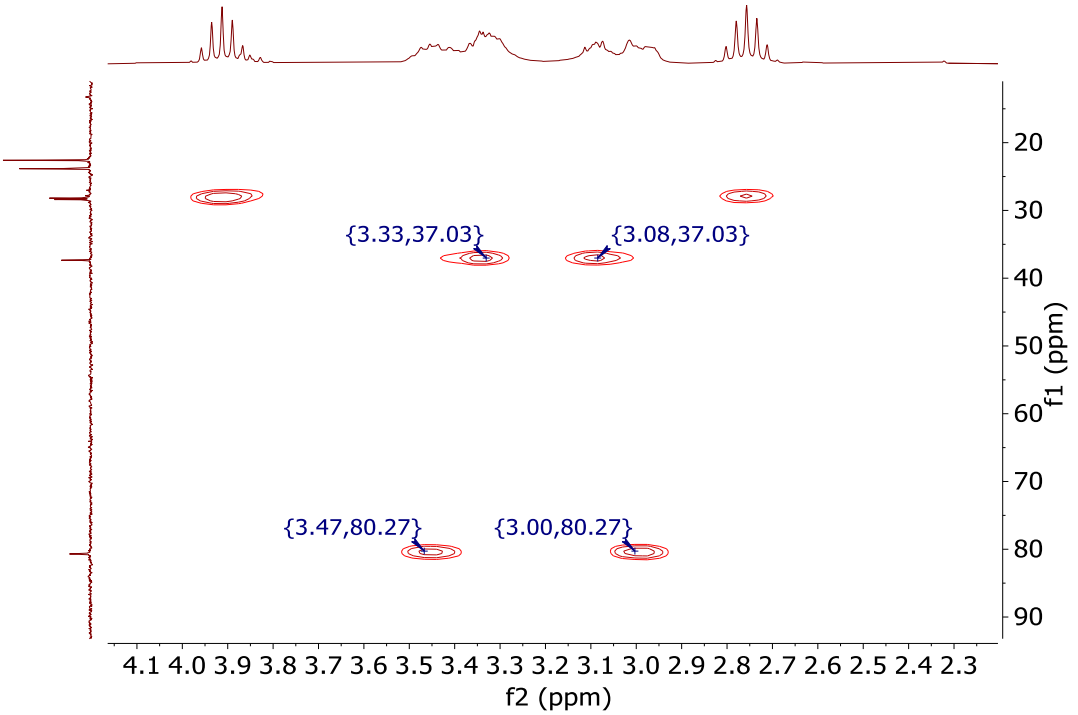

Figure S44. The aliphatic area of HSQC {^{1}H, ^{13}C} spectrum of the above reaction mixture (300 MHz, 298K) in C_6D_6.

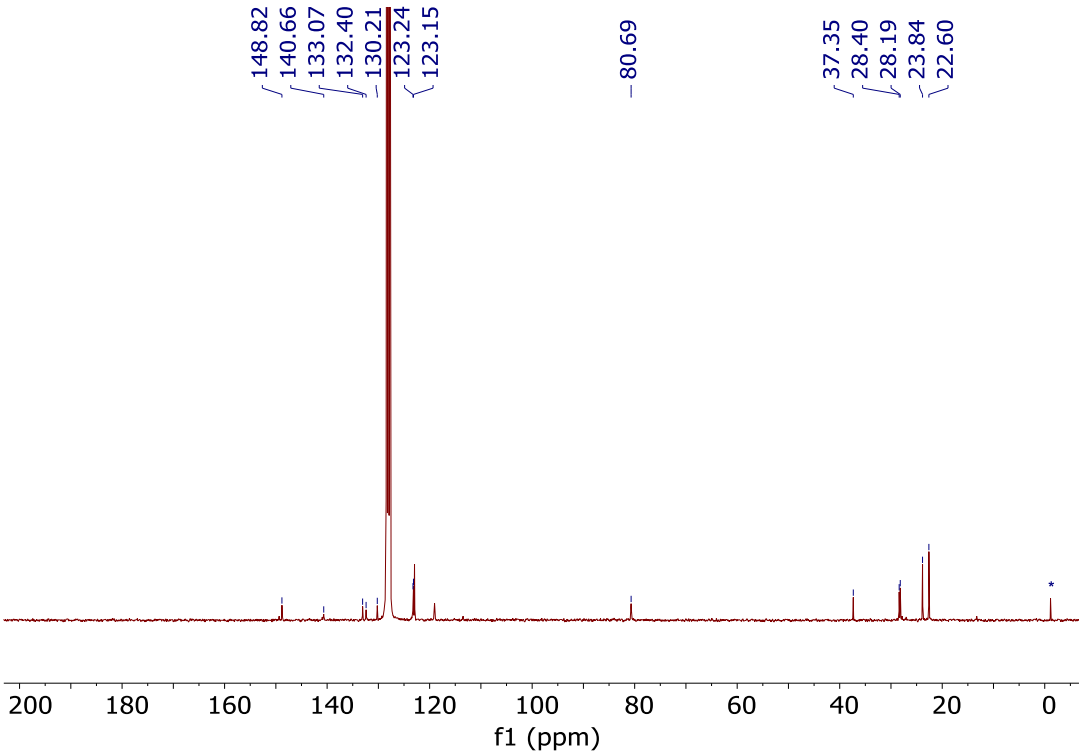

Figure S45. ^{13}C NMR spectrum of the above reaction mixture (75 MHz, 298K) in C_6D_6. *1,4-TMS benzene ($J_{W\text{-}C}$ = 73.8 Hz).

Reaction of $W(NAr)(OR_{F9})_2(C_2H_4)$ with ethylene

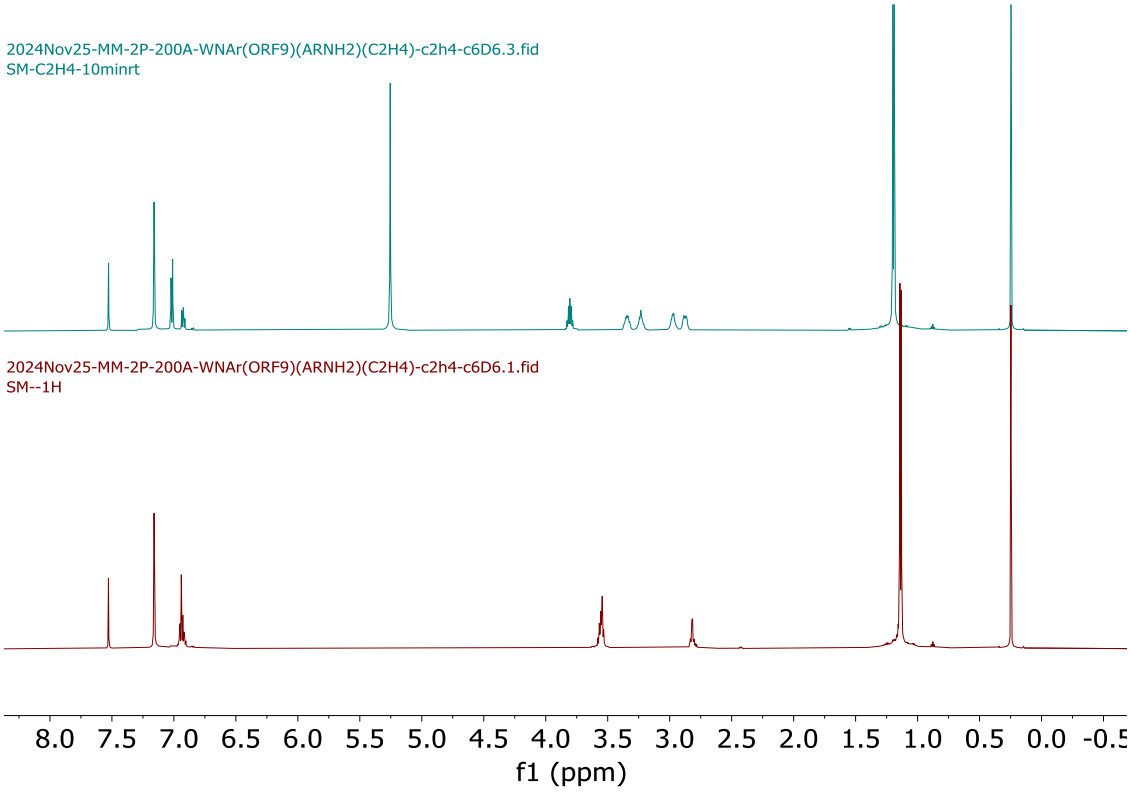

Figure S46. ^{1}H NMR spectra of $W(NAr)(OR_{F9})_2(C_2H_4)$ after 10 min of addition of ethylene (600 MHz, 298K) in C_6D_6.

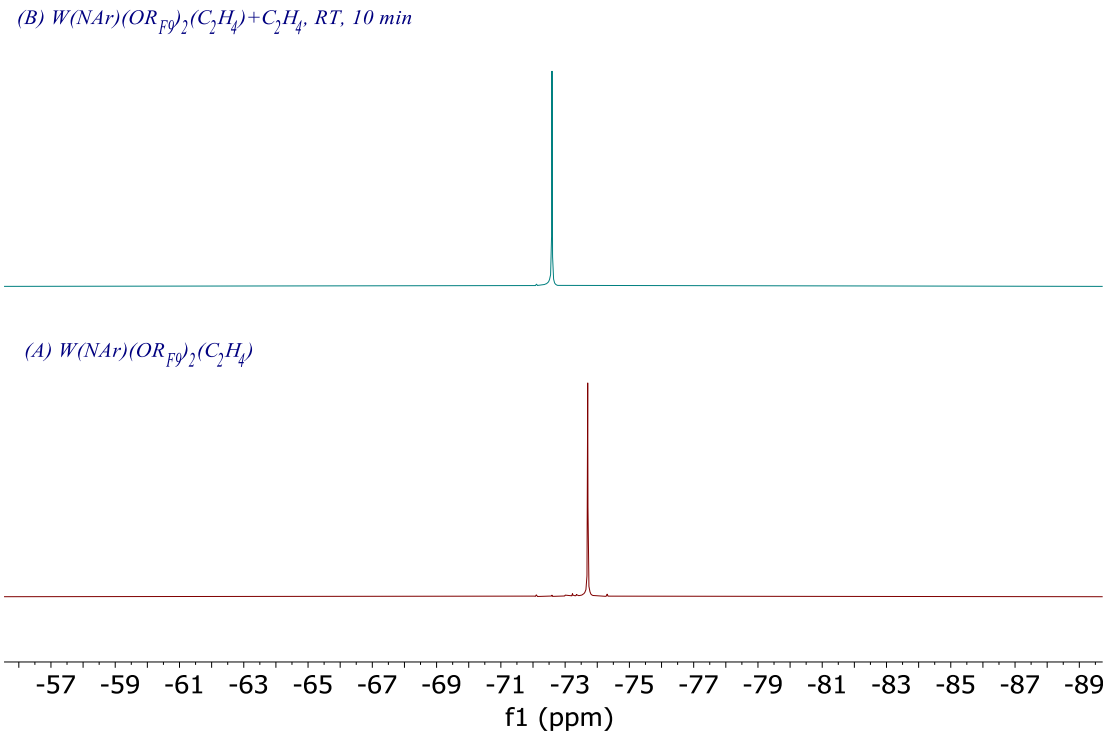

Figure S47. ^{19}F NMR spectra of A) $W(NAr)(OR_{F9})_2(C_2H_4)$**,** and B) after 10 min of addition of ethylene (564 MHz, 298K) in C_6D_6.

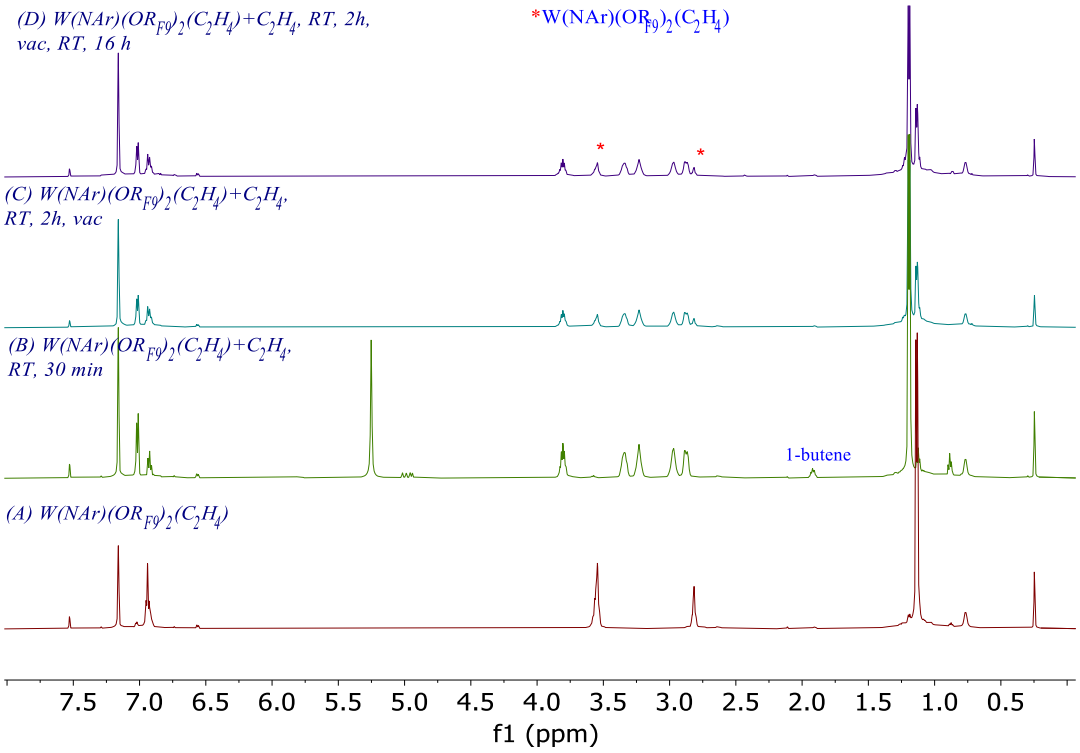

Figure S48. ^{1}H NMR (600 MHz, 298K) spectra showing the decomposition of W(NAr)(OR$_{F9}$)$_2$(C$_4$H$_8$) in absence of ethylene to a mixture of W(NAr)(OR$_{F9}$)$_2$(C$_2$H$_4$) and W(NAr)(OR$_{F9}$)$_2$(C$_4$H$_8$) in C$_6$D$_6$.

One pot formation of W(NAr)(OR$_{F9}$)$_2$(C$_4$H$_8$) that avoids formation of W(NAr)(Ar'NH)(ArNH$_2$)(OR$_{F9}$)

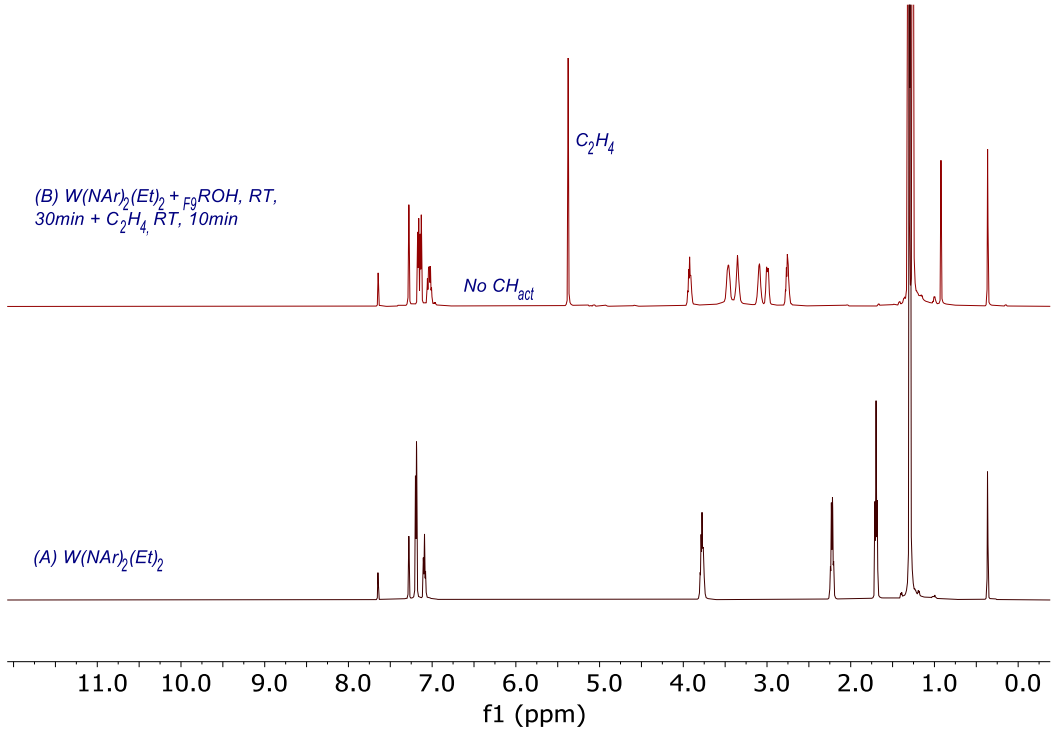

Figure S49. ^{1}H NMR spectra of A) W(NAr)$_2$Et$_2$ and B) upon successive addition of R$_{F9}$OH and C$_2$H$_4$ within 30 min (600 MHz, 298K) in C$_6$D$_6$.

Formation of 1-butene from ethylene by W(NAr)(ArNH$_2$)(OR$_{F9}$)$_2$(C$_2$H$_4$)

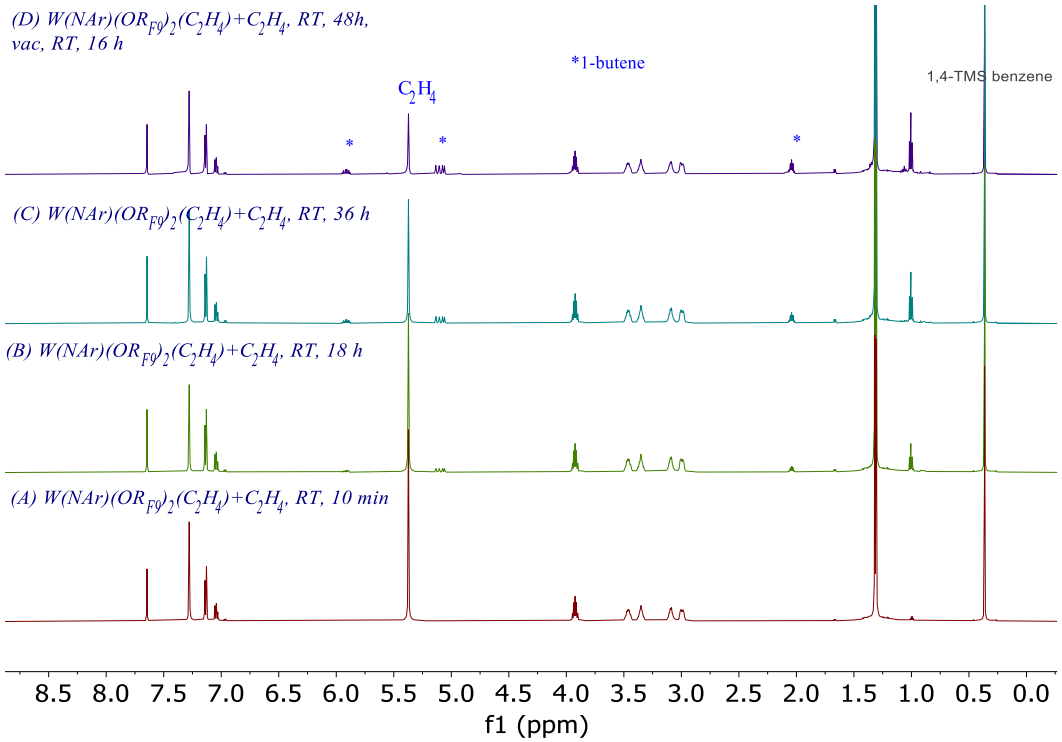

Figure S50. ^{1}H NMR spectra showing the slow formation of 1-butene from ethylene by W(NAr)(OR$_{F9}$)$_2$(C$_4$H$_8$) in absence of coordinated aniline (600 MHz, 298K) in C$_6$D$_6$.

Photolysis study of W(NAr)(OR$_{F9}$)$_2$(C$_4$H$_8$)

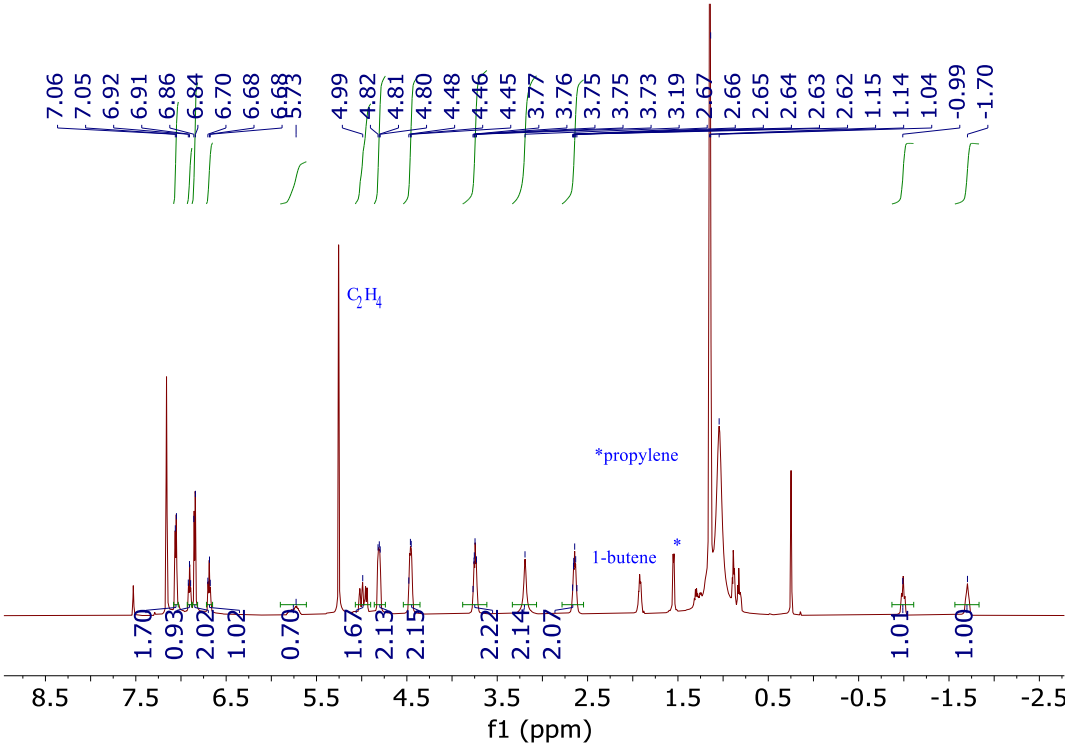

Figure S51. ^{1}H NMR spectra of the W(NAr)(C$_4$H$_8$)(OR$_{F9}$)$_2$ after blue LED irradiation (l=450 nm) for 12 h in presence of 15 psi ethylene (300 MHz, 298K) in C$_6$D$_6$.

Solution stability of W(NAr)(ArNH$_2$)(OR$_{F6}$)$_2$(C$_2$H$_4$)

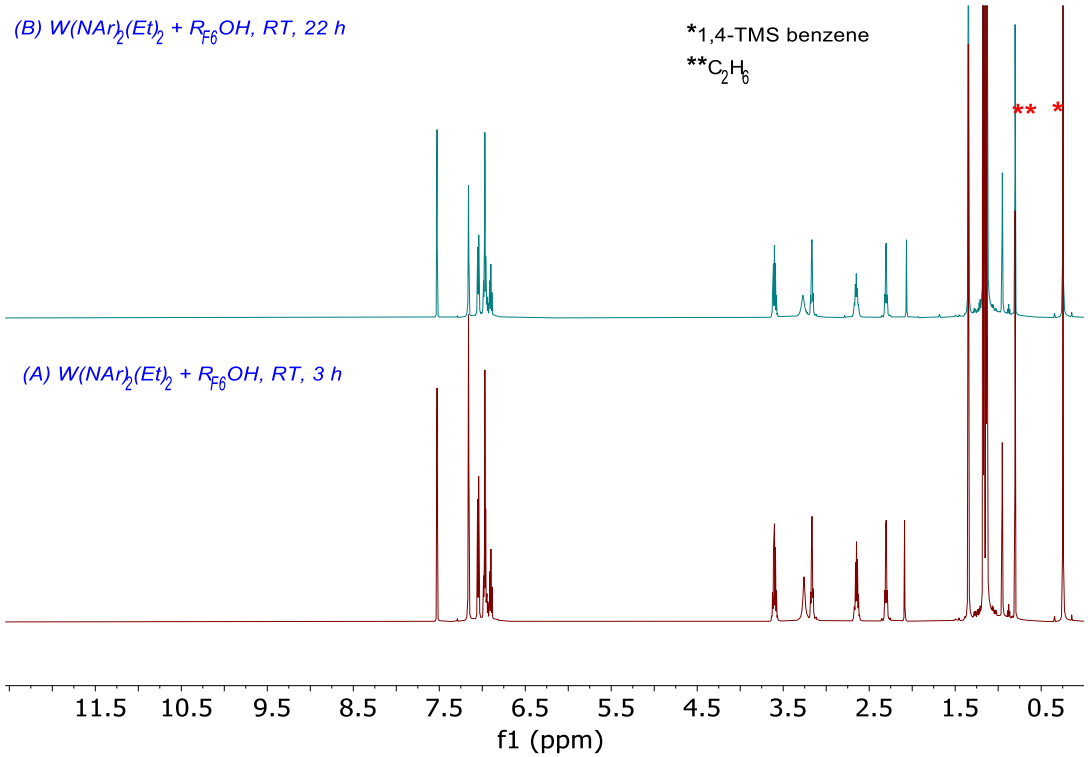

Figure S52. ^{1}H NMR spectra showing solution stability of W(NAr)(ArNH$_2$)(OR$_{F6}$)$_2$(C$_2$H$_4$) (600 MHz, 298K) in C$_6$D$_6$.

Reaction of W(NAr)(ArNH$_2$)(OR$_{F6}$)$_2$(C$_2$H$_4$) with ethylene

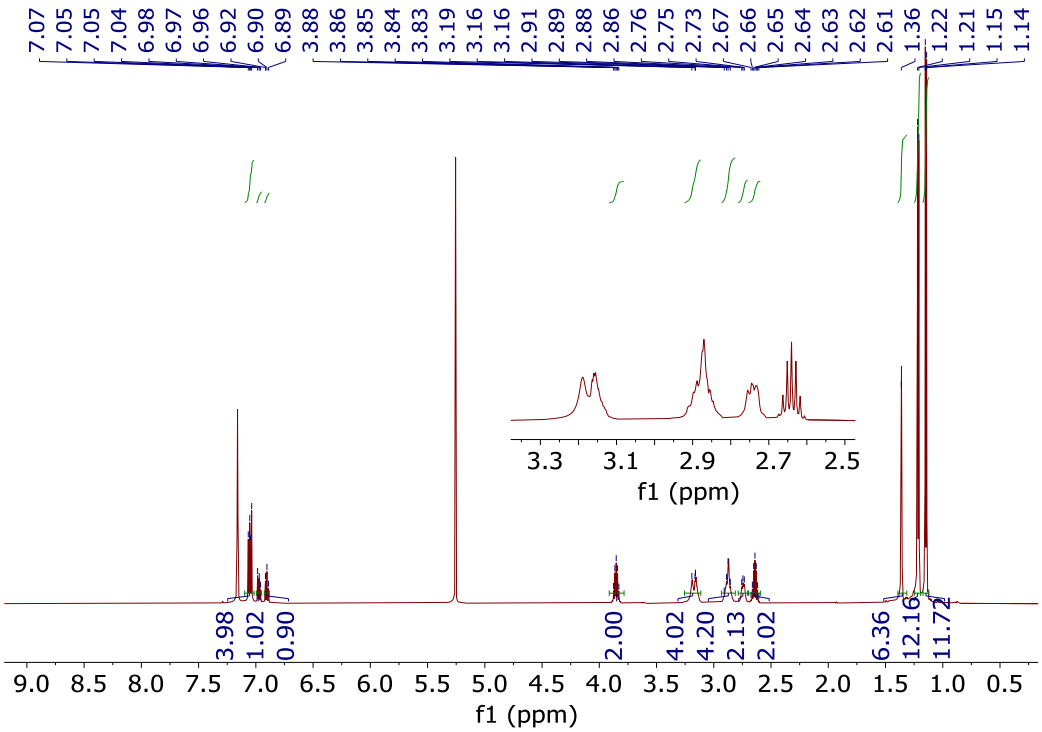

Figure S53. ^{1}H NMR spectra of W(ArNH$_2$)(NAr)(OR$_{F6}$)$_2$(C$_2$H$_4$) after 10 min of addition of ethylene (600 MHz, 298K) in C$_6$D$_6$.

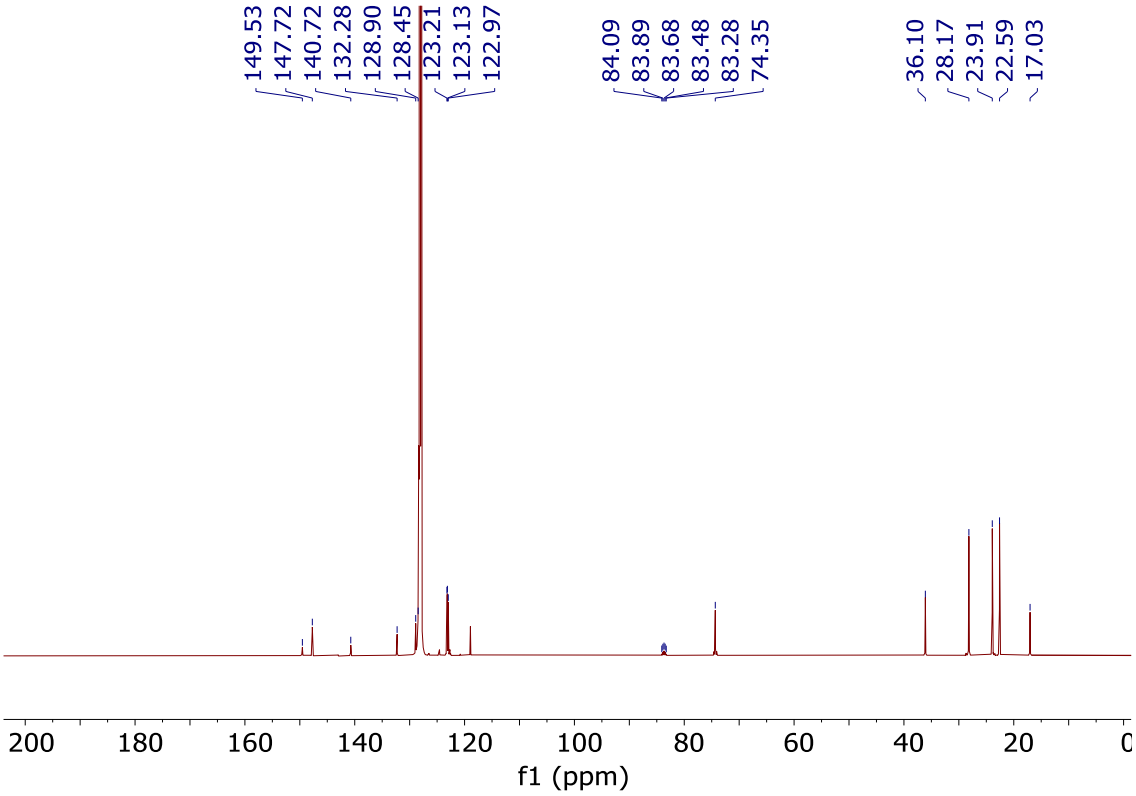

Figure S54. ^{13}C NMR spectrum of the above reaction mixture (151 MHz, 298K) in C_6D_6 ($J_{W\text{-}C}$ = 73.6 Hz).

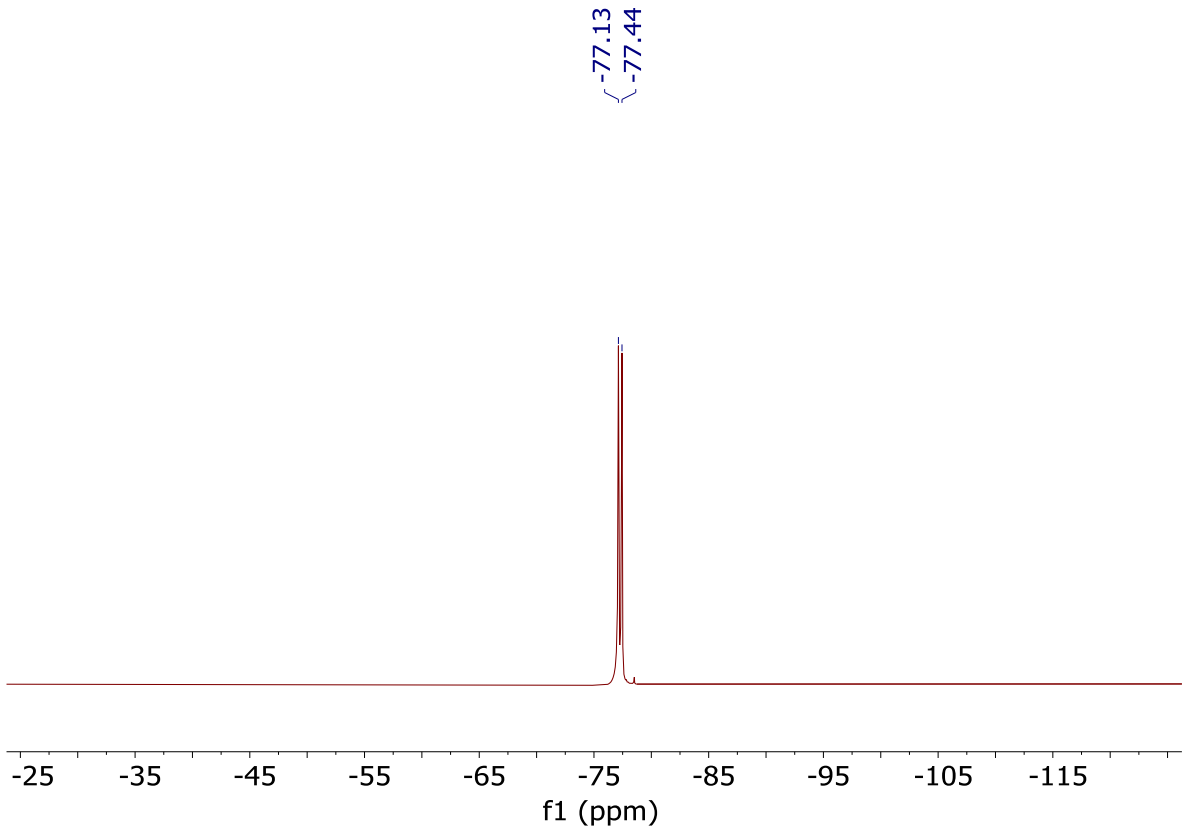

Figure S55. ^{19}F NMR spectra of the above reaction mixture (564 MHz, 298K) in C_6D_6.

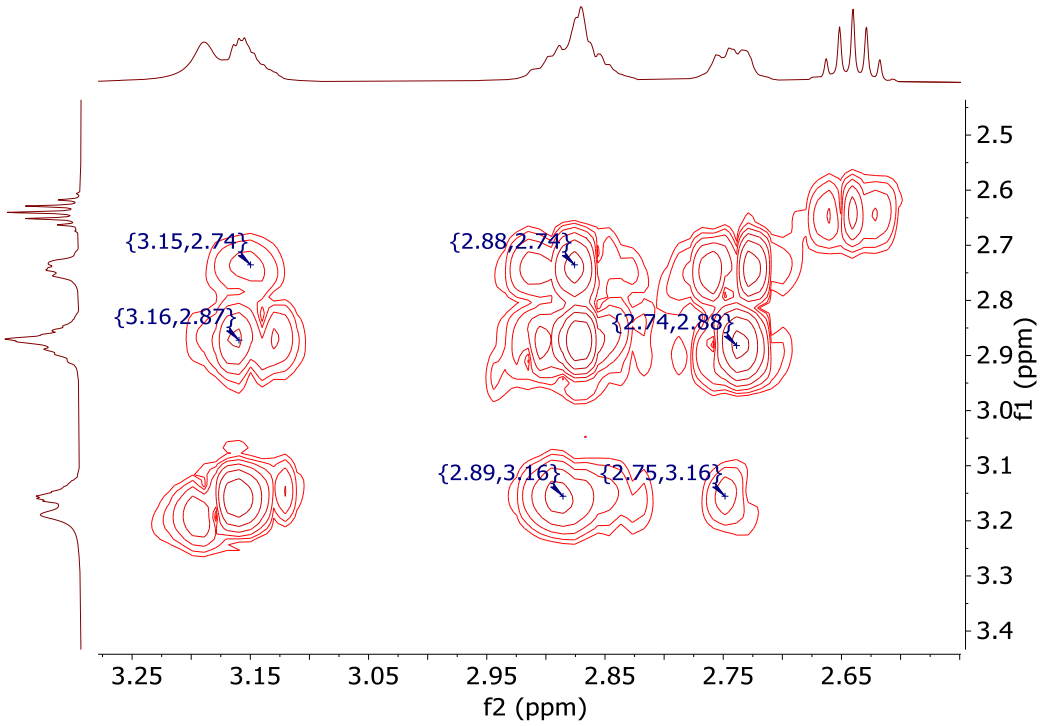

Figure S56. The aliphatic area of COSY spectrum of the above reaction mixture (600 MHz, 298K) in C_6D_6.

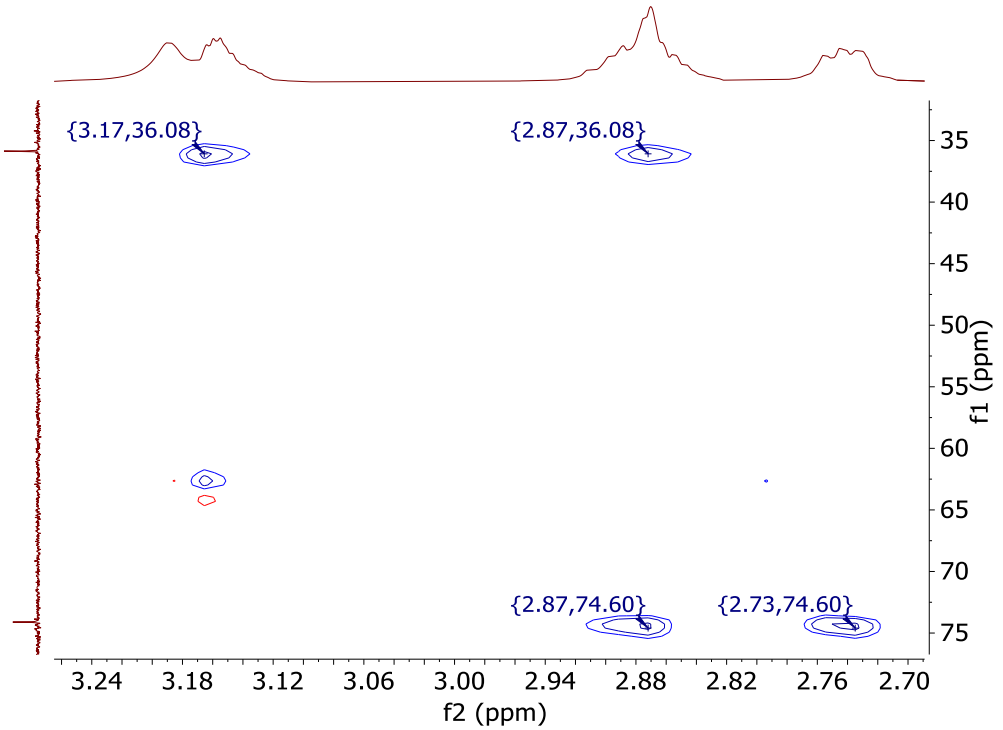

Figure S57. The Aliphatic area of HSQC {^{1}H, ^{13}C} spectrum of above reaction mixture (600 MHz, 298K) in C_6D_6.

Photolysis of W(NAr)(OR_{F6})$_2$(C_4H_8)

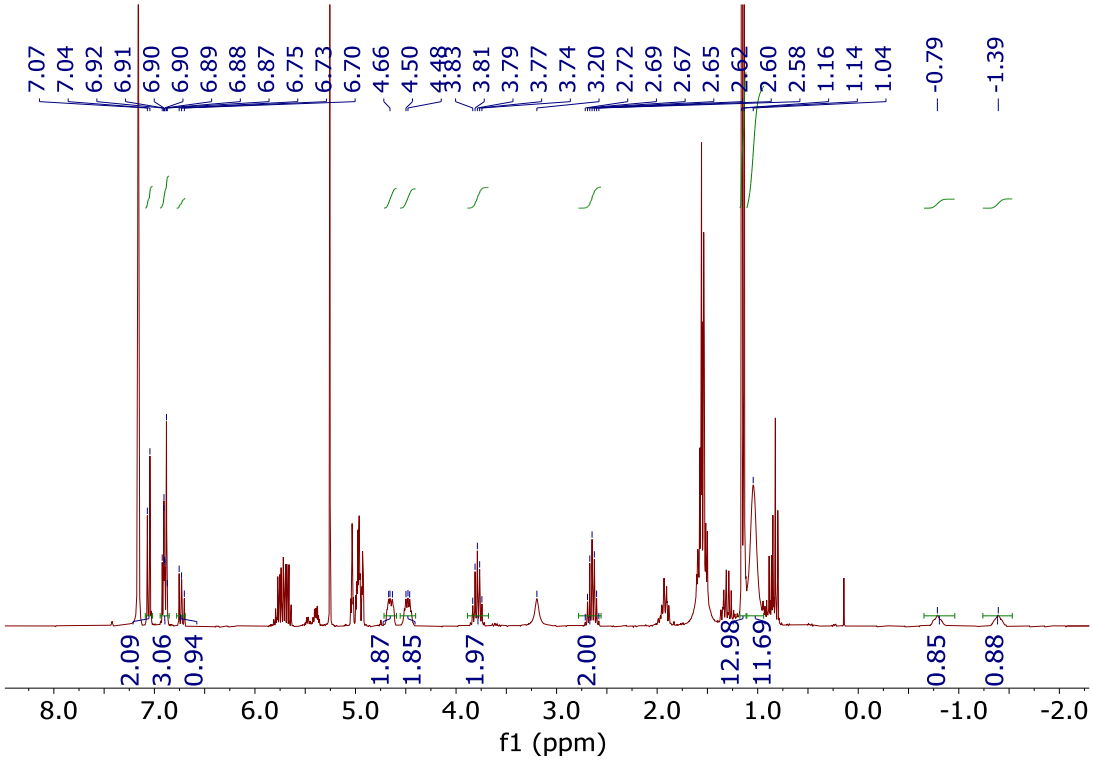

Figure S58. ^{1}H NMR spectra of the above reaction mixture after blue LED irradiation (450 nm) for 12 h after in presence of 15 psi ethylene (300 MHz, 298K) in C_6D_6.

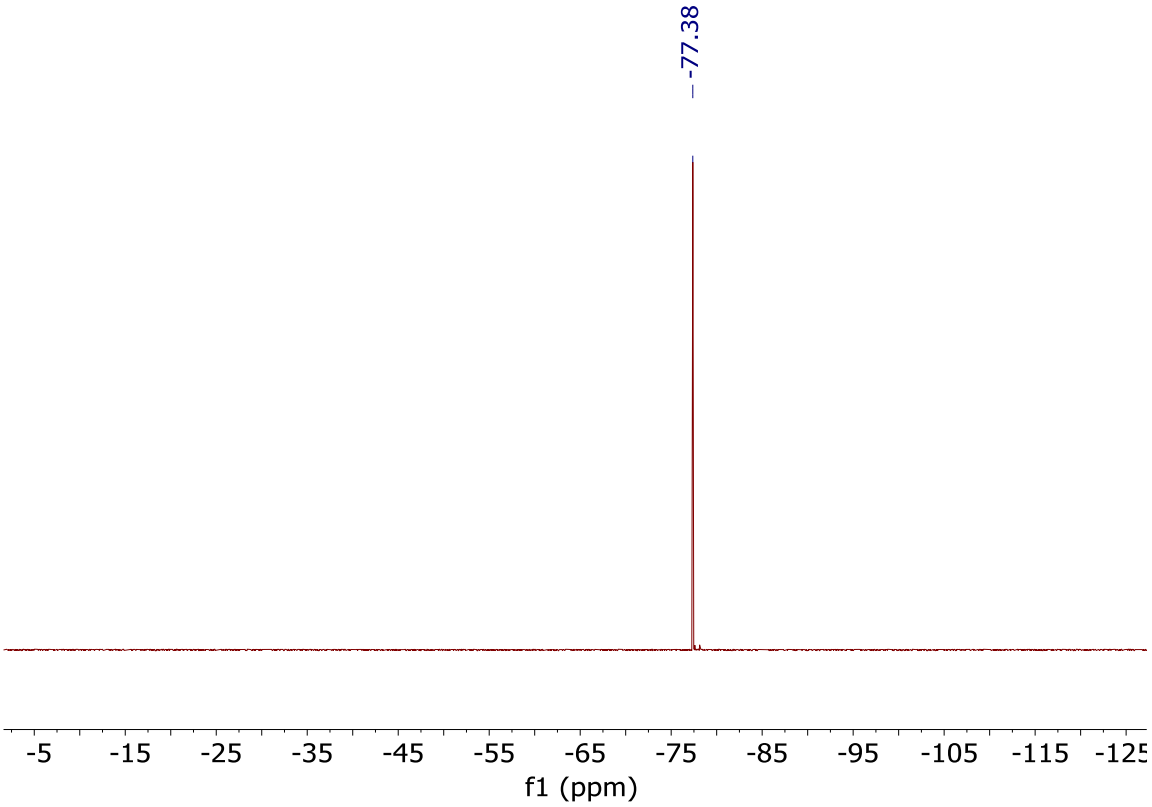

Figure S59. ^{19}F NMR spectra of the above reaction mixture (282 MHz, 298K) in C_6D_6.

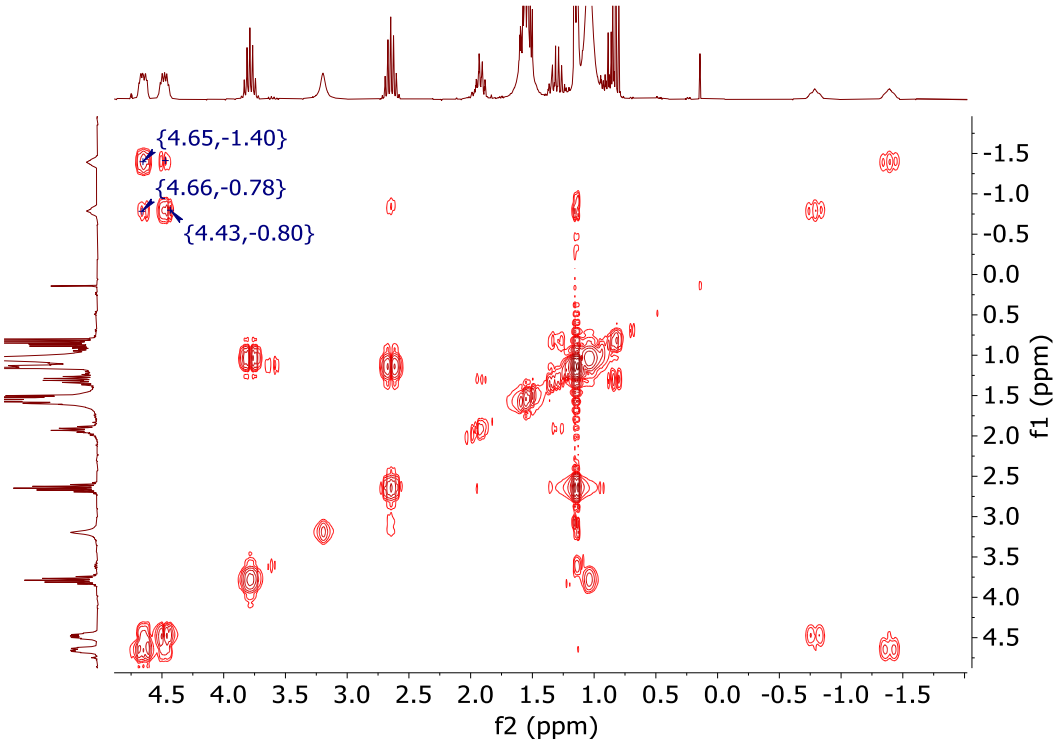

Figure S60. The aliphatic area of COSY spectrum of the above reaction mixture (300 MHz, 298K) in C_6D_6.

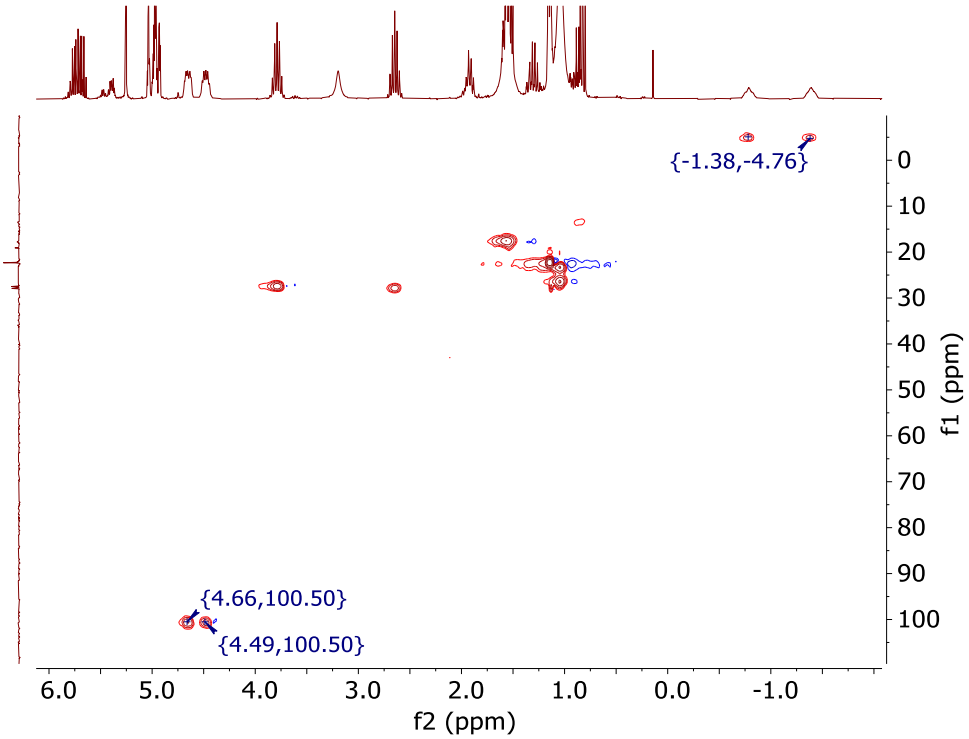

Figure S61. The Aliphatic area of HSQC {^{1}H, ^{13}C} spectrum of the above reaction mixture (300 MHz, 298K) in C_6D_6.

Reaction of W(NAr)(ArNH$_2$)(OR$_{F3}$)$_2$(C$_2$H$_4$) with ethylene

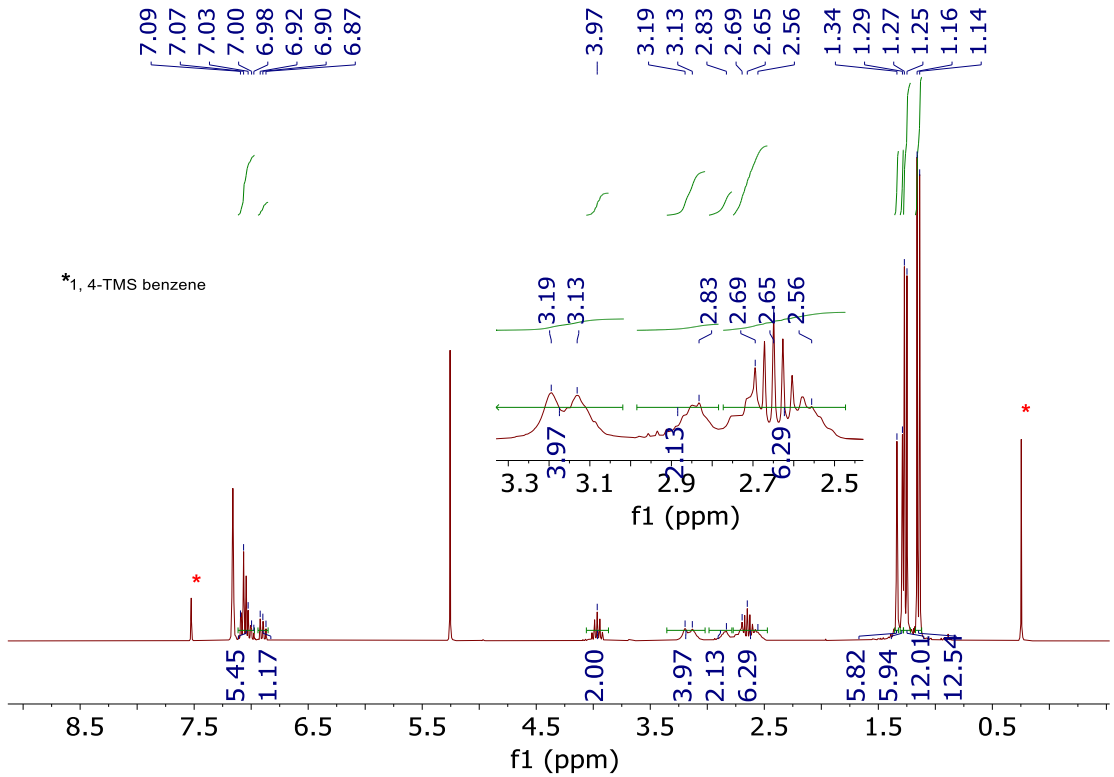

Figure S62. ^{1}H NMR spectra of **W(NAr)(ArNH$_2$)(OR$_{F3}$)$_2$(C$_2$H$_4$)** after 10 min of addition of ethylene (600 MHz, 298K) in C_6D_6.

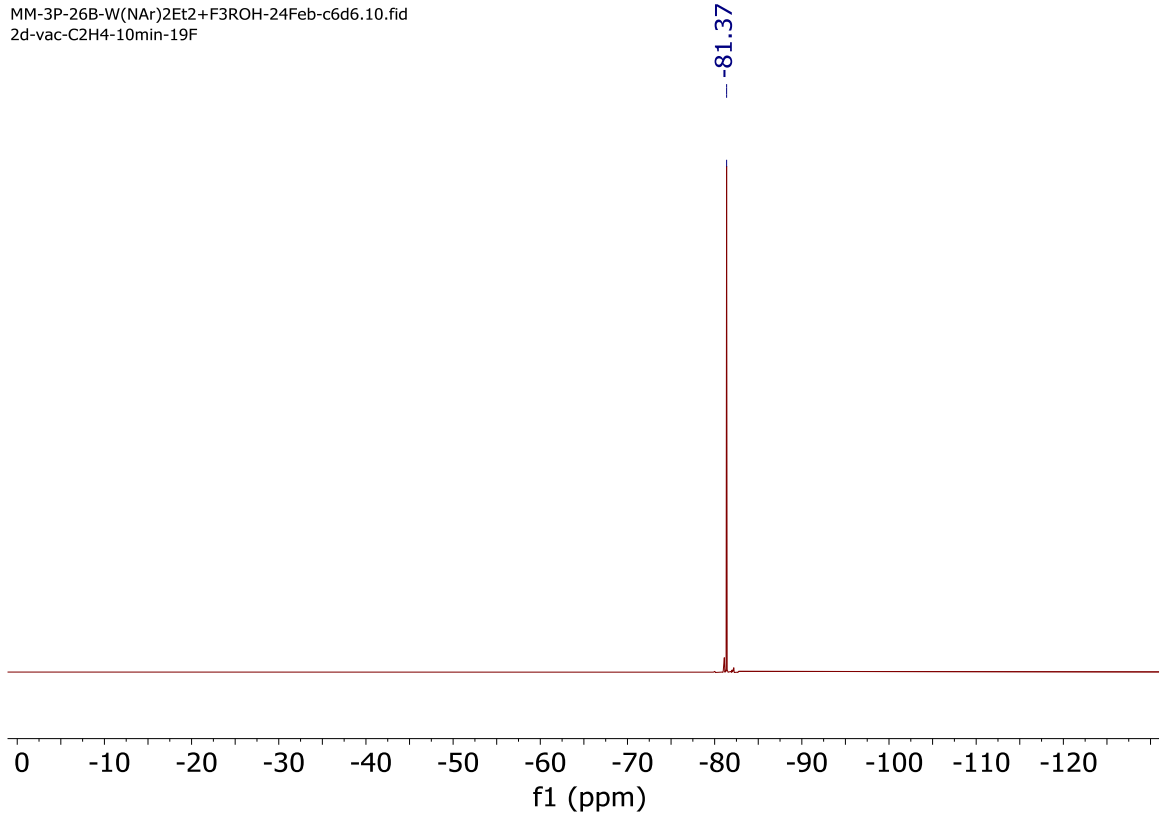

Figure S63. ^{19}F NMR spectra of the above reaction mixture (282 MHz, 298K) in C_6D_6.

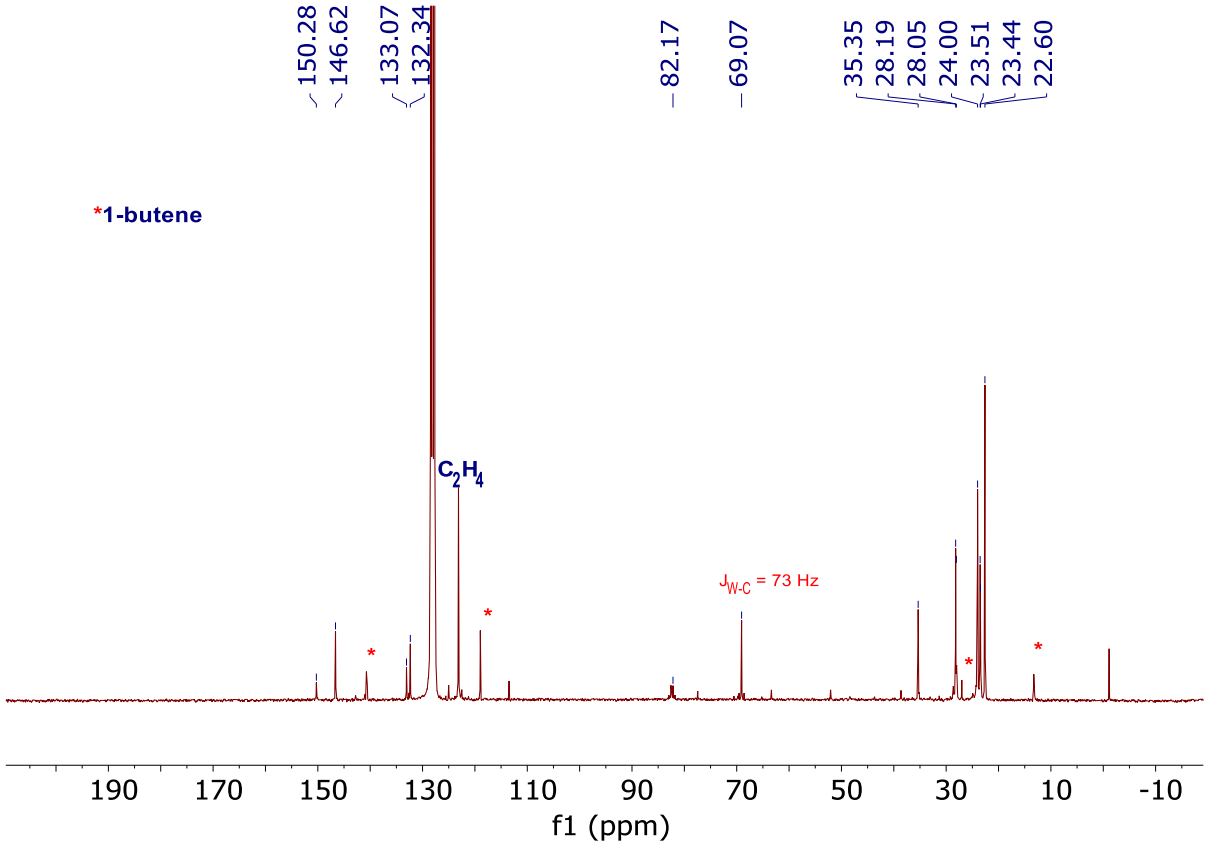

Figure S64. ^{13}C NMR spectrum of the above reaction mixture (75 MHz, 298K) in C_6D_6.

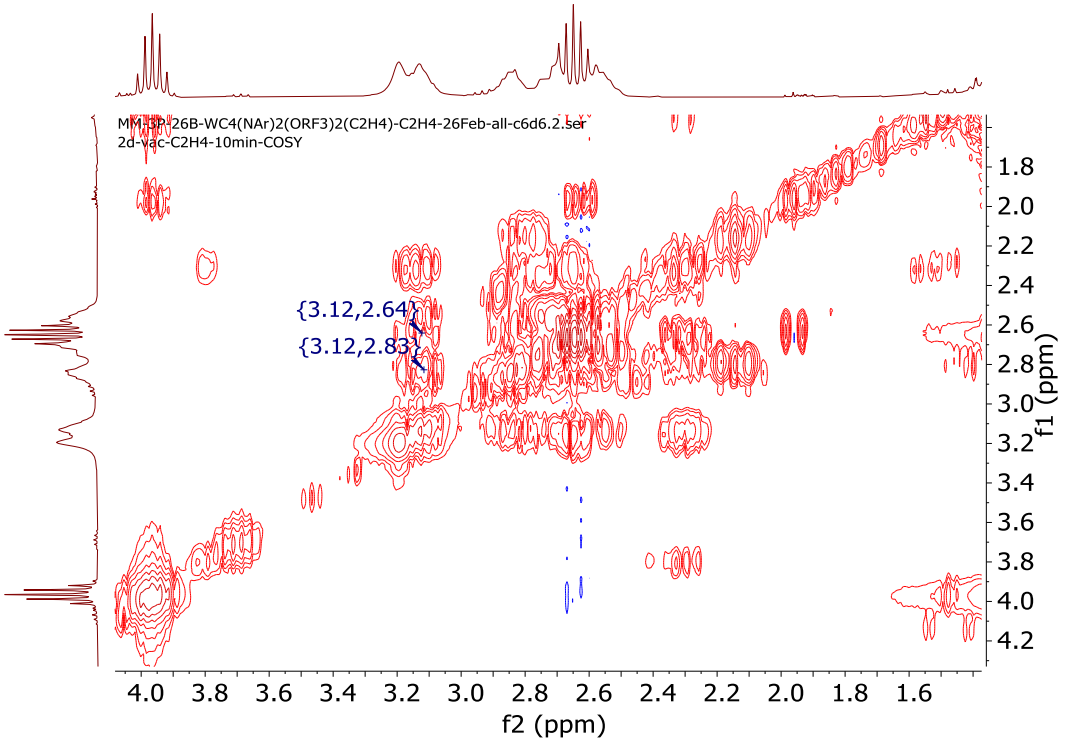

Figure S65. The Aliphatic area of COSY spectrum of the above reaction mixture (300 MHz, 298K) in C_6D_6.

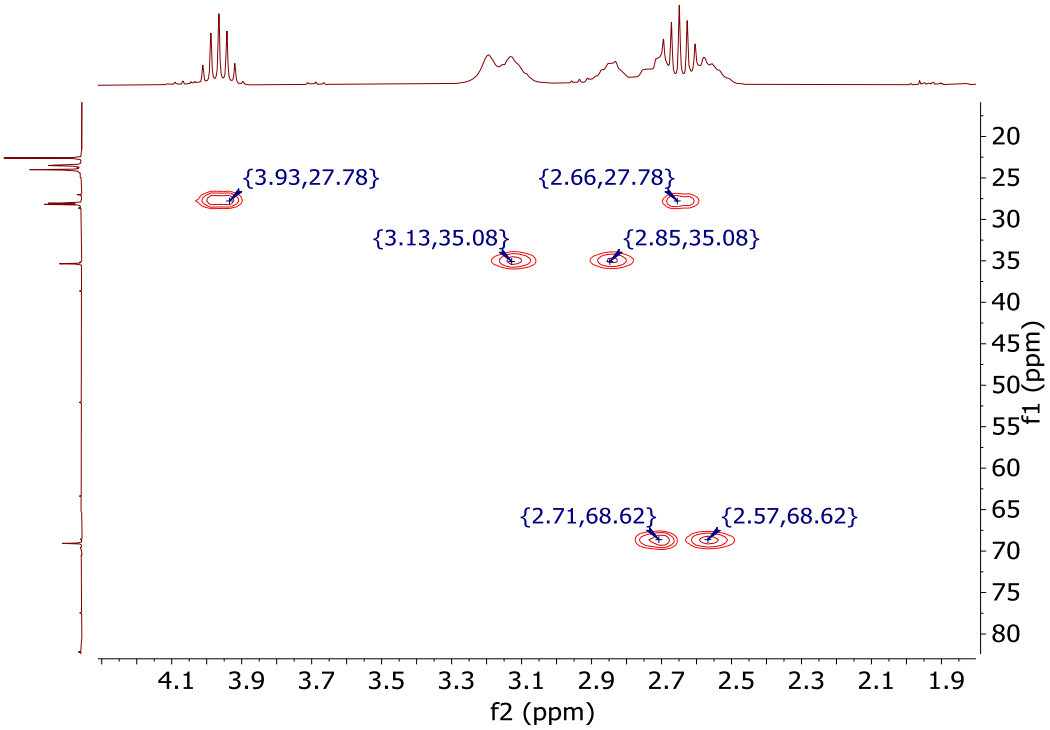

Figure S66. The aliphatic area of HSQC {^{1}H, ^{13}C} spectrum of the above reaction mixture (300 MHz, 298K) in C_6D_6.

$ArNH_2$ promoted formation of $W(NAr)(Ar'NH)(ArNH_2)(OR_{F9})$

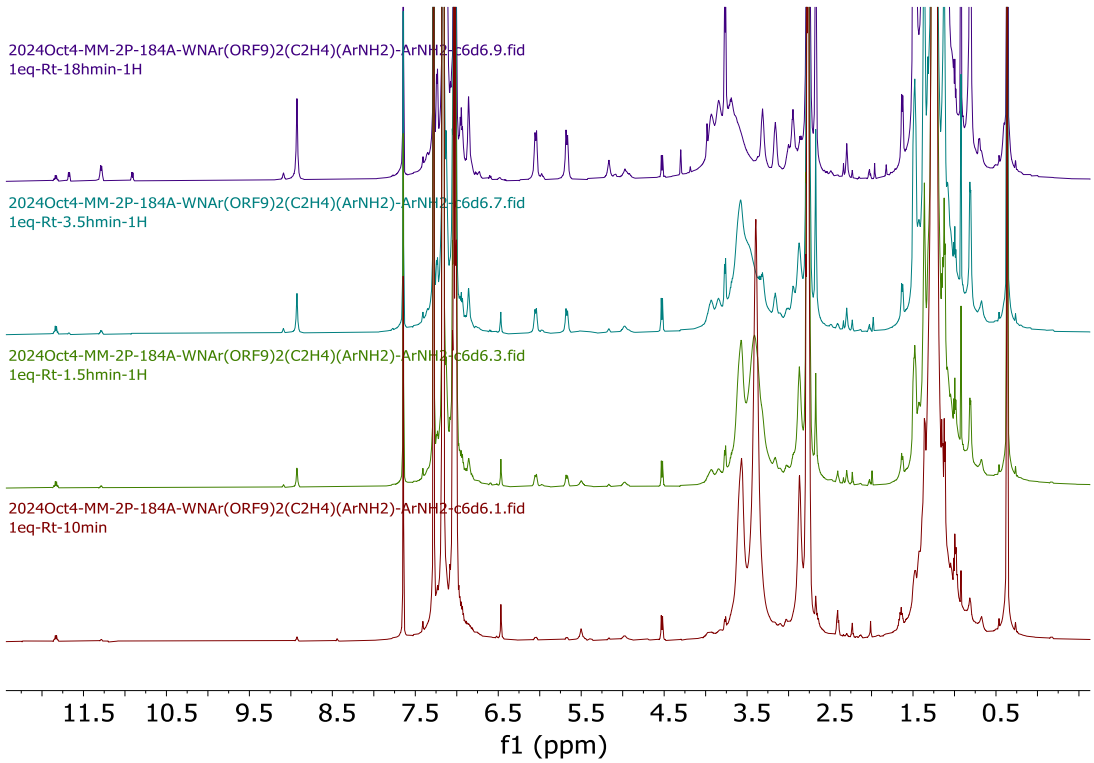

Figure S67. ^{1}H NMR spectra showing the reaction of $W(NAr)(ArNH_2)(OR_{F9})_2(C_4H_8)$ with $ArNH_2$ (1 eq) at ambient temperature (600 MHz, 298K) in C_6D_6.

Reaction of W(NAr)(ArNH$_2$)(OR$_{F9}$)$_2$(C$_2$H$_4$) with 2,6-lutidine

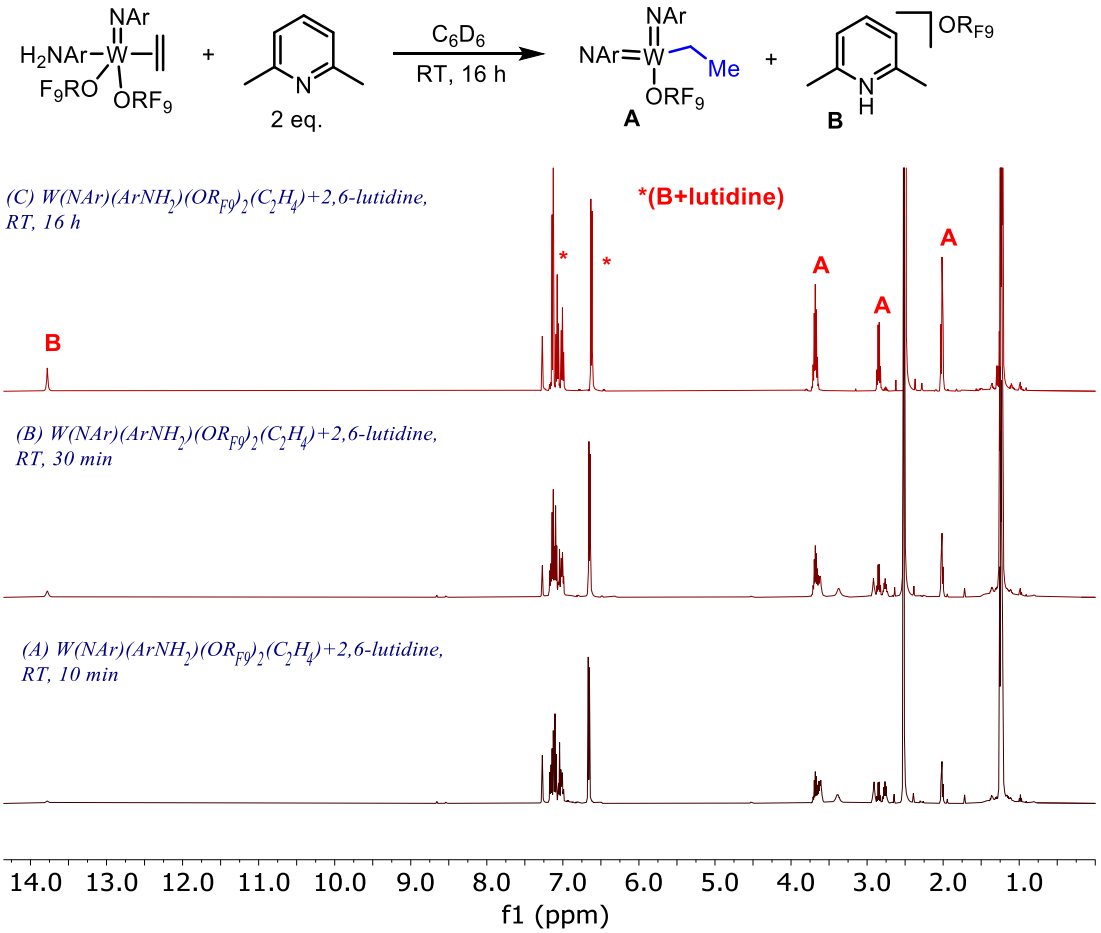

Figure S68. ^{1}H NMR spectra showing the reaction of W(NAr)(ArNH$_2$)(OR$_{F9}$)$_2$(C$_4$H$_8$) with 2,6-lutidine (2 equiv) at ambient temperature (600 MHz, 298K) in C$_6$D$_6$.

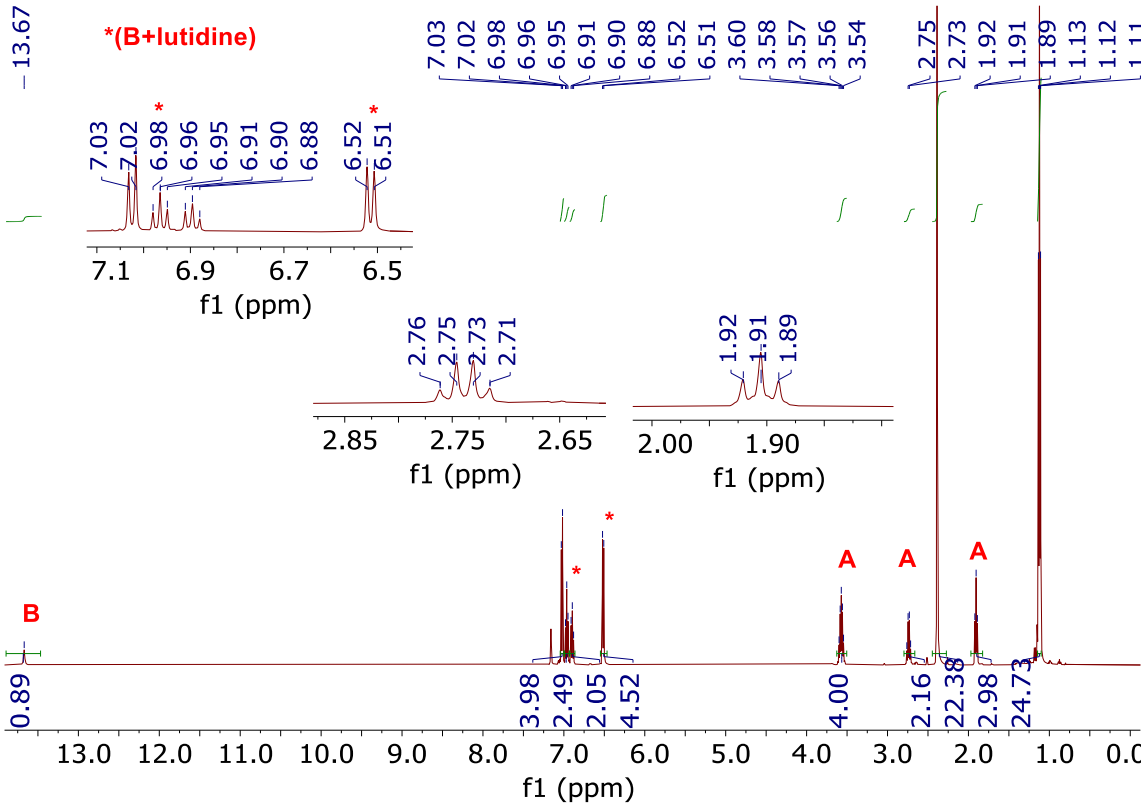

Figure S69. ^{1}H NMR spectra of the above reaction mixture (600 MHz, 298K) in C_6D_6.

Reaction of W(NAr)(ArNH$_2$)(OR$_{F9}$)$_2$(C$_2$H$_4$) with cyclohexene

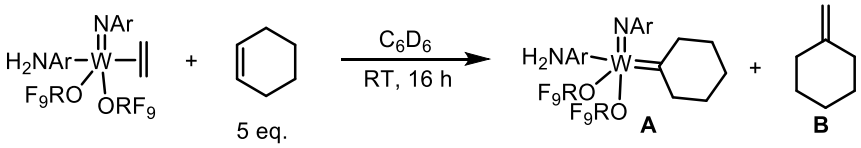

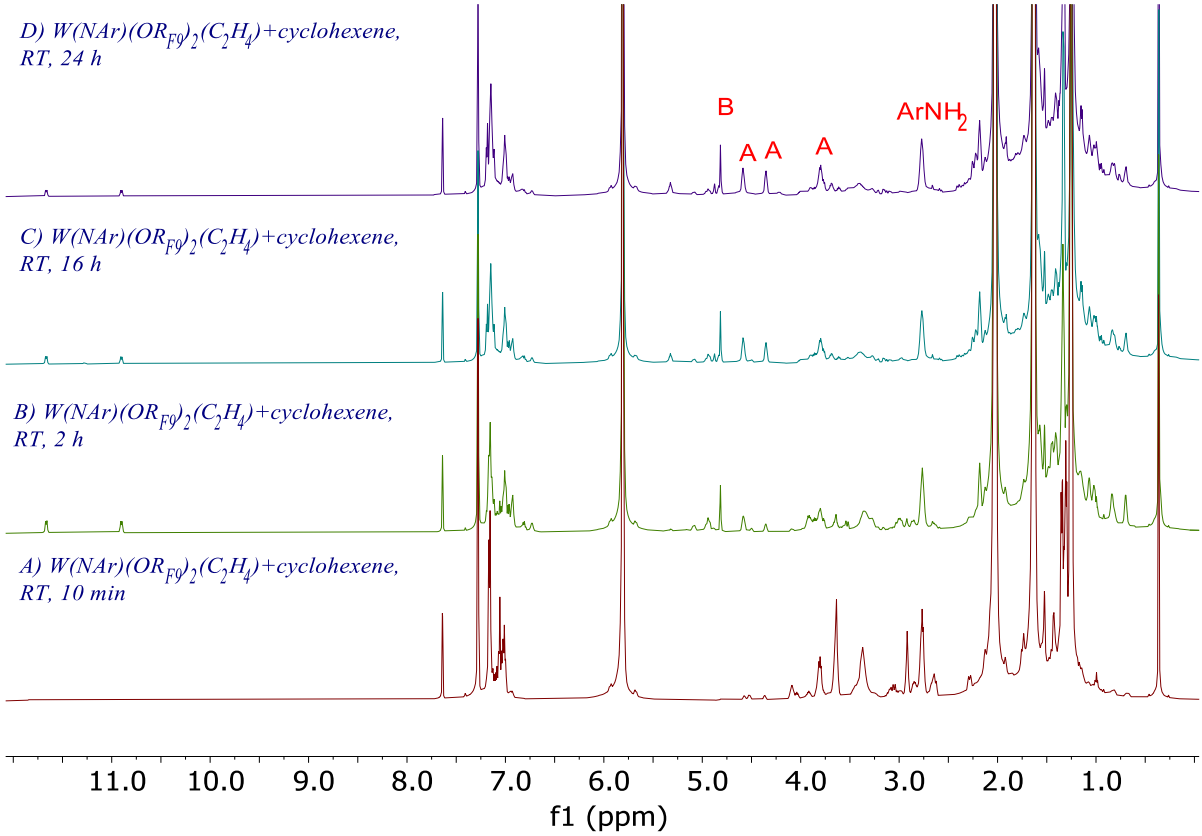

Figure S70. ^{1}H NMR spectra showing the reaction of W(NAr)(ArNH$_2$)(OR$_{F9}$)$_2$(C$_4$H$_8$) with cyclohexene (5 eq) at 100 °C (600 MHz, 298K) in C$_6$D$_6$.

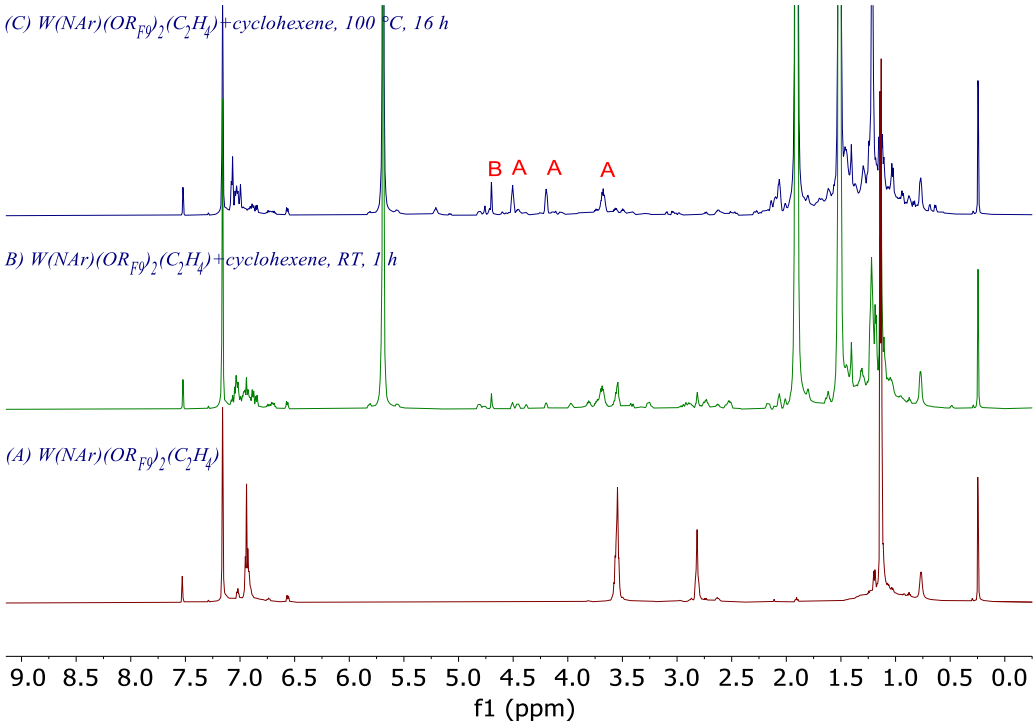

Figure S71. ^{1}H NMR spectra showing the reaction of W(NAr)(OR$_{F9}$)$_2$(C$_4$H$_8$) with cyclohexene (5 eq) at 100 °C (600 MHz, 298K) in C$_6$D$_6$.

Reaction of W(NAr)(Ar'NH)(ArNH$_2$)(OR$_{F9}$) with ethylene

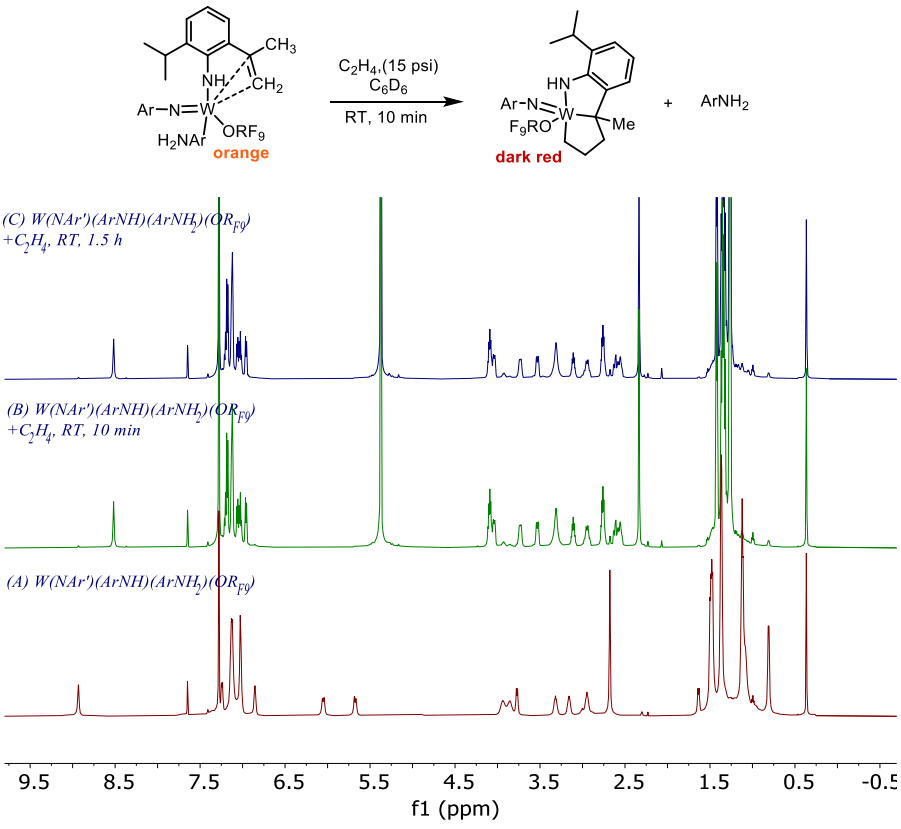

Figure S72. ^{1}H NMR spectra showing the reaction of W(NAr)(Ar'NH)(ArNH$_2$)(OR$_{F9}$) with ethylene at room temperature (600 MHz, 298K) in C$_6$D$_6$.

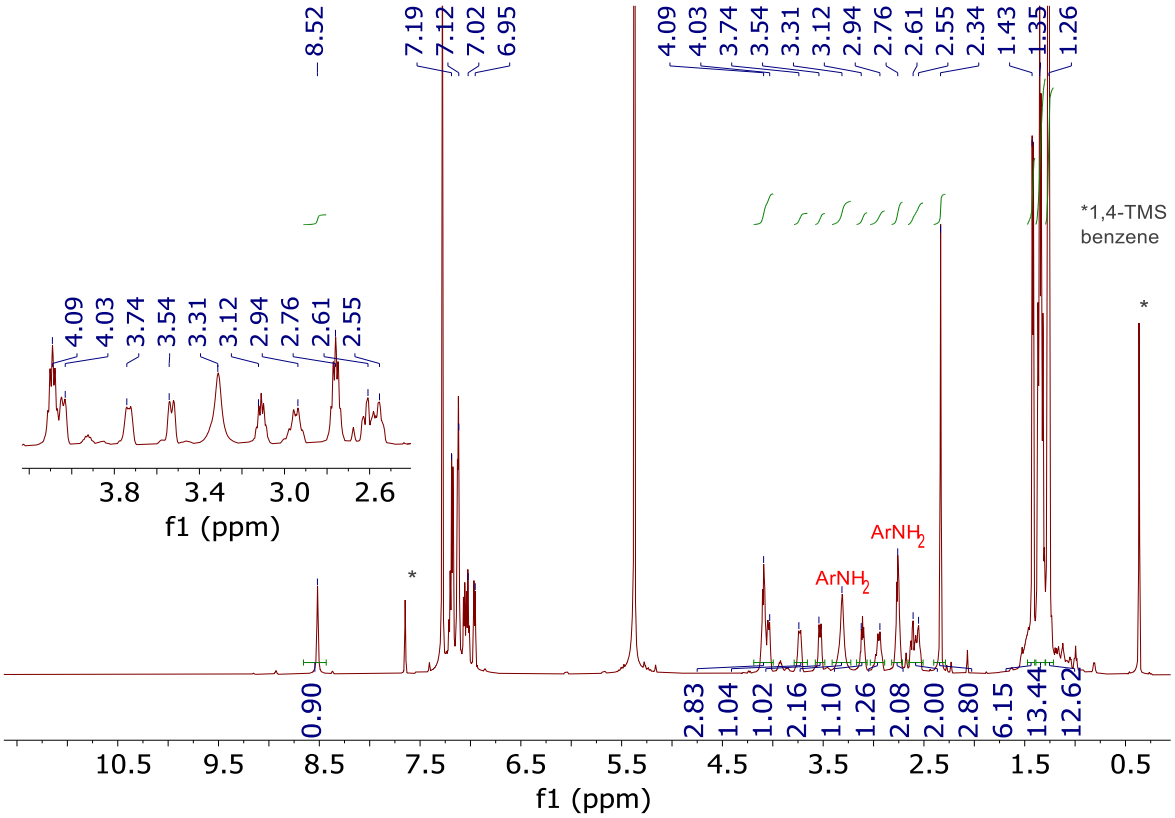

Figure S73. ^{1}H NMR spectra of the above reaction mixture (600 MHz, 298K) in C_6D_6.

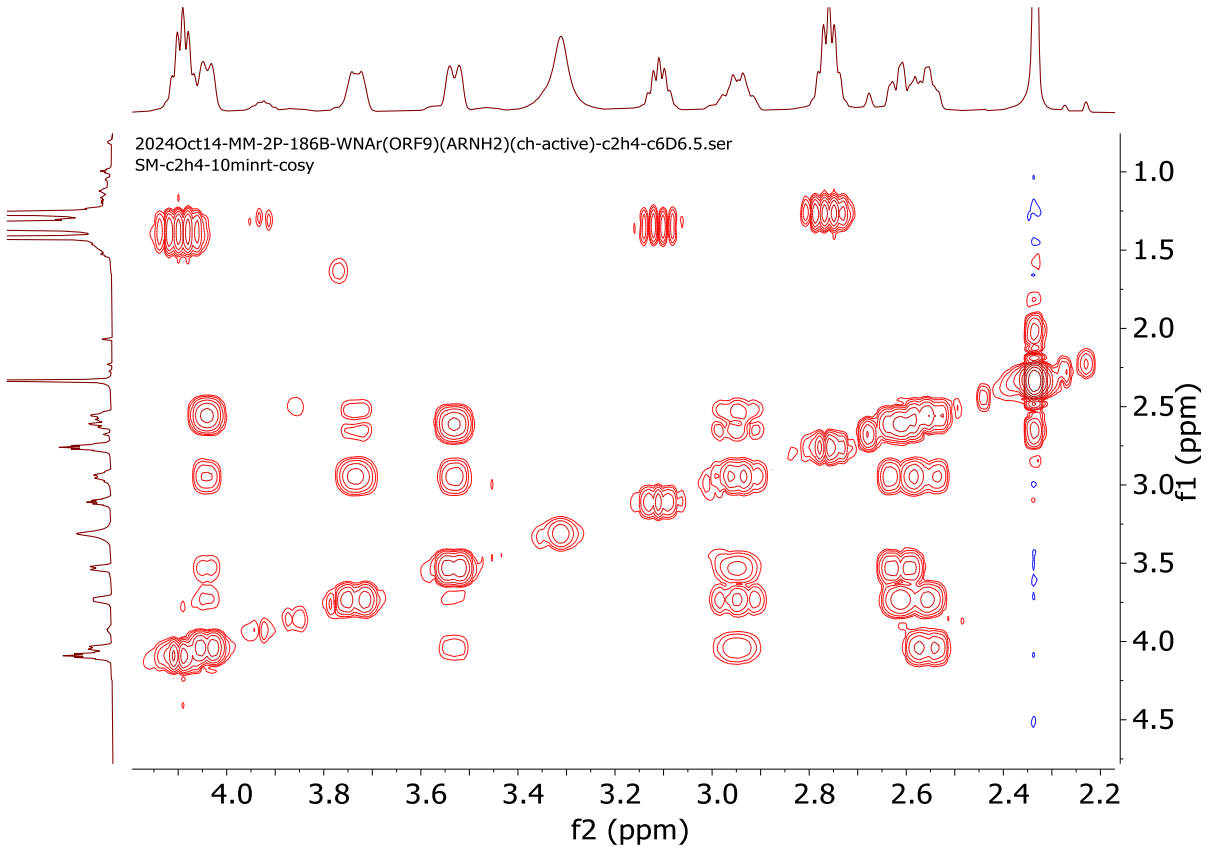

Figure S74. The aliphatic area of COSY spectrum of the above reaction mixture (600 MHz, 298K) in C_6D_6.

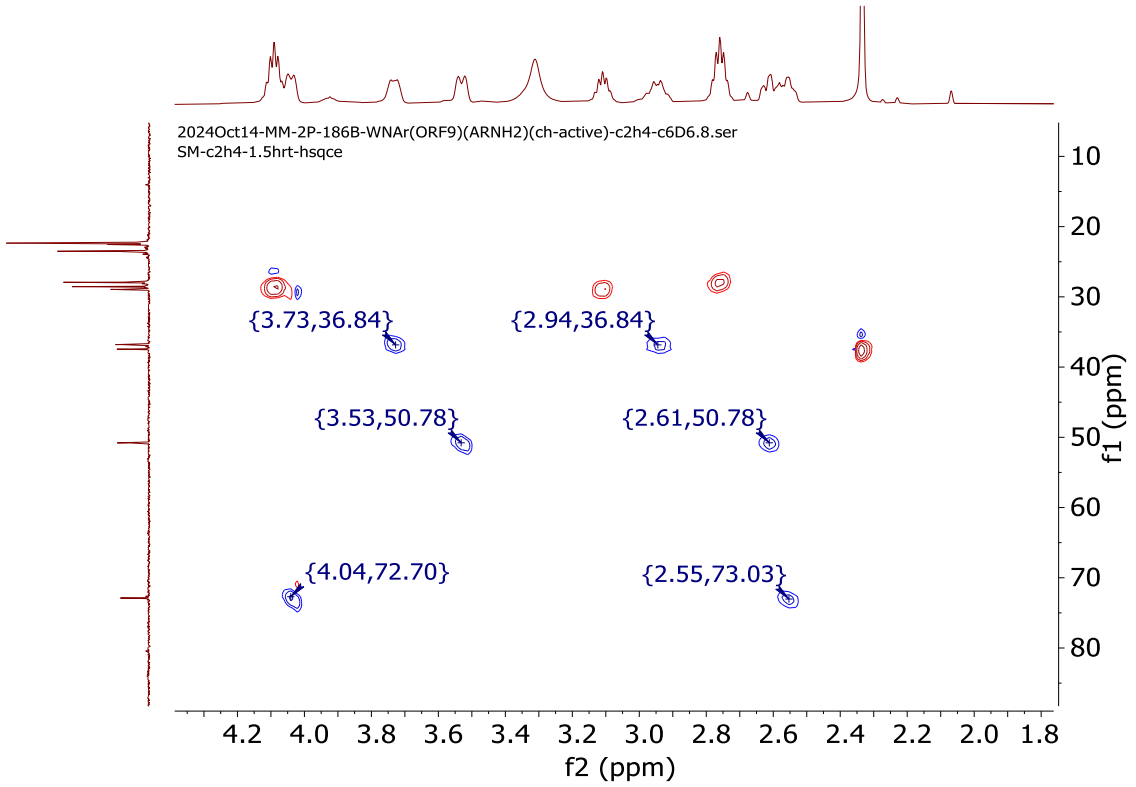

Figure S75. The aliphatic area of HSQC {^{1}H, ^{13}C} spectrum of the above reaction mixture (600 MHz, 298K) in C_6D_6.

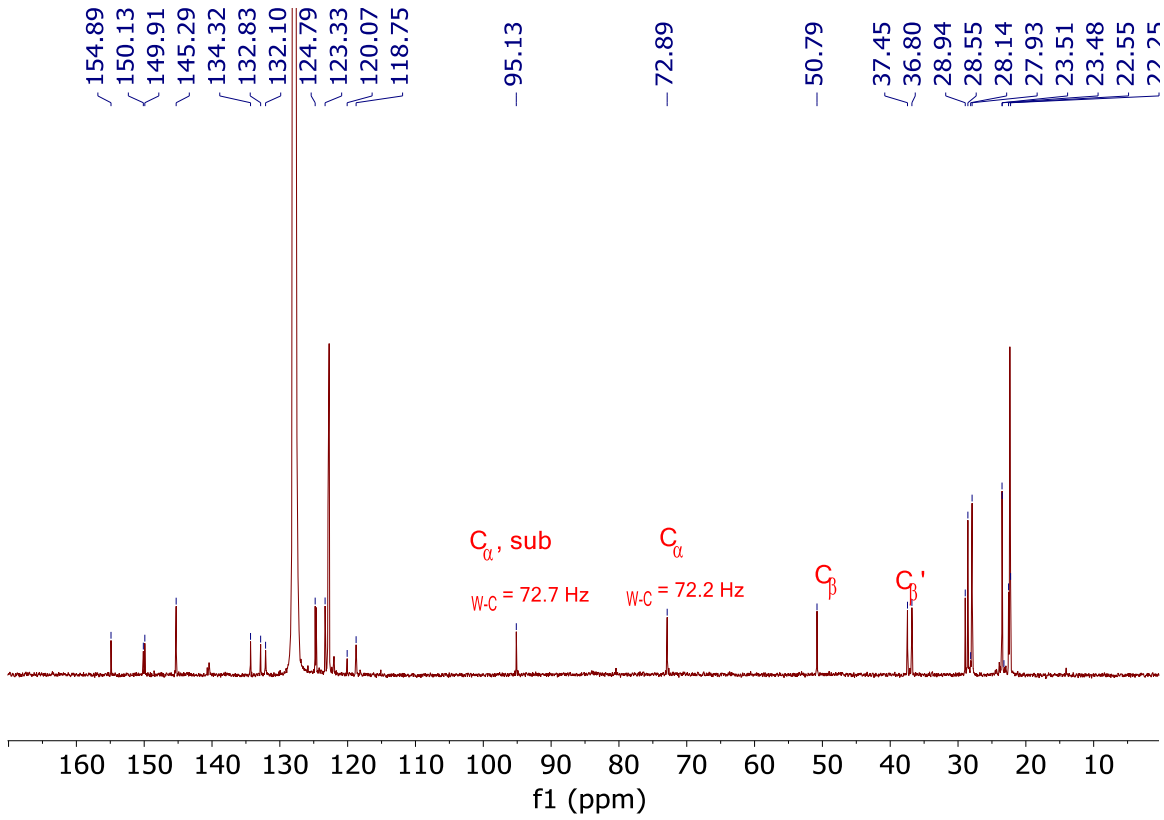

Figure S76. ^{13}C NMR spectrum of the above reaction mixture (75 MHz, 298K) in C_6D_6.

Solution stability of W(NAr)(Ar'NH)($ArNH_2$)(OR_{F9}) in absence of ethylene

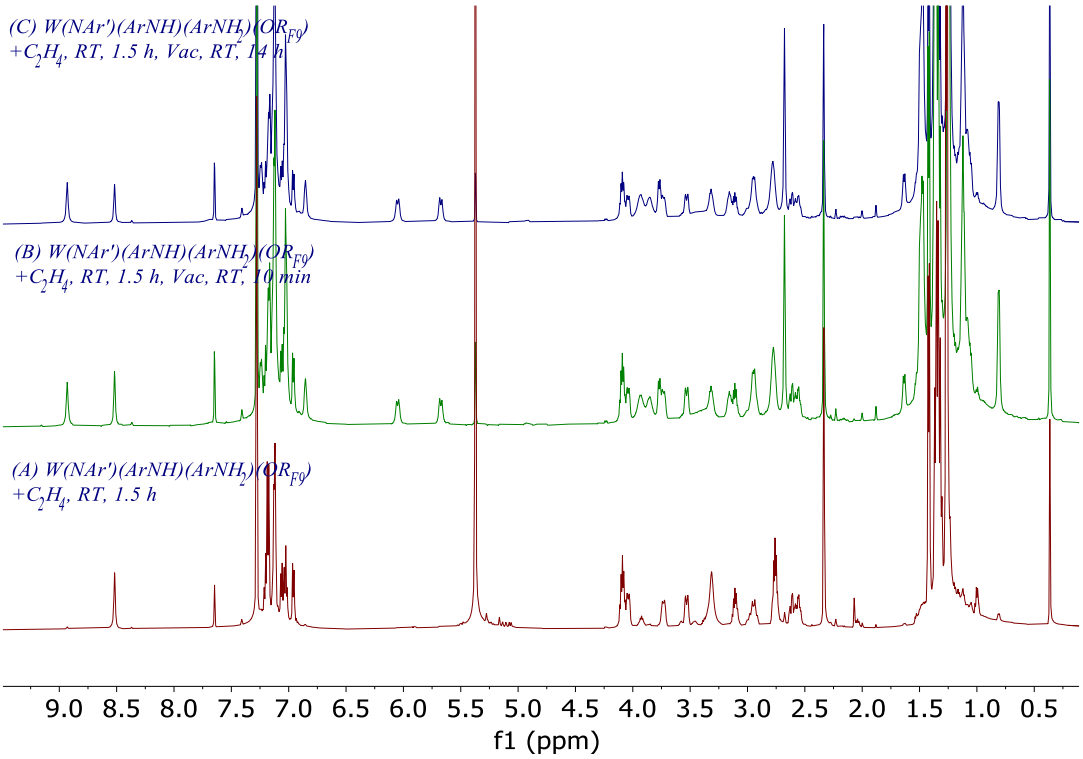

Figure S77. ^{1}H NMR spectra showing that the reaction mixture of figure S65 starts to form W(NAr)($ArNH_2$)(OR_{F9})$_2$(C_2H_4) in absence of ethylene (600 MHz, 298K) in C_6D_6.

Reaction of W(NAr)(Ar'NH)($ArNH_2$)(OR_{F9}) with cyclohexene

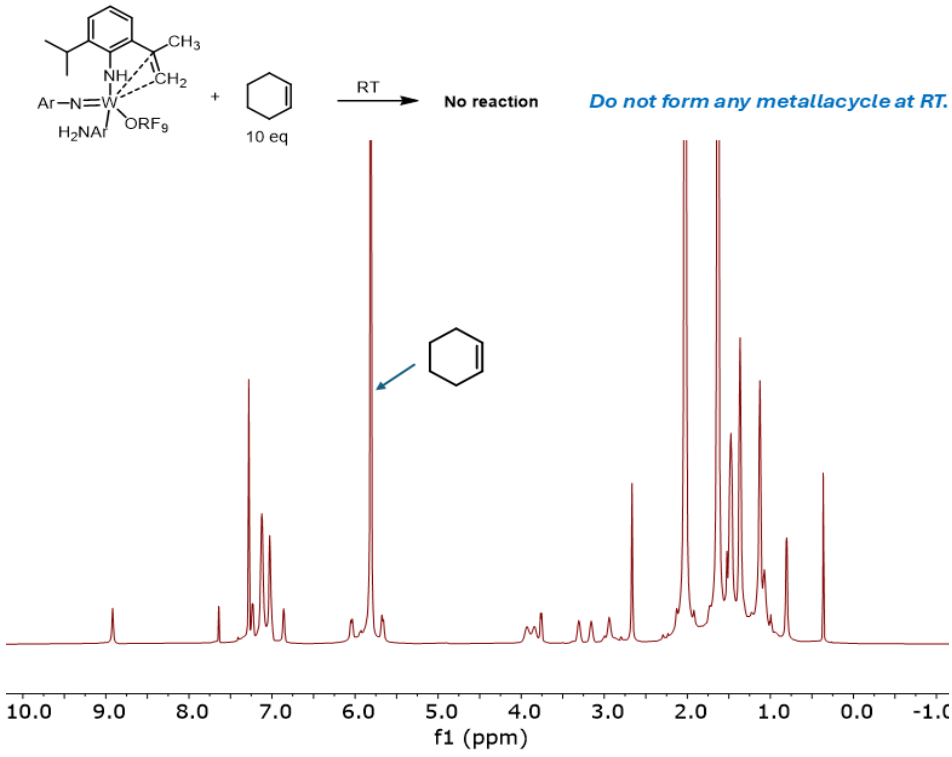

Figure S78. ^{1}H NMR spectra for the reaction of W(NAr)(Ar'NH)($ArNH_2$)(OR_{F9}) with cyclohexene at room temperature (600 MHz, 298K) in C_6D_6.

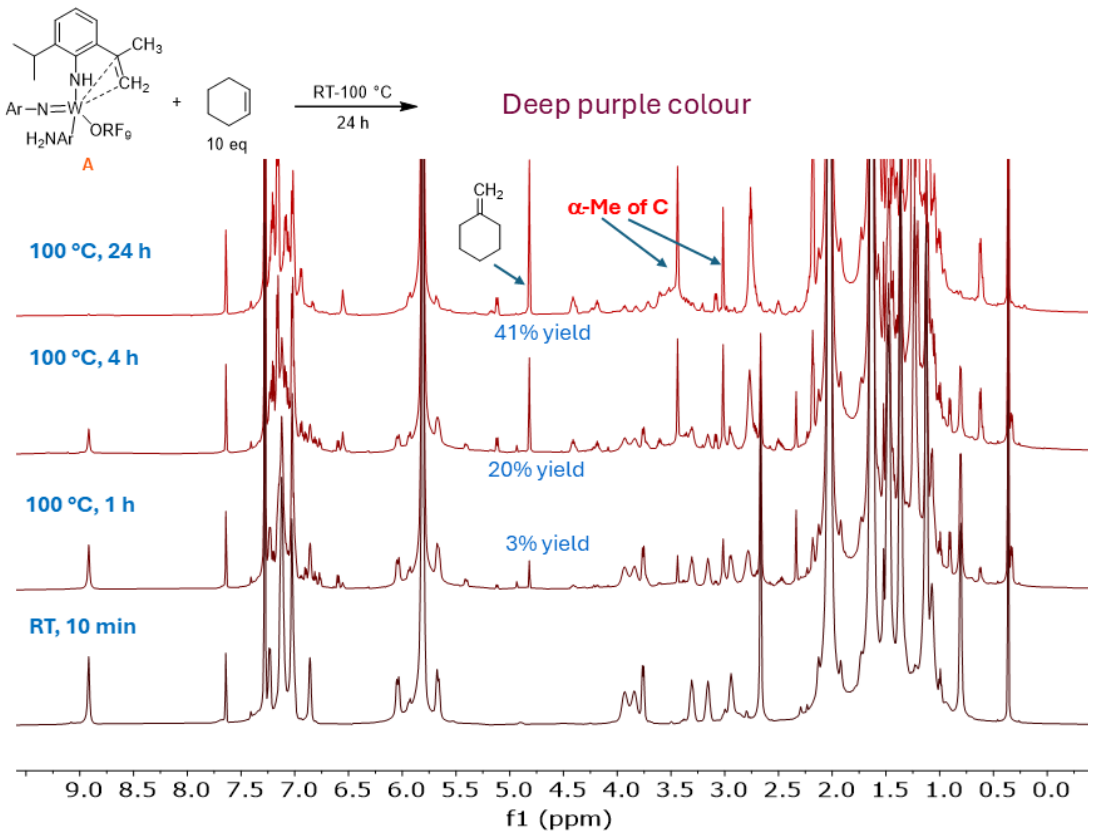

Figure S79. ^{1}H NMR spectra for the reaction of W(NAr)(Ar'NH)($ArNH_2$)(OR_{F9}) with cyclohexene at 100 °C for 24 h (600 MHz, 298K) in C_6D_6.

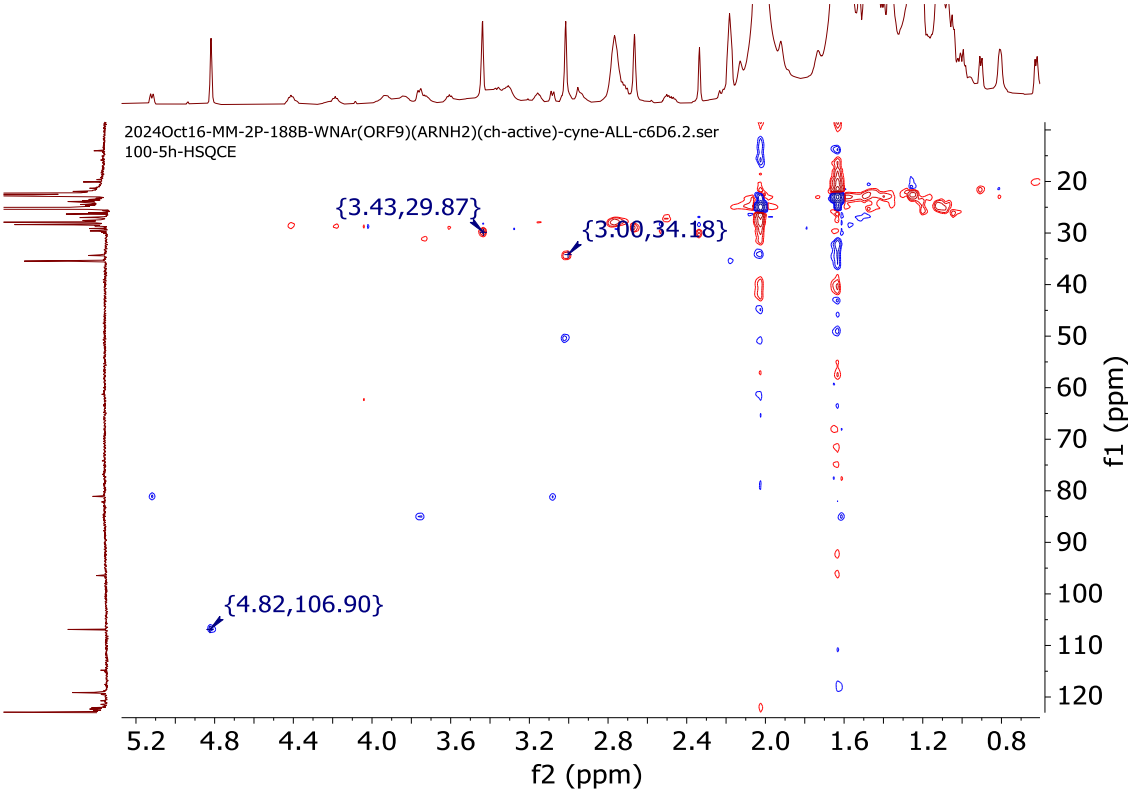

Figure S80. Aliphatic area of HSQC {^{1}H, ^{13}C} spectrum of the above mixture in C_6D_6 (151 MHz, 298K).

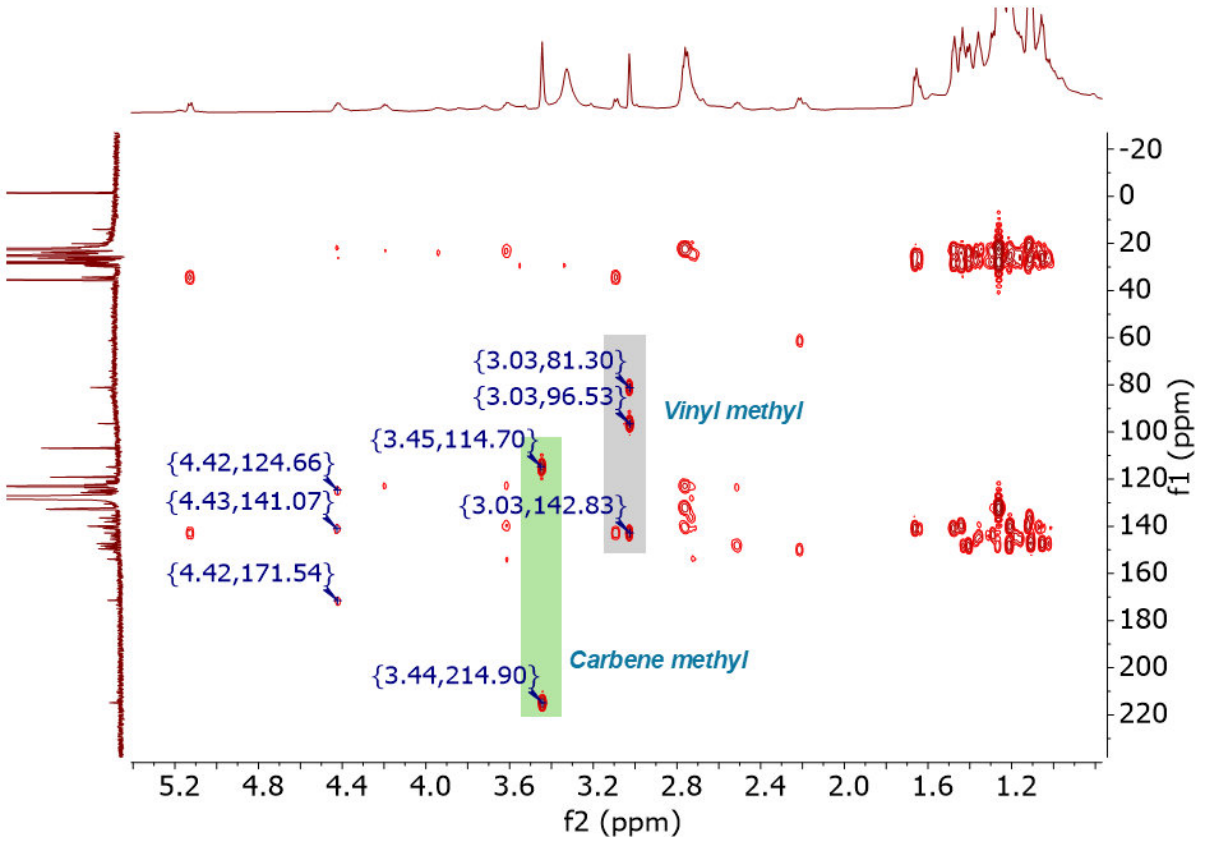

Figure S81. Aliphatic area of HMBC {^{1}H, ^{13}C} of the above reaction mixture in C_6D_6 (151 MHz, 298K).

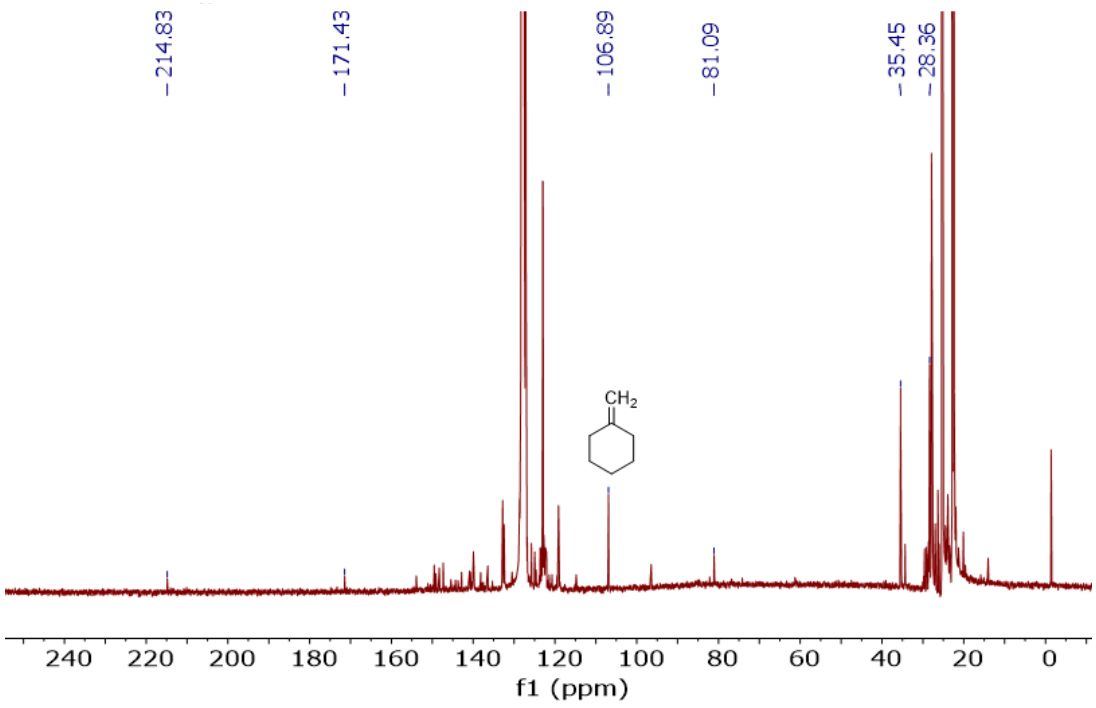

Figure S82. ^{13}C NMR spectra of the above reaction mixture in C_6D_6 (151 MHz, 298K).

4. Syntheses of other ethylene complexes

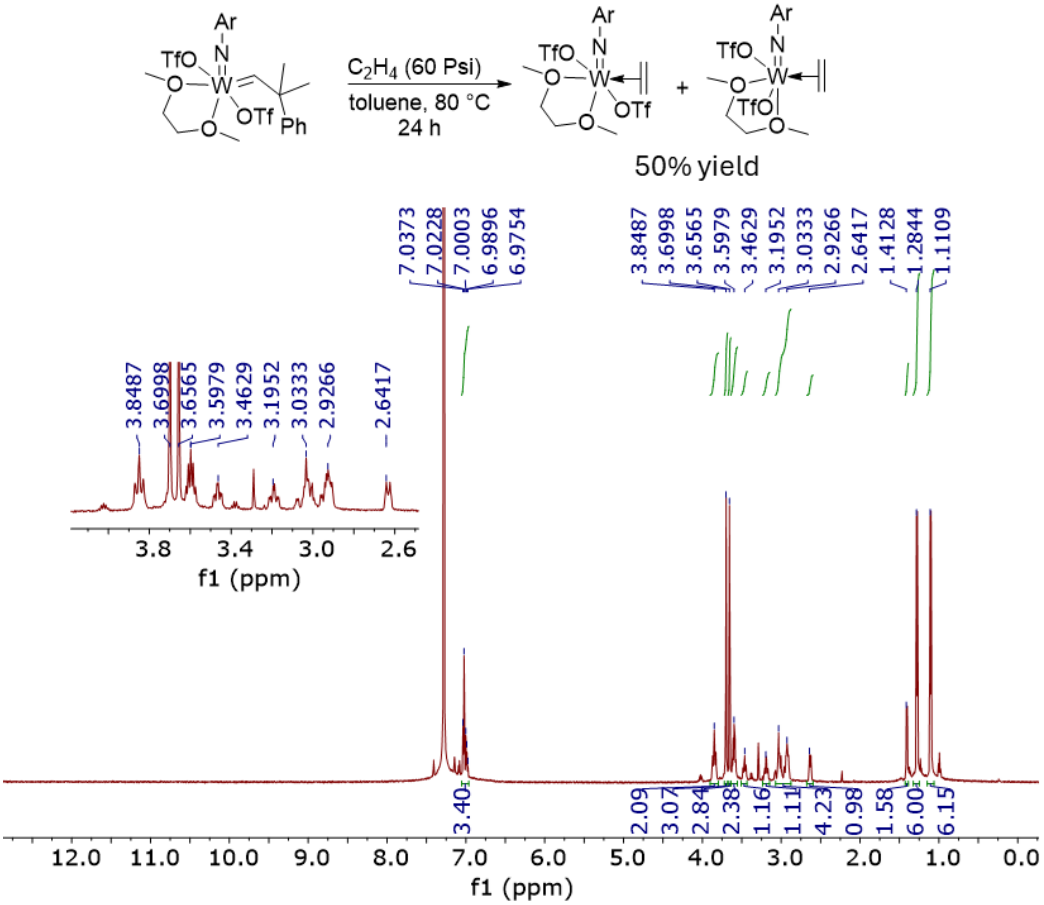

Figure S83. ^{1}H NMR spectra of the reaction of W(NAr)(CHCMe$_2$Ph)(OTf)$_2$(dme) with ethylene (60 psi) at 80 °C in toluene for 24 h (600 MHz, 298K, C_6D_6).

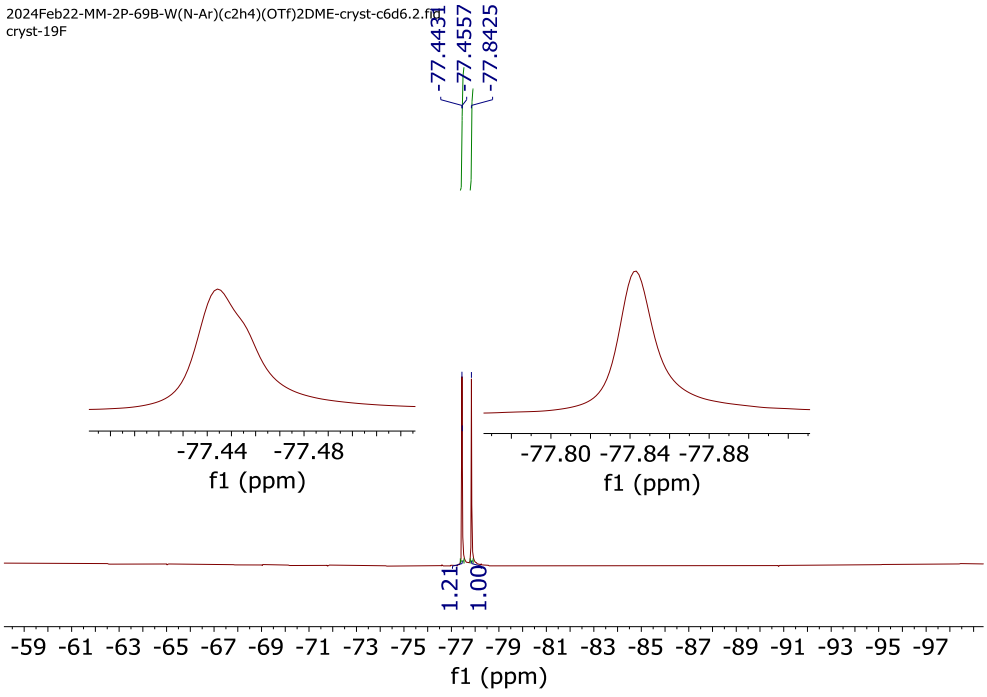

Figure S84. ^{19}F NMR spectra of W(NAr)(C_2H_4)(OTf)$_2$(dme) in C_6D_6 (564 MHz, 298K).

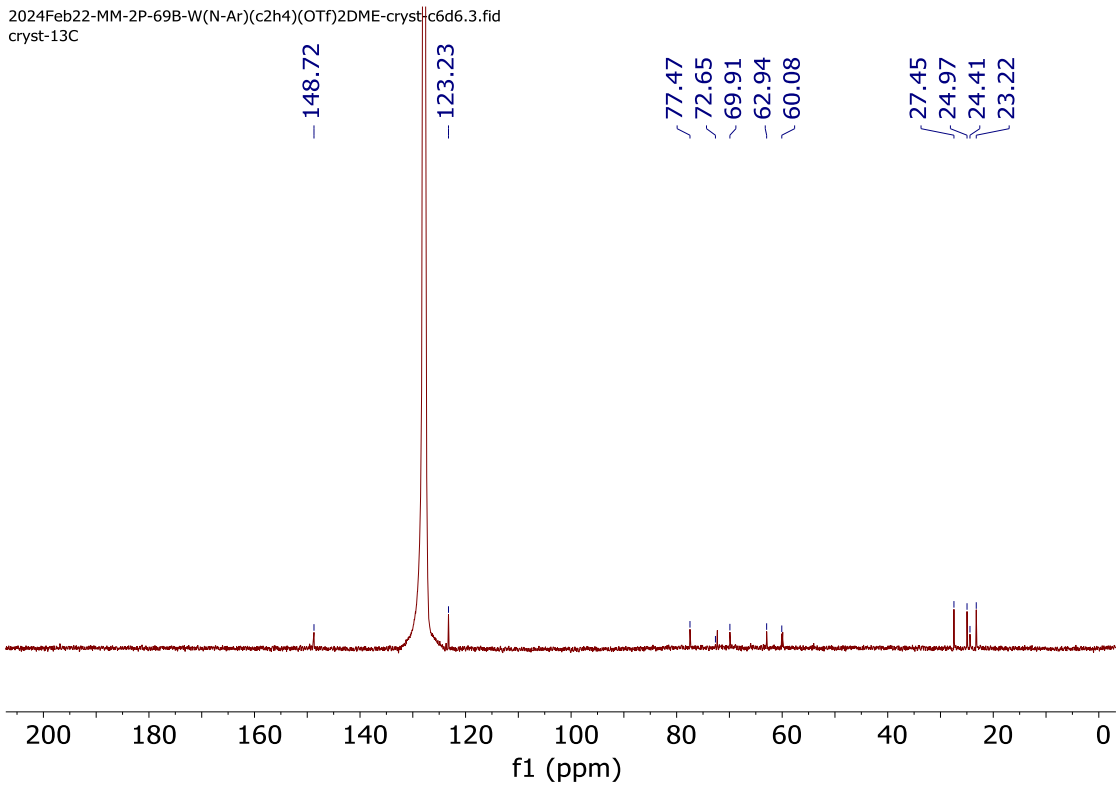

Figure S85. ^{13}C NMR spectra of W(NAr)(C_2H_4)($OTf)_2$(dme) in C_6D_6 (151 MHz, 298K).

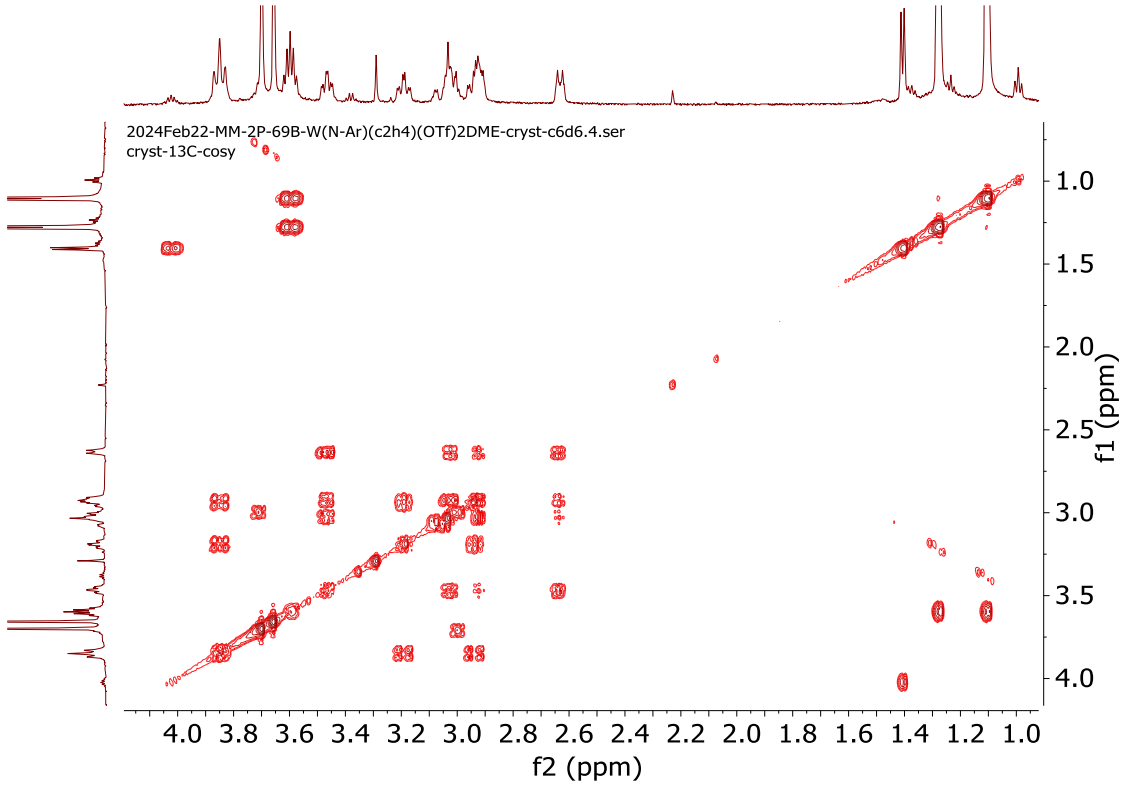

Figure S86. ^{1}H COSY NMR spectra of W(NAr)(C_2H_4)($OTf)_2$(dme) in C_6D_6 (151 MHz, 298K).

5. X-ray Crystallography

Data collection

Single crystals suitable for X-ray diffraction was placed onto the tip of a MiTeGen pin and mounted on a Bruker Venture D8 diffractometer equipped with a PhotonIII detector. The data collection was carried out using Mo Kα radiation (λ = 0.71073 Å)/ Cu Kα radiation (λ = 1.54178 Å) from an IμS micro-source. The frames were integrated with the Bruker SAINT[2] software package using a narrow-frame algorithm to 0.82 Å resolution. Data were corrected for absorption effects using the multi-scan method (SADABS).[3]

Structure solution and refinement

The space group was determined based on intensity statistics and systematic absences. The structure was solved using the SHELX suite of programs[4,5] and refined using full-matrix least-squares on F^2 within the OLEX2 suite,[6] An intrinsic phasing solution was calculated, which provided most non-hydrogen atoms from the E-map. Full-matrix least squares / difference Fourier cycles were performed, which located the remaining non-hydrogen atoms. All non-hydrogen atoms were refined with anisotropic displacement parameters. The hydrogen atoms were placed in ideal positions and refined as riding atoms with relative isotropic displacement parameters. Crystal and data quality details, as well as a summary of the residual refinement values, are listed in the following tables. All the crystallographic figures were generated using ORTEP-3 software.[7]

$W(NAr)_2Et_2$

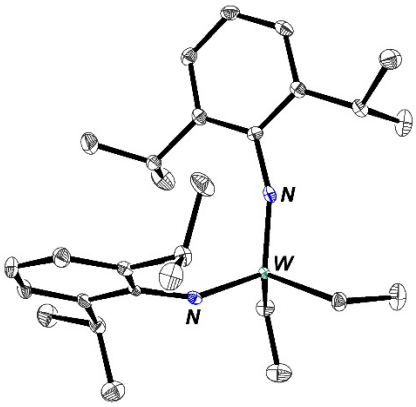

Figure S87. Thermal ellipsoid plot (40%) of $W(NAr)_2Et_2$ (hydrogen atoms have been omitted for clarity).

Table S1. Crystal data and structure refinement for compound $W(NAr)_2Et_2$ (deposition number 2419295).

Empirical formula	$C_{28}H_{44}N_2W$	
Formula weight	592.50	
Crystal color, shape, size	yellow block, 0.35 × 0.18 × 0.17 mm^3	
Temperature	100.00 K	
Wavelength	1.54178 Å	
Crystal system, space group	Monoclinic, P $2_1/n$	
Unit cell dimensions	a = 13.3829(9) Å	α = 90°.
	b = 18.8032(13) Å	β = 106.6806(19)°.
	c = 22.2737(15) Å	γ = 90°.
Volume	5369.1(6) $Å^3$	
Z	8	
Density (calculated)	1.466 g/cm^3	
Absorption coefficient	8.075 mm^{-1}	
F(000)	2400	

Data collection

Diffractometer	Bruker D8 Venture
Theta range for data collection	3.133 to 68.272°.
Index ranges	-16<=h<=16, -22<=k<=22, -26<=l<=26
Reflections collected	100571
Independent reflections	9678 [Rint = 0.0351]
Observed Reflections	9674
Completeness to theta = 67.679°	98.4 %

Solution and Refinement

Absorption correction	Semi-empirical from equivalents
Max. and min. transmission	0.7531 and 0.5008
Solution	Intrinsic methods
Refinement method	Full-matrix least-squares on F^2
Weighting scheme	$w = [\sigma^2 Fo^2 + AP^2 + BP]^{-1}$, with
	$P = (Fo^2 + 2\,Fc^2)/3$, A = 0.009, B = 10.4
Data / restraints / parameters	9678 / 0 / 579
Goodness-of-fit on F^2	1.285
Final R indices [I>2σ(I)]	R1 = 0.0217, wR2 = 0.0529
R indices (all data)	R1 = 0.0217, wR2 = 0.0529
Largest diff. peak and hole	0.980 and -1.279 $e.Å^{-3}$

W(NAr)(OR_{F9})$_2$(C_2H_4)($ArNH_2$)

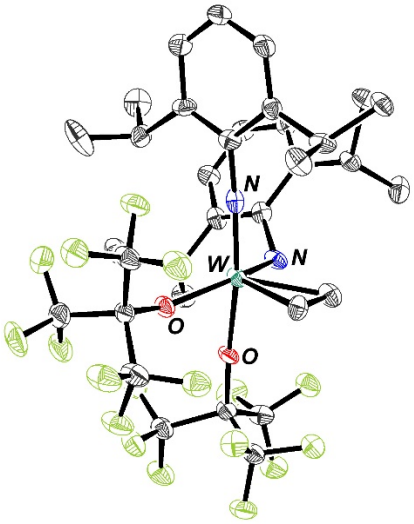

Figure 88. Thermal ellipsoid plot (40%) of W(NAr)(OR_{F9})$_2$(C_2H_4)($ArNH_2$) (hydrogen atoms have been omitted for clarity).

Table S2. Crystal data and structure refinement for W(NAr)(OR_{F9})$_2$(C_2H_4)($ArNH_2$) (deposition number 2419290).

Empirical formula	$C_{34}H_{40}F_{18}N_2O_2W$	
Formula weight	1034.53	
Crystal color, shape, size	yellow block, 0.08 × 0.06 × 0.04 mm^3	
Temperature	110.0 K	
Wavelength	1.54178 Å	
Crystal system, space group	Triclinic, $P\bar{1}$	
Unit cell dimensions	a = 10.5049(9) Å	α = 87.086(5)°.
	b = 13.5610(11) Å	β = 87.639(6)°.
	c = 13.6443(11) Å	γ = 81.043(6)°.
Volume	1916.4(3) $Å^3$	
Z	2	
Density (calculated)	1.793 g/cm^3	
Absorption coefficient	6.710 mm^{-1}	
F(000)	1020	

Data collection

Diffractometer	Bruker D8 Venture
Theta range for data collection	3.245 to 68.784°.
Index ranges	-12<=h<=12, -15<=k<=16, -16<=l<=16
Reflections collected	23570
Independent reflections	6900 [Rint = 0.0775]
Observed Reflections	5966
Completeness to theta = 67.679°	98.0 %

Solution and Refinement

Absorption correction	Semi-empirical from equivalents
Max. and min. transmission	0.7509 and 0.6109
Solution	Intrinsic methods
Refinement method	Full-matrix least-squares on F^2
Weighting scheme	$w = [\sigma^2 Fo^2 + AP^2 + BP]^{-1}$, with $P = (Fo^2 + 2\,Fc^2)/3$, A = 0.068, B = 28.9
Data / restraints / parameters	6900 / 0 / 522
Goodness-of-fit on F^2	1.094
Final R indices [I>2σ(I)]	R1 = 0.0665, wR2 = 0.1687
R indices (all data)	R1 = 0.0791, wR2 = 0.1793
Largest diff. peak and hole	4.716 and -1.914 e.Å^{-3}

W(NAr)(Ar'NH)($ArNH_2$)(OR_{F9})

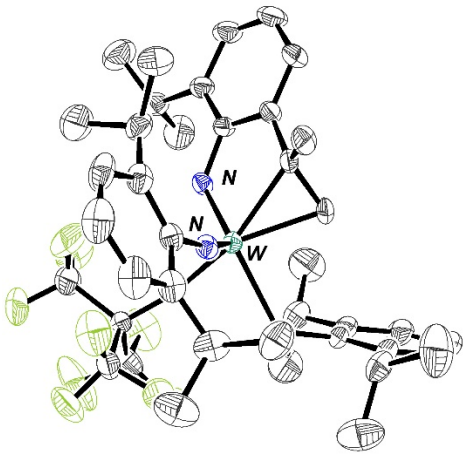

Figure S89. Thermal ellipsoid plot (40%) of W(NAr)(Ar'NH)($ArNH_2$)(OR_{F9}) (hydrogen atoms have been omitted for clarity).

Table S3. Crystal data and structure refinement for W(NAr)(Ar'NH)($ArNH_2$)(OR_{F9}) (deposition number 2419293).

Empirical formula	$C_{40}H_{52}F_9N_3OW$
Formula weight	945.69
Crystal color, shape, size	orange block, 0.4 × 0.36 × 0.22 mm^3
Temperature	298.0 K
Wavelength	0.71073 Å
Crystal system, space group	Triclinic, $P\bar{1}$
Unit cell dimensions	a = 11.223(9) Å α = 77.46(2)°.

	b = 12.684(10) Å β = 76.31(4)°.
	c = 16.267(13) Å γ = 70.79(2)°.
Volume	2100(3) $Å^3$
Z	2
Density (calculated)	1.496 g/cm^3
Absorption coefficient	2.824 mm^{-1}
F(000)	952

Data collection

Diffractometer	Bruker D8 Venture
Theta range for data collection	1.720 to 25.961°.
Index ranges	-13<=h<=13, -15<=k<=15, -19<=l<=19
Reflections collected	44071
Independent reflections	7966 [Rint = 0.0788]
Observed Reflections	6826
Completeness to theta = 25.242°	99.0 %

Solution and Refinement

Absorption correction	Semi-empirical from equivalents
Max. and min. transmission	0.7453 and 0.4929
Solution	Intrinsic methods
Refinement method	Full-matrix least-squares on F^2
Weighting scheme	$w = [\sigma^2 Fo^2 + AP^2 + BP]^{-1}$, with
	$P = (Fo^2 + 2\,Fc^2)/3$, A = 0.105, B = 0.000
Data / restraints / parameters	7966 / 0 / 498
Goodness-of-fit on F^2	1.077
Final R indices [I>2σ(I)]	R1 = 0.0506, wR2 = 0.1319
R indices (all data)	R1 = 0.0630, wR2 = 0.1462
Largest diff. peak and hole	2.239 and -2.427 $e.Å^{-3}$

W(NAr)(C_4H_8)(OR_{F9})$_2$

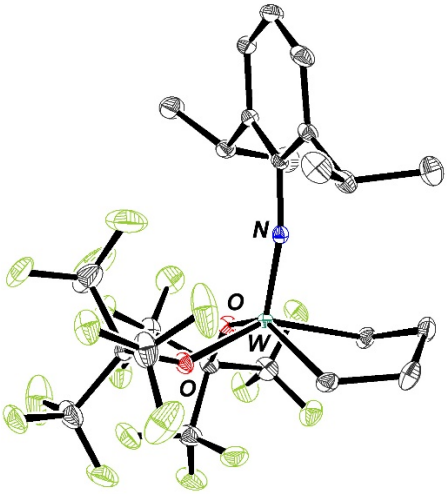

Figure S90. Thermal ellipsoid plot (40%) of compound W(NAr)(C_4H_8)(OR_{F9})$_2$ (hydrogen atoms have been omitted for clarity).

Table S4. Crystal data and structure refinement for compound W(NAr)(C_4H_8)(OR_{F9})$_2$ (deposition number 2419296).

Empirical formula	$C_{24}H_{25}F_{18}NO_2W$
Formula weight	885.30
Temperature/K	100.00
Crystal system	orthorhombic
Space group	Pbca
a/Å	10.2840(4)
b/Å	18.2199(7)
c/Å	30.9881(12)
α/°	90
β/°	90
γ/°	90
Volume/Å^3	5806.3(4)
Z	8
ρ_{calc}g/cm^3	2.025
μ/mm^{-1}	8.710
F(000)	3424.0
Crystal size/mm^3	0.18 × 0.17 × 0.09
Radiation	CuKα (λ = 1.54178)
2Θ range for data collection/°	10.12 to 140.122
Index ranges	$-12 \leq h \leq 12$, $-22 \leq k \leq 22$, $-37 \leq l \leq 37$
Reflections collected	130741
Independent reflections	5498 [R_{int} = 0.0451, R_{sigma} = 0.0164]

Data/restraints/parameters	5498/30/396
Goodness-of-fit on F^2	1.051
Final R indexes [I>=2σ (I)]	R_1 = 0.0331, wR_2 = 0.0795
Final R indexes [all data]	R_1 = 0.0335, wR_2 = 0.0797
Largest diff. peak/hole / e $Å^{-3}$	1.75/-1.47

W(NAr)(C_3H_6)(OR_{F9})$_2$

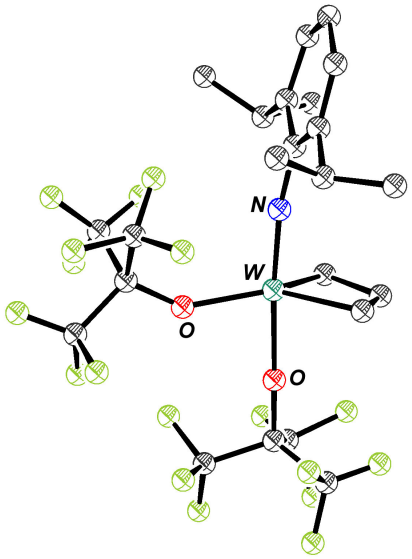

Figure S91. Thermal ellipsoid plot (40%) of compound W(NAr)(C_3H_6)(OR_{F9})$_2$ (hydrogen atoms have been omitted for clarity).

Table S5. Crystal data and structure refinement for compound W(NAr)(C_3H_6)(OR_{F9})$_2$ (deposition number 2419291).

Empirical formula	$C_{23}H_{23}F_{18}NO_2W$
Formula weight	871.27
Crystal color, shape, size	yellow block, 0.08 × 0.07 × 0.07 mm^3
Temperature	100.00 K
Wavelength	1.54184 Å
Crystal system, space group	Monoclinic, C 2
Unit cell dimensions	a = 20.517(2) Å
	b = 11.7363(13) Å
	c = 11.8494(11) Å
Volume	2834.1(5) $Å^3$
Z	4
Density (calculated)	2.042 g/cm^3
Absorption coefficient	8.910 mm^{-1}

F(000)	1680
Data collection	
Diffractometer	Bruker D8 Venture
Theta range for data collection	5.403 to 70.040°.
Index ranges	-24<=h<=24, -14<=k<=14, -13<=l<=14
Reflections collected	25024
Independent reflections	5212 [Rint = 0.0354]
Observed Reflections	5105
Completeness to theta = 67.684°	99.3 %
Solution and Refinement	
Absorption correction	Semi-empirical from equivalents
Max. and min. transmission	0.7533 and 0.6026

W(NAr)(py)[(μ-NAr')(μ-NHAr'')]W(NAr)(OR_{F9})

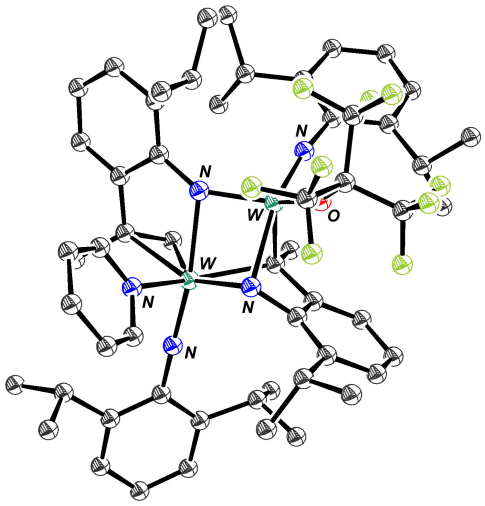

Figure S92. Thermal ellipsoid plot (40%) of W(NAr)(py)[(μ-NAr')(μ-NHAr'')]W(NAr)(OR_{F9}) (hydrogen atoms have been omitted for clarity).

Table S6. Crystal data and structure refinement for W(NAr)(py)[(μ-NAr')(μ-NHAr'')]W(NAr)(OR_{F9}) (deposition number 2480801).

Empirical formula	$C_{58}H_{73}F_9N_5O_{1.5}W_2$	
Formula weight	1402.91	
Crystal color, shape, size	red plate, 0.11 × 0.06 × 0.05 mm^3	
Temperature	100.0 K	
Wavelength	1.54178 Å	
Crystal system, space group	Orthorhombic, $Pna2_1$	
Unit cell dimensions	a = 20.8163(6) Å	α = 90°.
	b = 13.7960(4) Å	β = 90°.
	c = 39.1164(11) Å	γ = 90°.

Volume	11233.5(6) $Å^3$
Z	8
Density (calculated)	1.659 g/cm^3
Absorption coefficient	8.095 mm^{-1}
F(000)	5576

Data collection

Diffractometer	Bruker D8 VENTURE
Theta range for data collection	2.259 to 70.178°.
Index ranges	-25<=h<=25, -16<=k<=16, -47<=l<=47
Reflections collected	193781
Independent reflections	21316 [Rint = 0.0780]
Observed Reflections	20091
Completeness to theta = 67.679°	100.0 %

Solution and Refinement

Absorption correction	Semi-empirical from equivalents
Max. and min. transmission	0.7533 and 0.6014
Solution	Intrinsic methods
Refinement method	Full-matrix least-squares on F^2
Weighting scheme	$w = [\sigma^2 Fo^2 + AP^2 + BP]^{-1}$, with $P = (Fo^2 + 2\,Fc^2)/3$, A = 0.017, B = 187
Data / restraints / parameters	21316 / 1513 / 1210
Goodness-of-fit on F^2	1.132
Final R indices [I>2σ(I)]	R1 = 0.0493, wR2 = 0.1194
R indices (all data)	R1 = 0.0535, wR2 = 0.1219
Absolute structure parameter	0.242(18)
Largest diff. peak and hole	3.052 and -3.561 $e.Å^{-3}$

Twin Details

Type, twin law	inversion twin, -1 0 0, 0 -1 0, 0 0 -1
Twin element, domain ratio	inversion, 76:24

6. References

1. R. R. Schrock, R. T. DePue, J. Feldman, K. B. Yap, D. C. Yang, W. M. Davis, L. Park, M. DiMare, M. Schofield, *Organometallics* **1990,** *9*, 2262-2275.
2. SAINT, V8.30A, Bruker Analytical X-Ray Systems, Madison, WI, 2012.
3. SADABS, 2.03, Bruker Analytical X-Ray Systems Inc., Madison, WI, USA, 2016.
4. G. M. Sheldrick, *Acta Cryst*. **2008**, A64, 112-122.
5. G. M. Sheldrick, *Acta Cryst*. **2015**, A71, 3-8.
6. O. V. Dolomanov, L. J. Bourhis, R. J. Gildea, J. A. K. Howard, H. J. Puschmann, *Appl. Crystallogr.* **2009**, 42, 339-341.
7. M. N. Burnett, C. K. Johnson, ORTEP-III: Oak Ridge Thermal Ellipsoid Plot Program for Crystal Structure Illustrations, Oak Ridge National Laboratory Report ORNL-6895, 1996.